POLITECNICO

MILANO 1863

SCHOOL OF INDUSTRIAL AND INFORMATION ENGINEERING
MASTER DEGREE IN MECHANICAL ENGINEERING

Study of a pantographic linkage used as coordinate measuring arm for PKM applications

Supervisor

Prof. Hermes Giberti

Co-Supervisor

Eng. Patrick Maurine

Degree thesis of

Alessandro Villa

820366

Academic Year 2015/2016

Partner University

The present study have been proposed and developed at *Institut national des sciences appliquées de Rennes* in Rennes, France. The professors Patrick Maurine, Eric Courteille and Dominique Deblaise, from the Département Génie Mécanique et Automatique (GMA), have supported me during all the work.
All the experiments and tests have been achieved at INSA Rennes laboratories and facilities, under the supervision of the professors cited above.
Here the contact informations:

- INSA Rennes: www.insa-rennes.fr

- Eng. Patrick Maurine: Patrick.Maurine@insa-rennes.fr

- Eng. Eric Courteille: Eric.Courteille@insa-rennes.fr

- Eng. Dominique Deblaise: Dominique.Deblaise@insa-rennes.fr

Abstract

Parallel Kinematic Machines (PKMs), thanks to their speed, precision and high payload, are largely used in applications such as physical motion, space docking systems, machining, assembly, and also assisting surgeons during medical operations. Therefore a key factor is the PKM accuracy, for which the calibration plays a significant role. There are several ways to perform the calibration and in this work we focused on an external method, which uses a Coordinate Measuring Arm (CMA). This method was chosen because of being flexible (suitable for very different types of PKM), affordable and including a load compensator. We started from the creation of a geometrical and error model; therefore, an elastic model was created in order to identify the behaviour of the structure under a wrench. The calibration of the geometrical and elastic models was performed using measures on the real mock-up. This calibration allows the correction of the PKM end-effector position, measuring only three parameters on the CMA.

Sommario

I robot a cinematica parallela, o PKM (*Parallel Kinematic Machines*), grazie alla loro velocitá, precisione e al loro alto carico utile, sono largamente impiegati in applicazioni quali movimentazione, utilizzo in ambito spaziale, lavorazioni meccaniche, assemblaggio e in assistenza ai chirurghi durante le operazioni. Un aspetto chiave é quindi rappresentato dalla accuratezza dei PKM, in cui la calibrazione gioca un ruolo fondamentale. Vi sono diversi modi di eseguire la calibrazione e quello qui preso in considerazione fa parte della famiglia dei cosiddetti 'metodi esterni'. Si tratta di un *Coordinate Measuring Arm* (CMA), scelto perché economico, applicabile a diverse tipologie di PKM e poiché include un compensatore di carico. Sono stati creati un modello geometrico, un modello dell'errore, e infine un modello elastico, con lo scopo di identificare il comportamento della struttura soggetta a un carico. La calibrazione dei modelli geometrico ed elastico é stata effettuata utilizzando le misure sul modello reale. La calibrazione permette di correggere la posizione dell'*end-effector* del PKM misurando solo tre parametri sul CMA.

Contents

List of Figures

List of Tables

CHAPTER 1

Introduction and state of the art

Parallel kinematic machines (PKMs), also here called parallel kinematic manipulators, are closed-loop mechanisms, Figure 1.1 shows an example, presenting very good performances in terms of accuracy, rigidity and ability to manipulate large loads. Therefore, PKMs are used in various applications such as flight and automotive simulators, high speed and high accuracy positioning, material handling and medical fields. Comparing with the serial robots, the Parallel kinematic machines present higher structural stiffness, low inertia, a reduced sensitivity to certain errors and greater load capacity, thanks to the sharing of the load between the links connected to the fixed base. However there are some disadvantages especially in the writing of the kinematic model due to the presence of passive and multi-degrees of freedom (DoF) joints. PKMs are also affected by manufacturing errors and errors due to backlash and hysteresis [11], which are generally presented in all types of robot. These are the reasons why the calibration of PKMs is a critical aspect of the design.

Figure 1.1: PKM example

1.1 State of the art

The use in nowadays industries of parallel kinematic machines requires the development of calibration methods in order to increase the accuracy of these robots. Therefore the calibration is becoming an important aspect in the robots design and employment with the scope of compensating the PKM errors.

1.1.1 Error analysis

In order to better understand the calibration procedure, an analysis of the different types of error was performed, according to [9] and [7].

Geometrical errors   There are numerous factors that contribute to geometrical errors. The first ones are manufacturing errors, and they depend from how precisely the robot parts satisfy the design specifications. Further factors hail from the imperfections in the assembly procedures and errors of the joints. The last ones can cause deviation in the alignment of the centre of joints and actuators.
Geometrical errors do not depend on the robot configuration whereas their effect on the position and orientation accuracy depend on it. They can be identified through the geometrical model, where the position errors of the end-effector are function of the errors of the links.

Non-Geometrical errors   Non-geometrical errors depend on external conditions. They may result from friction, gravity, backlash, gear transmission and temperature. An additional error is the end-effector deflection caused by the force/torque associated with the purpose of the robot. It is called compliance error and it depends on the manipulator configuration. These different types of error do not have the same weight on the end-effector position error. The highest contribution is given, according to [9], by the joints and links flexibility with the $8\% - 10\%$, while the backlash contribution is about $0.5\% - 1\%$ and 0.1% due to temperature. The errors due to flexibility can be reduced using encoders on the passive joints, whereas the temperature errors are avoided controlling the room temperature or by using a dedicated thermal model.
The effect of geometrical and non-geometrical errors have to be separated, in order to identify, independently, the geometrical parameters, through a static calibration, and the non-geometrical ones by means of a dynamic calibration.

1.1.2 Types of calibration

Starting from the error types discussed, it is possible to split the calibration procedure in order to isolate the different types of error and achieve a better identification of the parameters influence, as suggested in [9]. The calibration procedure can be divided in three different steps:

- The calibration of the joints

- The kinematic calibration

- The dynamic calibration

Joints calibration has the scope to identify the differences between the theoretical and measured joints displacements, which are obtained from external data acquisitions.

The kinematic calibration attends the task of correcting the geometrical and assembly errors of the PKM. Through the geometrical model of the structure, we obtain the equations which contain the unknown geometrical errors, while boundary conditions are obtained from the errors on the end-effector positions and orientations. Using a numerical method we can perform the identification of the geometrical errors. The way in which the geometrical model is written highly influences the results of the assessment.

The compliance errors can be evaluated through a dynamic calibration (or kinetostatic in case of slow movements, minus than $1 \, \mathrm{m \, s^{-1}}$). Other types of error source, such as backlash and friction, are not being taken into account.

1.1.3   Calibration methods

The different calibration methods, as reported by [14], differ from the data-acquisition method and from its degree of automation. A summary of the main methods is reported below.

Self-calibration

Self-calibration consists in the addition of sensors to the passive joints. The number of the internal sensors have to be bigger than the DoF of the mechanism, in order to obtain an over-determined system. According to [15], self-calibration removes the dependence from external pose informations, generates measures with high accuracy in the entire workspace, allows on-line accuracy compensation and automates the measure process. The insertion of internal sensors could facilitate different control functionalities, however there are some disadvantages, such as the increase of the costs and difficulties in the insertion in a pre-existent structure or in the design process. Furthermore, environmental conditions of the joints, such as lubrication and vibration, can influence the measures. We have to consider that the weight and the dimension of the sensors have to be small in order not to influence the robot dynamic properties.

Some of these disadvantages entail difficulties in the application in the industrial environment.

Constrained calibration

Another method is to constrain the mobility of some passive joints through a physical constraint. This entails a reduction in the degrees of freedom of the structure, therefore the robot mobility is reduced. A way in which the constraint

is applied is to force the robot to follow the contour of a body, such as a cylinder or a plate. The robot end-effector is guided in a huge number of points around the shape and for each point the position of the end-effector is calculated through the kinematic model. The parameters of the model can be identified applying the least square method on the difference between the computed contour and the real one. This method is applicable to both serial and parallel robots.

A method which can be used only with parallel robots is to clamp some passive joints in order to remain in a fixed position. Therefore there is a reduction of the DoF of the structure and some geometric parameters will not change during the process. The calibration process uses the redundant informations coming from the position-sensors of the motors. This method has some drawbacks resulting from the restriction of the workspace and the interferences between links. Therefore some parameters related to the clamped joints can be unseen and the calibration is less accurate than external and self-calibration methods. An advantage of this method is that any extra sensors or external metrology equipment are required.

External calibration

Due to the difficulties in the addition of redundant sensors, the method which has become the most common is to acquire the necessary measurements with external devices, such as vision devices, laser trackers, inclinometers and coordinate measuring machines. Once the kinematic model of the robot is known, the identification can be performed measuring the end-effector position in different robot configurations and then using the gap between the measured and the theoretical positions of the end-effector to calibrate the robot model.

This type of calibration method is very general and can be applied on different types of robot, therefore it is largely used in industry as the standard calibration technique.

1.2   Case study

Literature proposes different approaches for the external calibration and the most common device used is a redundant leg. In [2] the redundant leg was mounted through magnetic ball joints between the machine frame and the HSK (German abbreviation for "hollow taper shank") interface and it was equipped with a linear measuring device. In a similar way, [10] chose to mount the leg between the end-effector and Stewart platform, a type of PKM (see Figure 1.2), frame. The leg was treated as a true leg of the robot. A different approach was proposed by [3] where the redundant leg, which contains a displacement sensor, was mounted through a ball joint to the manipulator base and through a precision adapter to the gripper. In this case the leg was inside the PKM and not linked to the external frame.
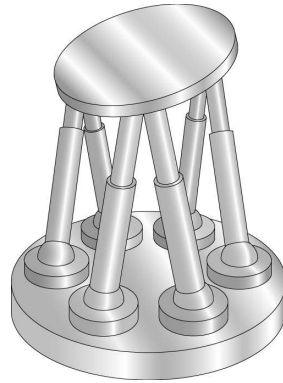
Figure 1.2: Stewart Platform

In agreement with [6] external calibration methods have the drawback of being expensive, limiting the workspace and need a considerable effort in setting-up system, nevertheless they provide better accuracy compared with the redundant sensors method. Considering the advantages and drawbacks of the methods reported above, we here propose an external calibration method which can improve the accuracy of the PKM with a simple, affordable and reusable tool.

Therefore the purpose of this work is to revise, correct and continue the work of [13] as a means to understand the potentiality of the coordinate measuring arm (CMA), also here called pantograph or pantographic linkage. The pantograph, shown in Figure 1.3 and mounted on the PKM in Figure 1.4, was modelled and calibrated with the scope of calculating the accuracy of the CMA. The mathematical model is made by a geometrical and elastic model and the calibration of both the models was accomplished with intensive simulations and experiments on the real mock-up.
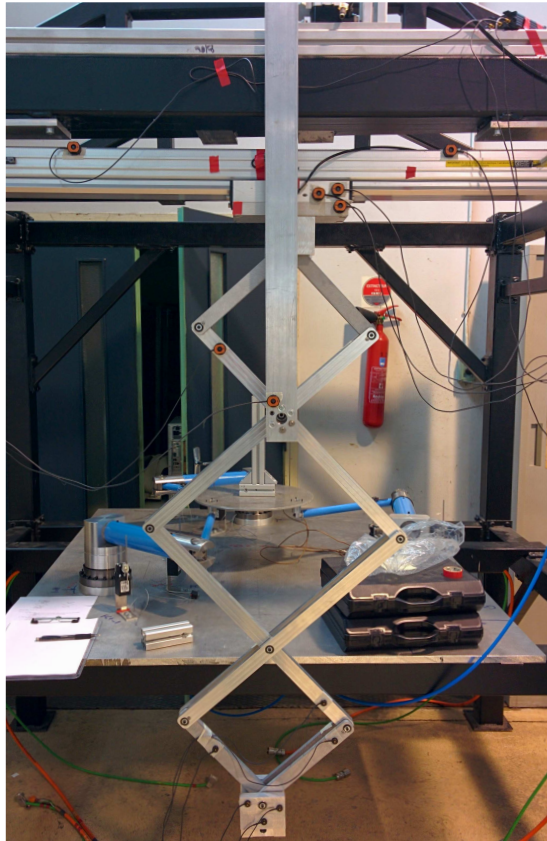
Figure 1.3: Parallel kinematic manipulator

Figure 1.4: Parallel kinematic manipulator plus the coordinate measuring arm

CHAPTER 2

Geometrical and Error models

The geometrical model is necessary to identify, through the geometrical characteristics, the position of the end-effector and of the joints of the structure. Therefore the procedure proposed by [13] describes how to implement the geometrical model of the pantograph.

2.1 System description and notation

The notation used in this thesis is shown in Figure 2.1. Points $A_{i,j}$ are the joints which connect the upper and lower links of a loop, points B_i are the joints between the loops, and the end-effector position is $\boldsymbol{P} = [\, x \; y \; z \,]^T$. The system is driven by the coordinates $\boldsymbol{q} = [q_1 \; q_2 \; q_3]$, where q_1 represents the horizontal translation of the point B_0, q_2 the vertical translation of the point B_1 and q_3 the rotation of the base around the $\vec{z}$ axis. The length of the links is named $L_{i,j}^u$ for the upper part of the loop and $L_{i,j}^l$ for the lower part, where $i = 1 \ldots 3$ represents the number of the loop and j represents the side, 1 for the left side and 2 for the right side. The pantograph is composed by eight links where, in order to apply the finite element method, the four longest links (the first one from A_{11} to A_{22}, the second one from A_{12} to A_{21}, the third one from A_{21} to A_{32} and the last one from A_{22} to A_{31}) are split in two parts. The division points are B_1 and B_2 because they represent rotation joints and therefore are points of discontinuity. Joints A and B are rotational joints which let the pantograph moves.
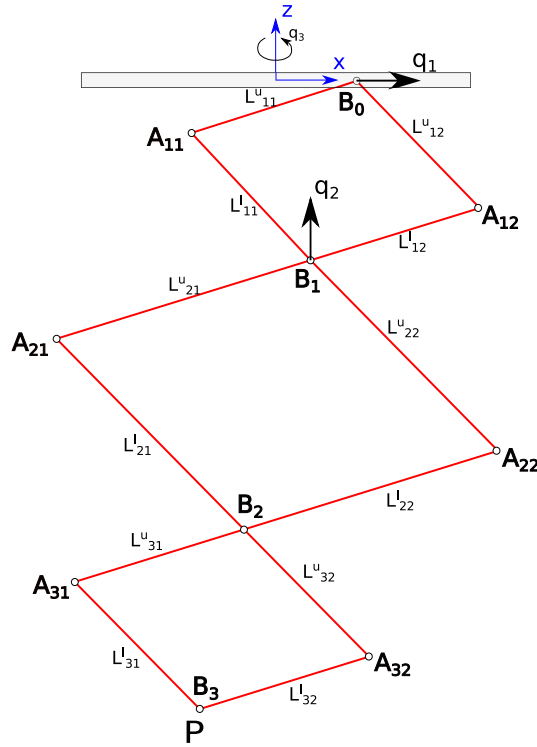
Figure 2.1: Scheme of the structure and notation

2.2 Geometrical model

Once are known the geometrical properties of the pantograph and its configuration through the imposed coordinates q_1, q_2 and q_3, it is possible to calculate the position of the points $A_{i,j}$ and B_i. Because of the structure properties it has to be $\boldsymbol{B_0} = [\, q_1 \; 0 \; 0 \,]^T$ and $\boldsymbol{B_1} = [\, 0 \; q_2 \; 0 \,]^T$, therefore the point B_0 can only translate in horizontal direction whereas the point B_1 can only translate in vertical direction. The geometrical model is written, firstly, considering the pantograph in the plane and then, with the introduction of the coordinate q_3, projecting the structure in the space. The coordinate q_3 represents the rotation of the structure around the axis $\vec{z}$, therefore, it gives the orientation in the space. Starting from the first loop, the position of joints A_{11} and A_{12} is calculated considering the intersection of two circles, as shown in Equation (2.1). The calculation of the point A_{11} is made considering a first circle centred in B_0 with radius L^u_{11}, and a second one centred in B_1 with radius L^l_{11}. Regarding A_{12} the centres are the same while the radius are L^u_{12} and L^l_{12}, as described in Figure 2.2.

$$
\begin{cases}
(x_{A_{1,j}} - x_{B_0})^2 + (z_{A_{1,j}} - z_{B_0})^2 = {L^u_{1,j}}^2 \\[2mm]
(x_{A_{1,j}} - x_{B_1})^2 + (z_{A_{1,j}} - z_{B_1})^2 = {L^l_{1,j}}^2
\end{cases}
\tag{2.1}
$$
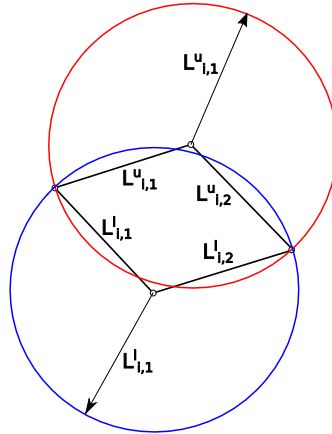
Figure 2.2: Definition of the two circles centred in B_0 and B_1

Once the positions of the first loop joints are known, we can calculate the position of A_{21} and A_{22} through the Equation (2.2), which describes, along $\vec{x}$ and $\vec{z}$, the extension of the link L_{11}^l and L_{12}^l in the second loop.

$$
\begin{cases}
A_{i,1} = A_{i-1,2} + \frac{L_{i-1,2}^l + L_{i,1}^u}{L_{i-1,2}^l}(B_{i-1} - A_{i-1,2}) \\[2mm]
A_{i,2} = A_{i-1,1} + \frac{L_{i-1,1}^l + L_{i,2}^u}{L_{i-1,1}^l}(B_{i-1} - A_{i-1,1})
\end{cases}
\tag{2.2}
$$

The position of the point B_2 is obtained by the intersection of two circles, as reported in Equation (2.3).

$$
\begin{cases}
(x_{B_i} - x_{A_{i,1}})^2 + (z_{B_i} - z_{A_{i,1}})^2 = {L_{i,1}^l}^2 \\[2mm]
(x_{B_i} - x_{A_{i,2}})^2 + (z_{B_i} - z_{A_{i,2}})^2 = {L_{i,2}^l}^2
\end{cases}
\tag{2.3}
$$

A_{31} and A_{32} position are obtained by Equation (2.2), whereas for point B_3 Equation (2.3) is used. The end-effector position P in the plane is equal to the position of point B_3. The coordinate q_3 is necessary to give the pantograph orientation in the space. Therefore a rotation matrix $\boldsymbol{R}$ is needed.

$$
\boldsymbol{P} = \begin{bmatrix} x_p & y_p & z_p \end{bmatrix}^T = \boldsymbol{R} \begin{bmatrix} x_{B_3} & y_{B_3} & z_{B_3} \end{bmatrix}^T
\tag{2.4}
$$

where

$$
\boldsymbol{R} = \begin{bmatrix} \cos(q_3) & -\sin(q_3) & 0 \\ \sin(q_3) & \cos(q_3) & 0 \\ 0 & 0 & 1 \end{bmatrix}
\tag{2.5}
$$

The geometrical model was written in Matlab®.

2.2.1   Pantograph ratio and amplification factor

The pantograph end-effector position is directly linked to the two driven coordinates. Through the Matlab® model we calculate a specific ratio that links the

movement on the driven coordinates to the movement of the end-effector. This ratio is -2.5 for the $\vec{x}$ direction and 3.5 for the $\vec{z}$ direction. This means that if the coordinate q_1 increases by $1\,\text{mm}$, the end-effector will have a movement along $\vec{x}$ of $-2.5\,\text{mm}$. The same also for the coordinate q_2. This factor is a characteristic of the pantograph and depends on its geometrical properties.

The length of the links influence the pantograph ratio, therefore an error in the length cause a modification in this ratio, and then in the end-effector position. An error on the length of a link affect in a different way the end-effector position depending from the position of the link. For example an error on a link of the first loop (which is the loop between B_0 and B_1) entail a bigger error in the end-effector position than a error on a link in the last loop.

2.2.2 Geometrical model test

The verification of the accuracy of the geometrical model (called also Matlab® model) was performed using both measures on the real model and a Catia® model of the pantograph. The Catia® geometrical model was made in a previous study ([13]). The measures on the mock-up were considered only as purely indicative because they are effected by manufacturing and assembly errors, by elastic deformations due to the structure weight and by the errors of the measuring system. They are closed to the values obtained by the Matlab® model but they are affected by a not-negligible error. Therefore the measures on the mock-up were considered as coherent with the results of the geometrical model but they are not accurate enough for a validation.

Taking into account the previous observations, the Catia® model is the only precise tool for verifying the geometrical model.

2.2.2.1 Verification through the Catia® model

The comparison between Matlab® and Catia® geometrical models was performed through numerous configurations. For a simple dissertation only three configurations are compared. Table 2.1 and Figure 2.3 report the comparison with a focus on the end-effector positions. The results of the two models are exactly the same, therefore, taking into account the coherence of the measure on the mock-up, we can conclude that the Matlab® model is correct.

Table 2.1: Comparison between the Matlab® and Catia® geometrical models in three different configurations

Position	Matlab® model		Catia® model	
	$\vec{x}$ [mm]	$\vec{z}$ [mm]	$\vec{x}$ [mm]	$\vec{z}$ [mm]
1	-0.3750	-0.7875	-0.3750	-0.7875
2	-0.5000	-0.5250	-0.5000	-0.5250
3	-0.3750	-1.1375	-0.3750	-1.1375
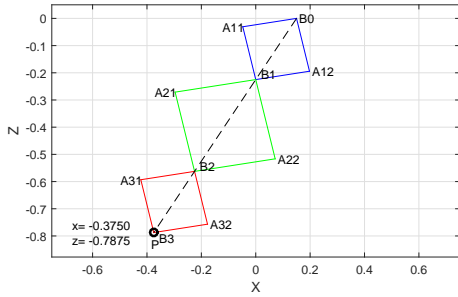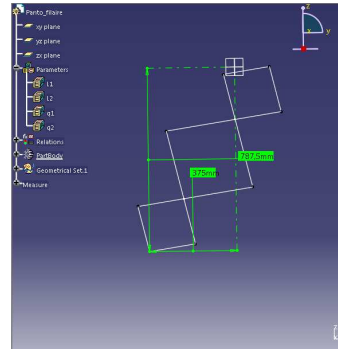
(a.1) Matlab® geometrical model   (a.2) Catia® geometrical model

(a) First comparison
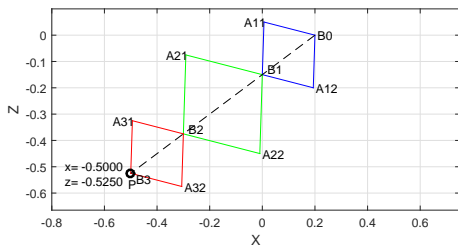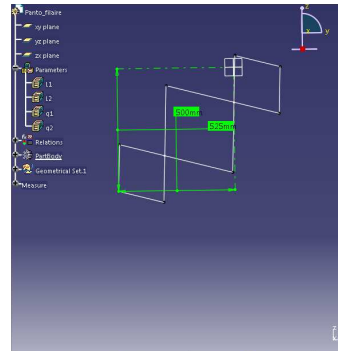
(b.1) Matlab® geometrical model   (b.2) Catia® geometrical model

(b) Second comparison
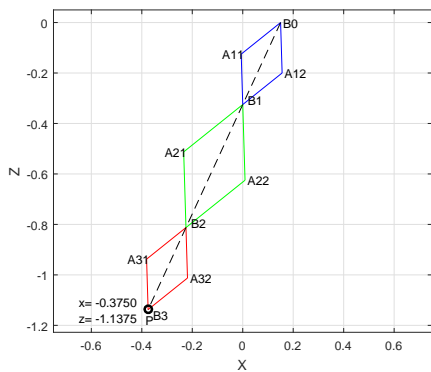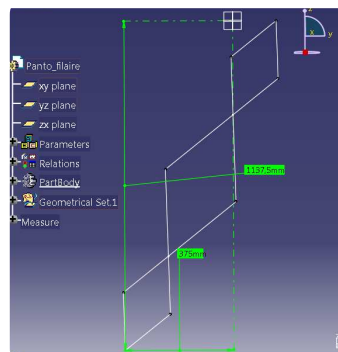
(c.1) Matlab® geometrical model   (c.2) Catia® geometrical model

(c) Third comparison

Figure 2.3: Comparison between the Matlab® and Catia® geometrical models in three different configurations

2.3   Error model

Manufacturing and assembling errors could entail a position of the pantograph which differs from the one obtained through the geometrical model. It is therefore necessary to take into account the effects of these errors.

2.3.1   Description of the method used

The geometrical errors are described by the vector

$$\boldsymbol{\delta K} = \begin{bmatrix} \boldsymbol{\delta q}^T \\ \boldsymbol{\delta L}^T \end{bmatrix} \tag{2.6}$$

where

$$\boldsymbol{\delta q} = [\ \delta q_1 \quad \delta q_2 \quad \delta q_3\ ]^T \tag{2.7}$$

$$\boldsymbol{\delta L} = [\ \boldsymbol{\delta L}_1^T \ \ldots \ \boldsymbol{\delta L}_n^T\ ]^T \tag{2.8}$$

$$\boldsymbol{\delta L}_i = [\ \delta L_{i,1}^u \quad \delta L_{i,2}^u \quad \delta L_{i,1}^l \quad \delta L_{i,2}^l\ ]^T \tag{2.9}$$

$\boldsymbol{\delta q}$ contains the errors on the driven coordinates and $\boldsymbol{\delta L}$ the errors on the length of the links.

To perform the calculation of the real end-effector position the Jacobian matrix $\boldsymbol{J}$, which links the geometrical errors to the end-effector position errors, is used, as shown in Equation (2.10).

$$\boldsymbol{\delta P} = \boldsymbol{J}\,\boldsymbol{\delta K} \tag{2.10}$$

where

$$\boldsymbol{\delta P} = [\delta x_P \quad \delta y_P \quad \delta z_P]^T \tag{2.11}$$

is the vector of the displacement of the end-effector position due to the geometrical errors. The calculation of the Jacobian matrix is made deriving the equations of the geometrical model, starting from the first loop, in order to provide a dependence of the end-effector position from each parameter of the pantograph.

First loop

The calculation of the Jacobian matrices is done deriving Equation (2.12) to obtain $\boldsymbol{J}_{B_0}$ and $\boldsymbol{J}_{B_1}$ and deriving Equation (2.1) to obtain $\boldsymbol{J}_{A_{1,1}}$, $\boldsymbol{J}_{A_{1,2}}$.

$$\begin{cases} x_{B_0} = q_1 \\ z_{B_0} = 0 \end{cases}$$
$$\begin{cases} x_{B_1} = 0 \\ z_{B_1} = q_2 \end{cases} \tag{2.12}$$

Therefore the gap between the position of the points $A_{1,j}$ and B_i calculated with and without the geometrical errors can be obtained as follow

$$
\begin{cases}
\delta \boldsymbol{A}_{1,j} = \boldsymbol{J}^i_{A_{1,j}} [\ \delta x_{B_0} \quad \delta z_{B_0} \quad \delta x_{B_1} \quad \delta z_{B_1} \quad \delta \boldsymbol{L}^T_{1,j} \ ]^T \\
\delta \boldsymbol{B}_i = \boldsymbol{J}_{B_i} [\ \delta q_1 \quad \delta q_2 \quad \delta \boldsymbol{L}^T_{1,j} \ ]^T
\end{cases}
\tag{2.13}
$$

For $\delta \boldsymbol{A}_{1,j}$ it is necessary to refer the Jacobian matrix to the parameters which describe the system instead of the coordinates of the point B_0 and B_1, therefore a permutation matrix $\boldsymbol{P}_{A_{i,j}}$ is used.

$$
\boldsymbol{P}_{A_{i,j}} = \begin{bmatrix} \boldsymbol{J}_{B_0} \\ \boldsymbol{J}_{B_1} \\ \boldsymbol{0}_{4,2} \quad \boldsymbol{I}_4 \end{bmatrix}
\tag{2.14}
$$

Hence one obtains

$$
\delta \boldsymbol{A}_{1,j} = \boldsymbol{J}_{A_{1,j}} [\ \delta q_1 \quad \delta q_2 \quad \delta \boldsymbol{L}^T_{1,j} \ ]^T
\tag{2.15}
$$

where

$$
\boldsymbol{J}_{A_{1,j}} = \boldsymbol{J}^i_{A_{1,j}} \boldsymbol{P}_{A_{i,j}}
\tag{2.16}
$$

Second and third loop

The calculation of the Jacobian matrices $\boldsymbol{J}_{A_{i,1}}$, $\boldsymbol{J}_{A_{i,2}}$ $\boldsymbol{J}_{B_i}$ is made considering the propagation of the errors from the first loop. With this scope the matrices $\boldsymbol{J}^i_{A_{i,1}}$, $\boldsymbol{J}^i_{A_{i,2}}$ $\boldsymbol{J}^i_{B_i}$ are defined as the Jacobian matrices which consider only the errors of the geometrical parameters involved in the second loop. They are calculated deriving Equation (2.2) and Equation (2.3), therefore we obtain

$$
\begin{cases}
\delta \boldsymbol{A}_{i,1} = \boldsymbol{J}^i_{A_{i,1}} [\ \delta \boldsymbol{A}_{i-1,2} \quad \delta \boldsymbol{B}_{i-1} \quad \delta \boldsymbol{L}^T_{i-1} \quad \delta \boldsymbol{L}^T_{i-1} \ ]^T \\
\delta \boldsymbol{A}_{i,2} = \boldsymbol{J}^i_{A_{i,2}} [\ \delta \boldsymbol{A}_{i-1,1} \quad \delta \boldsymbol{B}_{i-1} \quad \delta \boldsymbol{L}^T_{i-1} \quad \delta \boldsymbol{L}^T_{i-1} \ ]^T \\
\delta \boldsymbol{B}_i = \boldsymbol{J}^i_{B_i} [\ \delta \boldsymbol{A}_{i,1} \quad \delta \boldsymbol{A}_{i,2} \quad \delta \boldsymbol{L}^T_{i-1} \ ]^T
\end{cases}
\tag{2.17}
$$

The Jacobian matrices have to be referred to every geometrical parameters placed before the considered loop, therefore three permutation matrices are needed.
The variation of the position of the points $A_{i,j}$ and B_i with and without the errors is defined as below

$$
\begin{cases}
\delta \boldsymbol{A}_{i,j} = \boldsymbol{J}_{A_{i,j}} [\ \delta q_1 \quad \delta q_2 \quad \delta \boldsymbol{L}^T_1 \quad \dots \quad \delta \boldsymbol{L}^T_i \ ]^T \\
\delta \boldsymbol{B}_i = \boldsymbol{J}_{B_i} [\ \delta q_1 \quad \delta q_2 \quad \delta \boldsymbol{L}^T_1 \quad \dots \quad \delta \boldsymbol{L}^T_i \ ]^T
\end{cases}
\tag{2.18}
$$

where

$$
\begin{cases}
\boldsymbol{J}_{A,j} = \boldsymbol{J}^i_{A_{i,j}} \boldsymbol{P}_{A_{i,j}} \\
\boldsymbol{J}_{B_i} = \boldsymbol{J}^i_{B_i} \boldsymbol{P}_{B_i}
\end{cases}
\tag{2.19}
$$

Once $\boldsymbol{J}_{A_j}$ and $\boldsymbol{J}_{B_i}$ are known, it is possible to define the permutation matrices as[1]:

$$\boldsymbol{P}_{A_{i,1}} = \begin{bmatrix} \boldsymbol{J}_{A_{i-1,2}} & \boldsymbol{0}_{2,4} \\ \boldsymbol{J}_{B_{i-1}} & \boldsymbol{0}_{2,4} \\ \boldsymbol{0}_{8,a} & \boldsymbol{I}_8 \end{bmatrix}$$

$$\boldsymbol{P}_{A_{i,2}} = \begin{bmatrix} \boldsymbol{J}_{A_{i-1,1}} & \boldsymbol{0}_{2,4} \\ \boldsymbol{J}_{B_{i-1}} & \boldsymbol{0}_{2,4} \\ \boldsymbol{0}_{8,a} & \boldsymbol{I}_8 \end{bmatrix} \qquad (2.20)$$

$$\boldsymbol{P}_{B_i} = \begin{bmatrix} \boldsymbol{J}_{A_{i,1}} \\ \boldsymbol{J}_{A_{i,2}} \\ \boldsymbol{0}_{8,b} \quad \boldsymbol{I}_4 \end{bmatrix}$$

where

$$a = \begin{cases} 2 & \text{for the second loop} \\ 6 & \text{for the third loop} \end{cases}$$

$$b = \begin{cases} 6 & \text{for the second loop} \\ 10 & \text{for the third loop} \end{cases}$$

It is now possible to calculate the end-effector position error in the plane as:

$$\begin{bmatrix} \delta x_{B_3} & \delta z_{B_3} \end{bmatrix}^T = \boldsymbol{J}_{B_3} \begin{bmatrix} \delta q_1 & \delta q_2 & \boldsymbol{\delta L}_1^T & \boldsymbol{\delta L}_2^T & \boldsymbol{\delta L}_3^T \end{bmatrix}^T \qquad (2.21)$$

The calculation of the end-effector position error in the space needs the coordinate q_3 because it gives the rotation of the structure around the axis $\vec{z}$, see Figure 2.1. For this purpose we define:

$$\boldsymbol{\delta P} = \boldsymbol{J}_p \begin{bmatrix} \delta q_3 & \delta x_{B_3} & \delta z_{B_3} \end{bmatrix}^T \qquad (2.22)$$

The end-effector position is described by:

$$\boldsymbol{P} = \begin{bmatrix} x_p \\ y_p \\ x_p \end{bmatrix} = \begin{bmatrix} \cos(q_3) & -\sin(q_3) & 0 \\ \sin(q_3) & \cos(q_3) & 0 \\ 0 & 0 & 1 \end{bmatrix} \begin{bmatrix} x_{B_3} \\ 0 \\ z_{B_3} \end{bmatrix} \qquad (2.23)$$

The Jacobian matrix J_P is calculated deriving the Equation (2.23) by the vector $\begin{bmatrix} \delta q_3 & \delta x_{B_3} & \delta z_{B_3} \end{bmatrix}^T$. Therefore the Jacobian matrix is:

$$\boldsymbol{J}_p = \begin{bmatrix} -x_{B_3}\sin(q_3) & \cos(q_3) & 0 \\ x_{B_3}\cos(q_3) & \sin(q_3) & 0 \\ 0 & 0 & 1 \end{bmatrix} \qquad (2.24)$$

Known the Jacobian matrix of the end-effector in the space, we have to consider the errors given by the previous loops, therefore we introduce the permutation matrix:

$$\boldsymbol{P}_p = \begin{bmatrix} \boldsymbol{0}_{1,2} & 1 & \boldsymbol{0}_{1,12} \\ \boldsymbol{J}_{B_3}(1:2,1:2) & \boldsymbol{0}_{2,1} & \boldsymbol{J}_{B_3}(1:2,3:14) \end{bmatrix} \qquad (2.25)$$

---

[1]Despite from what is reported in [13] the permutation matrices are the ones reported in Equation (2.20)

The global Jacobian matrix becomes

$$\boldsymbol{J} = \boldsymbol{J}_p \, \boldsymbol{P}_p \qquad (2.26)$$

and the equation which describes the errors of the structure is

$$\begin{bmatrix} \delta x_p & \delta y_p & \delta z_p \end{bmatrix}^T = \boldsymbol{J} \begin{bmatrix} \delta q_1 & \delta q_2 & \delta q_3 & \boldsymbol{\delta L}_1^T & \boldsymbol{\delta L}_2^T & \boldsymbol{\delta L}_3^T \end{bmatrix}^T \qquad (2.27)$$

For the details of the calculation of the Jacobian matrices see Appendix A.

2.3.1.1 Jacobian test

The verification of the accuracy of the Jacobian matrix was performed analytically imposing an error on all the geometrical parameters and verifying the position displacement calculated in two different ways. The first displacement was obtained by Equation (2.27) while the second one was calculated as the difference between the geometrical model output with and without the imposed errors. In a first attempt, the influence of each parameter, considered individually, was tested to verify the accuracy of the Jacobian. For conciseness only a few results, in one of the configuration tested, are reported. In Figure 2.4 we can see a comparison between the displacement of the end-effector due to an error on the driven coordinates. We could note that the calculation of the displacement through the Jacobian matrix is very close to the displacement obtained through the geometrical model, which represents the real displacement. Furthermore Figure 2.4 shows how the position of the end-effector changes with an error in the driven coordinates. The coordinate q_1, as expected, influences only the horizontal position of the end-effector whereas q_2 influences only the vertical position.

Figure 2.5 is similar to the figure described above but it considers an error on the length of a link, firstly (Figure 2.5a) on a link of the first loop, then (Figure 2.5b) on a link of the third loop. We observe that the end-effector displacement is smaller for an error applied on a link of the third loop and the reason is explained in Section 2.2.1. In Figure 2.5b.2 we note that for values of the link error close to 1 mm the accuracy of the Jacobian matrix decreases because of the linear approximation of the Jacobian. The difference between the values obtained through the geometrical model and the ones obtained with the Jacobian is less then 10% therefore it is considered acceptable for a linear approximation.

(a.1) δx_p (a.2) δz_p
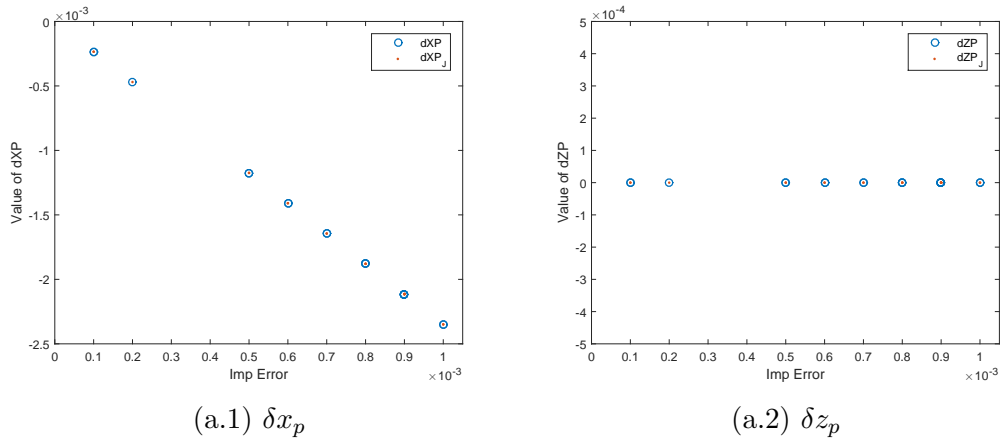
(a) Error applied on q_1

(b.1) δx_p (b.2) δz_p
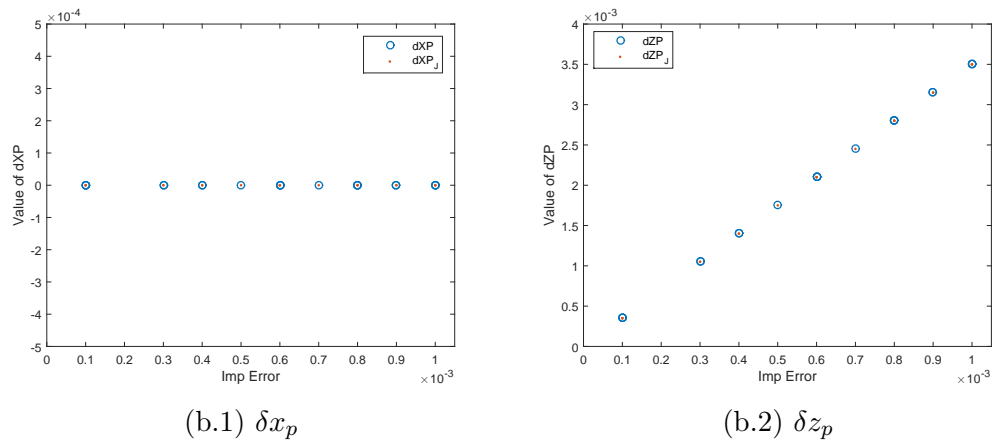
(b) Error applied on q_2

Figure 2.4: Comparison between the end-effector displacement, due to an error on a driven coordinate, calculated with the Jacobian matrix and through the geometrical model

(a.1) δx_p

(a.2) δz_p

(a) Error applied on $L_{1,2}^u$

(b.1) δx_p

(b.2) δz_p

(b) Error applied on $L_{3,2}^u$
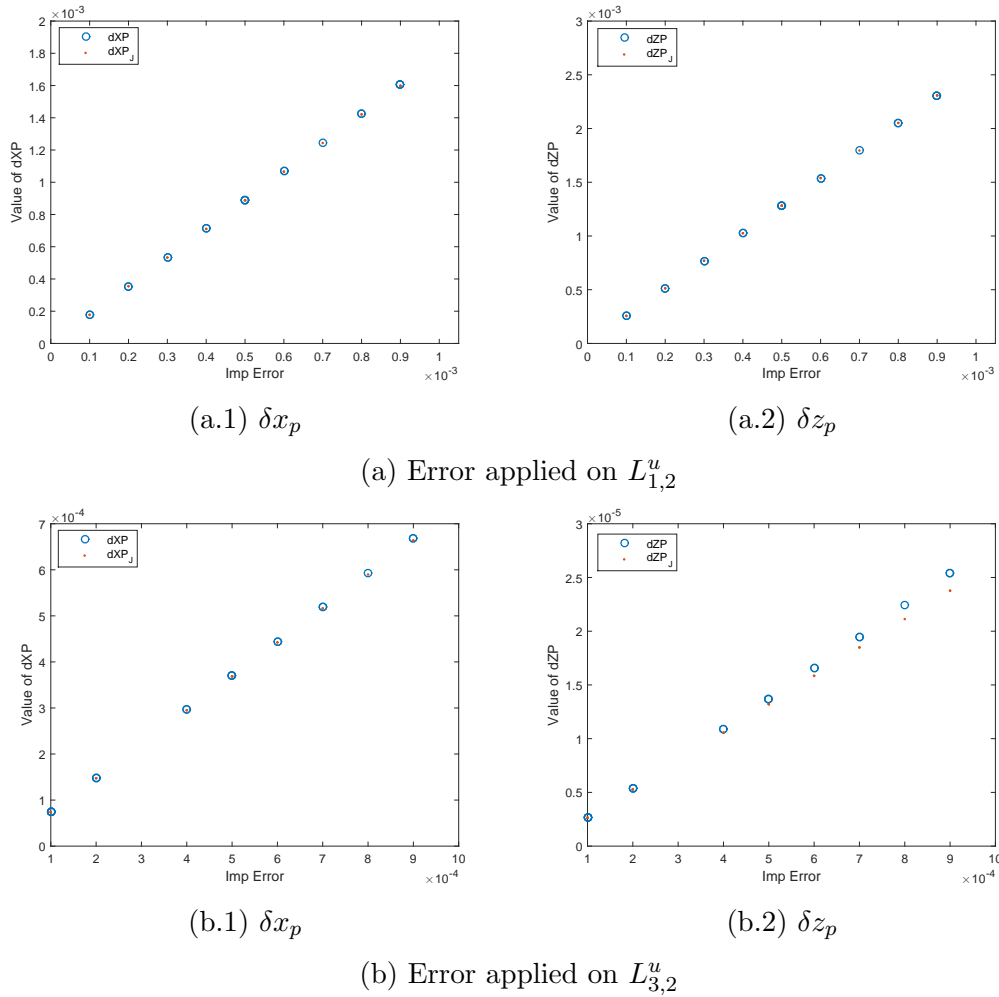
Figure 2.5: Comparison between the end-effector displacement, due to an error in length of a link, calculated with the Jacobian matrix and with the geometrical model

The displacements obtained through the geometrical model and with the Jacobian
are very similar, therefore one can consider the method accurate. To verify in a
more precise way the accuracy of the Jacobian, some tests were performed. We
observed that using the same error for each geometrical parameter entails more
understandable results, therefore we chose to consider different errors (but equal
for all the parameters) in different configurations of the pantograph to evaluate
the accuracy of the model. In Table 2.2 and Figure 2.6 one can find the tested
configuration where the values of the errors applied go from $0.1\,\mathrm{mm}$ to $2\,\mathrm{mm}$.

Table 2.2: Pantograph configurations tested

	$q_1\ [m]$	$q_2\ [m]$	$q_3\ [m]$
1	0.15	-0.075	pi/6
2	0.1	-0.125	pi/9
3	-0.05	-0.175	pi/18
4	0.01	-0.225	0
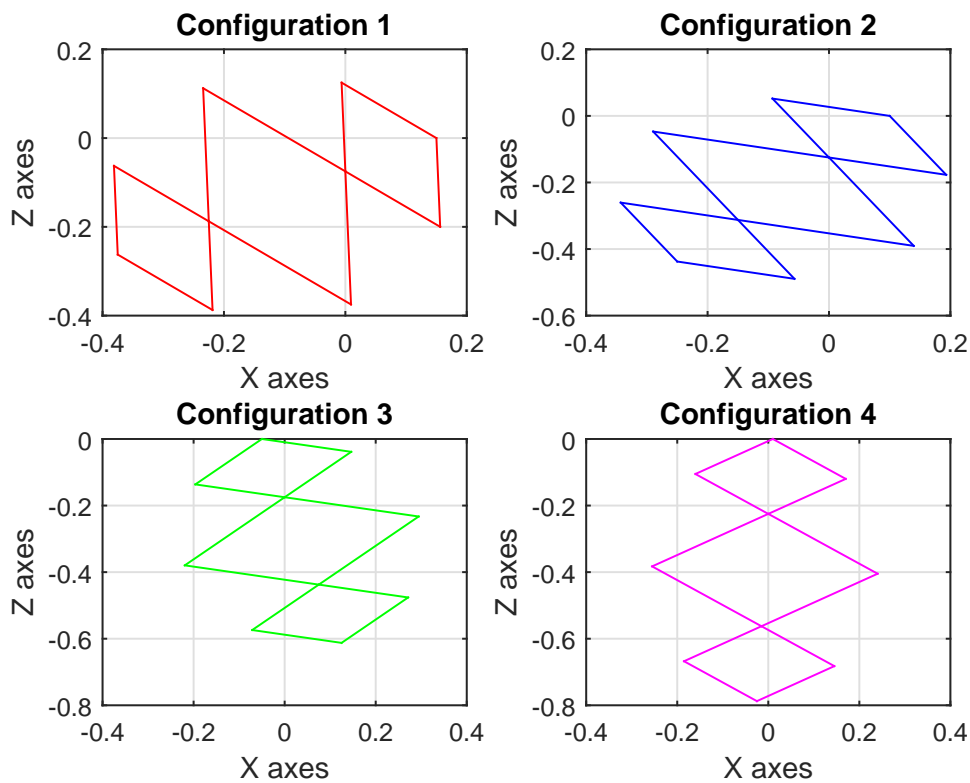
Figure 2.6: Pantograph configurations tested

In Figure 2.7 one sees that for different configurations the exact value, calculated
through the geometrical model, and the approximated value, calculated with the

Jacobian matrix, are very similar for both the $\vec{x}$ and $\vec{z}$ axis. Figure 2.8 shows the mean values of the error between δP and δP_J for the different configurations tested. The difference between the two end-effector displacement has an increasing trend, with a parabolic law. Despite from that, the maximum error is around 10^{-5} m for the $\vec{x}$ direction and 2×10^{-5} m for the $\vec{z}$. The maximum difference between the two displacements is calculated with an error, applied to all the elements, equal to 2 mm, which represents the worst case possible, therefore the Jacobian matrix has a good accuracy.
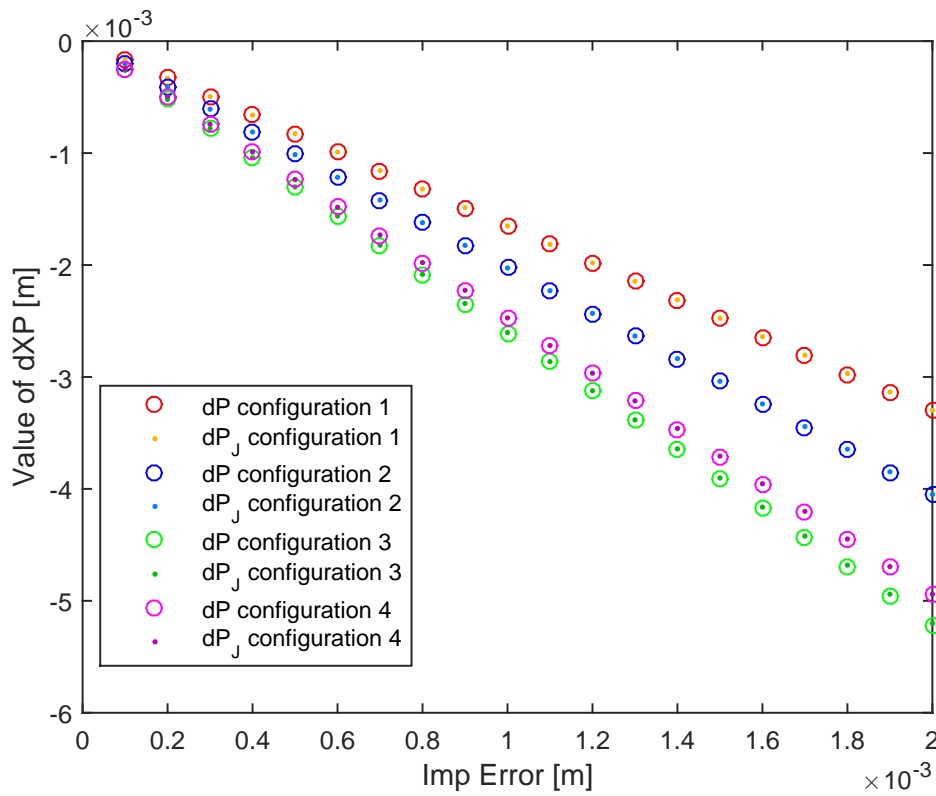
(a) X direction
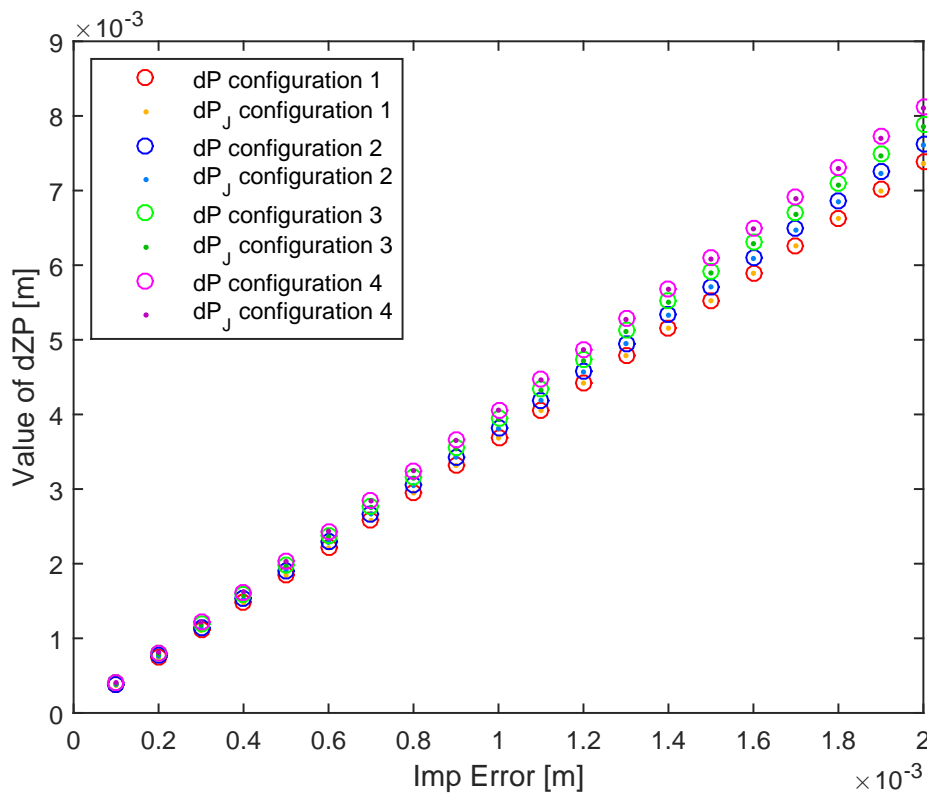
(b) Z direction

Figure 2.7: Comparison between the displacement of the end-effector position calculated from the geometrical model and obtained from the Jacobian
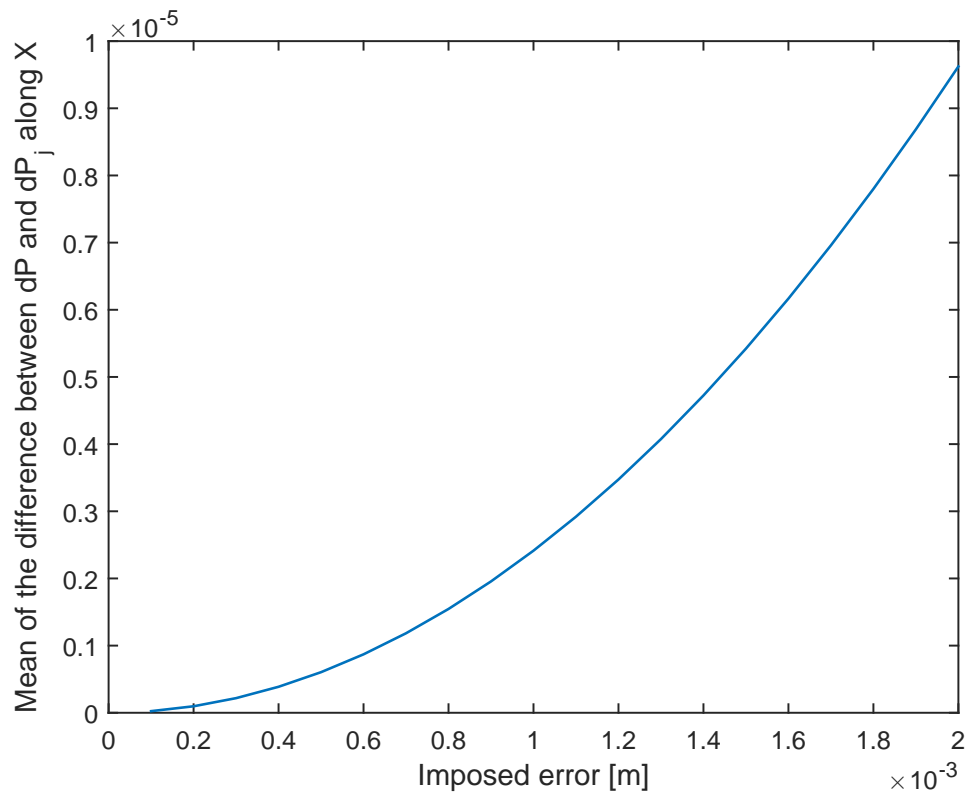
(a) X direction
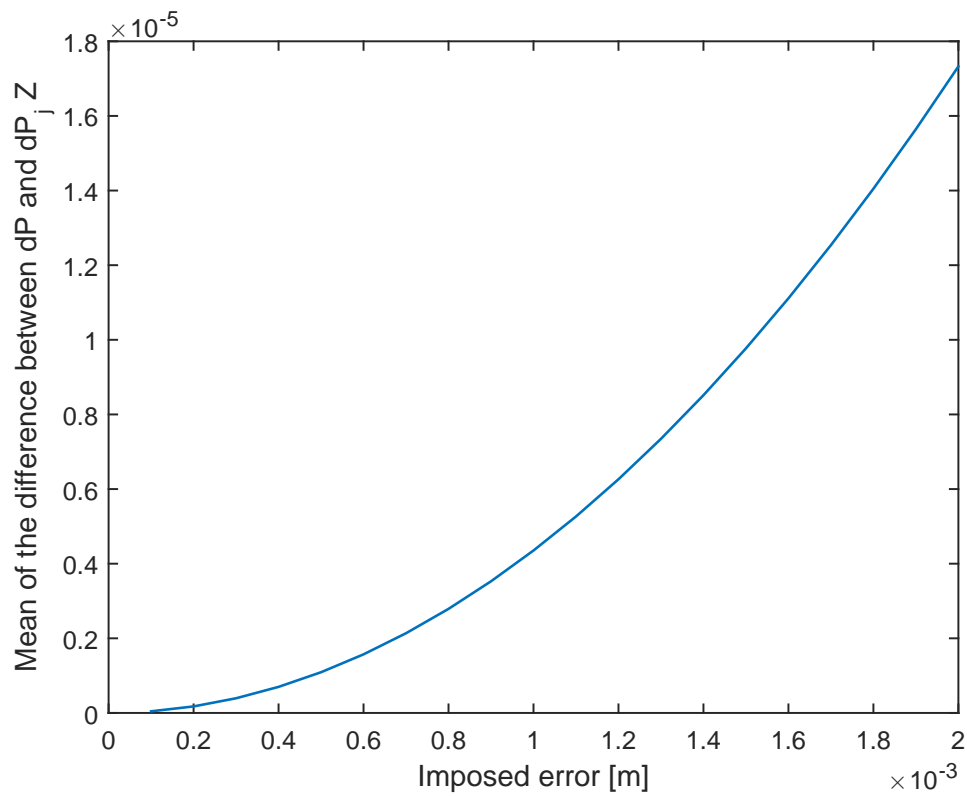
(b) Z direction

Figure 2.8: Mean value of the difference between the calculation of δP obtained through the geometrical model and through the Jacobian matrix for the configurations tested

CHAPTER 3

Elastic model

The main purpose of the elastic model is to calculate the deformations of the pantograph under a load. This means consider the external wrenches plus the weight of the structure. The elastic model is developed using the finite element method following the guidelines reported in [13].

3.1 Hypotheses

The pantograph was analysed considering a quasistatic condition (the velocity is under $1\,\mathrm{m\,s^{-1}}$) therefore the inertial forces of the structure were not taken into account and only the kinetostatic behaviour was considered.

Moreover the following hypotheses were chosen in order to simplify the elastic problem:

- Beam geometry: one dimension is bigger than the others.

- Euler-Bernoulli beam theory: the section, during the deformation, remains perpendicular to the neutral line.

- The material was considered as homogeneous, isotropic and with a linear behaviour.

- The axial, torsional and bending movement were considered as decoupled.

With these hypotheses we considered all the elements of the pantograph as beam elements and nodes.

3.2 System description

The nodes of the beam elements correspond to discontinuities in the structure, such as joints or points in which a force is applied. Therefore the finite elements are placed as in Figure 3.1. This set-up was chosen in order to insert in the model the rotation joints.
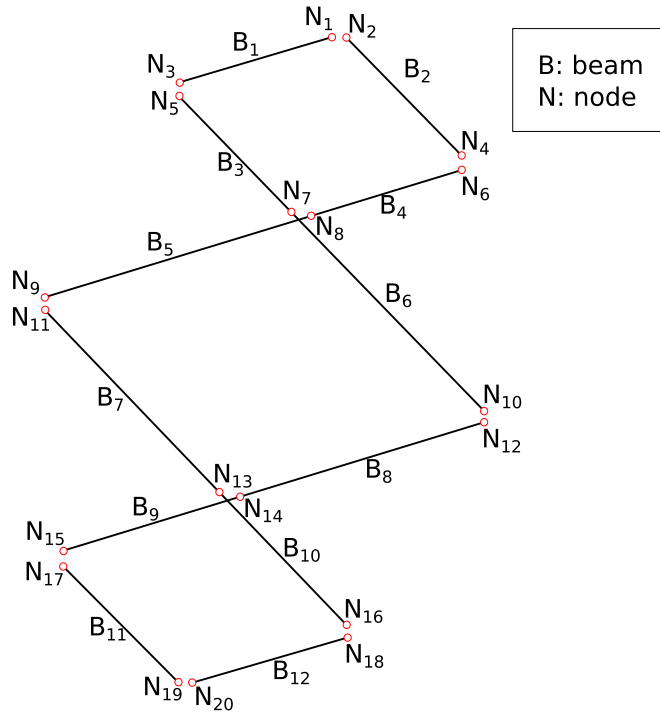
Figure 3.1: Beams and nodes notation

3.3   Displacements and wrenches

The force acting on a node, according to the *Finite Element Method*, is described by a vector containing six elements (Equation (3.1)), which corresponds to the six degrees of freedom (DoF).

$$\boldsymbol{F}_i = \begin{bmatrix} F_{x_i} \ F_{y_i} \ F_{z_i} \ M_{x_i} \ M_{y_i} \ M_{z_i} \end{bmatrix}^T \tag{3.1}$$

A force applied on a node generates a deformation in the structure that entails a displacement on the considered node and also on the other nodes of the structure, as shown in Figure 3.2. The displacement can be a translation or a rotation, therefore, to describe the effects of the applied load, the vector $\boldsymbol{\Delta X}$ is used. It is expressed in the following way:

$$\boldsymbol{\Delta X} = \begin{bmatrix} \delta \boldsymbol{P}^T \ \delta \boldsymbol{\theta}_p^T \end{bmatrix}^T \tag{3.2}$$

where

$$\delta \boldsymbol{P} = \begin{bmatrix} u_i \ v_i \ w_i \end{bmatrix}^T$$
$$\delta \boldsymbol{\theta}_p = \begin{bmatrix} \theta_{x_i} \ \theta_{y_i} \ \theta_{z_i} \end{bmatrix}^T$$
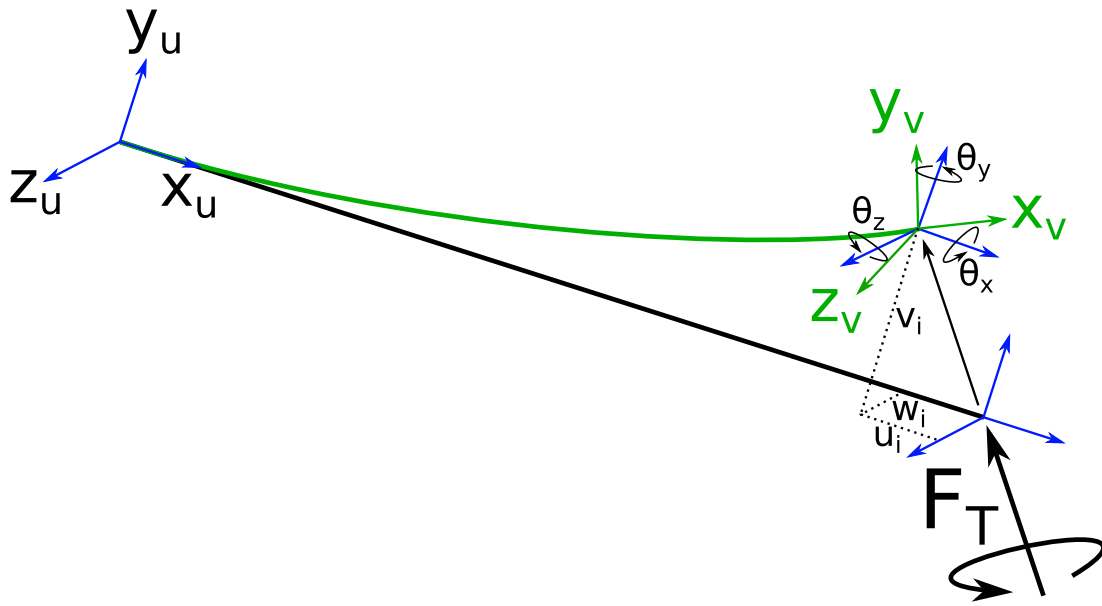
Figure 3.2: Beam element

3.3.1   Weight of the structure

The weight of the structure is considered as a distributed load applied on each beam of the structure. The theory of the beam element asserts that it is equivalent to a couple of forces and momentum applied on the edges of the beam element, as shown in Figure 3.3.

Figure 3.3: Beam element with forces and momentum instead of a distributed load

The weight of the structure is added to the vector containing the external forces and momentum.

3.4   Stiffness matrix

The stiffness matrix, according to [4, 5], is defined through the potential energy. It is referred to the local reference system $\boldsymbol{R_i}$ of the beam. The beam element starts with the node u and ends with the node v, each node has six degrees of freedom therefore the beam element in the space has twelve degrees of freedom. Hence the stiffness matrix of one beam is a 12 square matrix. The parameters to consider for writing the stiffness matrix are:

- The geometrical properties (length and cross sectional area).

- The Young's modulus.

- The Coulomb's modulus.

- Poisson coefficient.

- The quadratic and polar moments of area.

The stiffness matrix in the beam reference system $\boldsymbol{R_i}$ is expressed by four sub-matrices as reported in Equation (3.3).

$$
{}^{R_i}\mathbf{K}^i = \left[\begin{array}{cc} {}^{R_i}\boldsymbol{K}^i_{u,u} & {}^{R_i}\boldsymbol{K}^i_{u,v} \\ {}^{R_i}\boldsymbol{K}^i_{v,u} & {}^{R_i}\boldsymbol{K}^i_{v,v} \end{array} \right] \tag{3.3}
$$

The four sub-matrices are the nodal stiffness matrices, defined as follow:

$$
{}^{R_i}\boldsymbol{K}^i_{uu} = \left[\begin{array}{cccccc} \frac{E_{u,v}\,S_{u,v}}{L_{u,v}} & 0 & 0 & 0 & 0 & 0 \\ 0 & \frac{12\,E_{u,v}\,Iz_{u,v}}{L_{u,v}^3} & 0 & 0 & 0 & \frac{6\,E_{u,v}\,Iz_{u,v}}{L_{u,v}^2} \\ 0 & 0 & \frac{12\,E_{u,v}\,Iy_{u,v}}{L_{u,v}^3} & 0 & -\frac{6\,E_{u,v}\,Iy_{u,v}}{L_{u,v}^2} & 0 \\ 0 & 0 & 0 & \frac{G_{u,v}\,Jy_{u,v}}{L_{u,v}} & 0 & 0 \\ 0 & 0 & -\frac{6\,E_{u,v}\,Iy_{u,v}}{L_{u,v}^2} & 0 & \frac{4\,E_{u,v}\,Iy_{u,v}}{L_{u,v}} & 0 \\ 0 & \frac{6\,E_{u,v}\,Iz_{u,v}}{L_{u,v}^2} & 0 & 0 & 0 & \frac{4\,E_{u,v}\,Iz_{u,v}}{L_{u,v}} \end{array} \right] \tag{3.4}
$$

$$
{}^{R_i}\boldsymbol{K}^i_{uv} = \left[\begin{array}{cccccc} -\frac{E_{u,v}\,S_{u,v}}{L_{u,v}} & 0 & 0 & 0 & 0 & 0 \\ 0 & -\frac{12\,E_{u,v}\,Iz_{u,v}}{L_{u,v}^3} & 0 & 0 & 0 & \frac{6\,E_{u,v}\,Iz_{u,v}}{L_{u,v}^2} \\ 0 & 0 & -\frac{12\,E_{u,v}\,Iy_{u,v}}{L_{u,v}^3} & 0 & -\frac{6\,E_{u,v}\,Iy_{u,v}}{L_{u,v}^2} & 0 \\ 0 & 0 & 0 & -\frac{G_{u,v}\,Jy_{u,v}}{L_{u,v}} & 0 & 0 \\ 0 & 0 & \frac{6\,E_{u,v}\,Iy_{u,v}}{L_{u,v}^2} & 0 & \frac{2\,E_{u,v}\,Iy_{u,v}}{L_{u,v}} & 0 \\ 0 & -\frac{6\,E_{u,v}\,Iz_{u,v}}{L_{u,v}^2} & 0 & 0 & 0 & \frac{2\,E_{u,v}\,Iz_{u,v}}{L_{u,v}} \end{array} \right] \tag{3.5}
$$

$$
{}^{R_i}\boldsymbol{K}^i_{vu} = \left[\begin{array}{cccccc} -\frac{E_{u,v}\,S_{u,v}}{L_{u,v}} & 0 & 0 & 0 & 0 & 0 \\ 0 & -\frac{12\,E_{u,v}\,Iz_{u,v}}{L_{u,v}^3} & 0 & 0 & 0 & -\frac{6\,E_{u,v}\,Iz_{u,v}}{L_{u,v}^2} \\ 0 & 0 & -\frac{12\,E_{u,v}\,Iy_{u,v}}{L_{u,v}^3} & 0 & \frac{6\,E_{u,v}\,Iy_{u,v}}{L_{u,v}^2} & 0 \\ 0 & 0 & 0 & -\frac{G_{u,v}\,Jy_{u,v}}{L_{u,v}} & 0 & 0 \\ 0 & 0 & -\frac{6\,E_{u,v}\,Iy_{u,v}}{L_{u,v}^2} & 0 & \frac{2\,E_{u,v}\,Iy_{u,v}}{L_{u,v}} & 0 \\ 0 & \frac{6\,E_{u,v}\,Iz_{u,v}}{L_{u,v}^2} & 0 & 0 & 0 & \frac{2\,E_{u,v}\,Iz_{u,v}}{L_{u,v}} \end{array} \right] \tag{3.6}
$$

$$
{}^{R_i}\boldsymbol{K}^i_{vv} = \left[\begin{array}{cccccc} \frac{E_{u,v}\,S_{u,v}}{L_{u,v}} & 0 & 0 & 0 & 0 & 0 \\ 0 & \frac{12\,E_{u,v}\,Iz_{u,v}}{L_{u,v}^3} & 0 & 0 & 0 & -\frac{6\,E_{u,v}\,Iz_{u,v}}{L_{u,v}^2} \\ 0 & 0 & \frac{12\,E_{u,v}\,Iy_{u,v}}{L_{u,v}^3} & 0 & \frac{6\,E_{u,v}\,Iy_{u,v}}{L_{u,v}^2} & 0 \\ 0 & 0 & 0 & \frac{G_{u,v}\,Jy_{u,v}}{L_{u,v}} & 0 & 0 \\ 0 & 0 & \frac{6\,E_{u,v}\,Iy_{u,v}}{L_{u,v}^2} & 0 & \frac{4\,E_{u,v}\,Iy_{u,v}}{L_{u,v}} & 0 \\ 0 & -\frac{6\,E_{u,v}\,Iz_{u,v}}{L_{u,v}^2} & 0 & 0 & 0 & \frac{4\,E_{u,v}\,Iz_{u,v}}{L_{u,v}} \end{array} \right] \tag{3.7}
$$

The stiffness matrix in the global reference system is obtained by multiplying the stiffness matrix in the local reference system (see Figure 3.4) for a permutation matrix (reported in Equation (3.8)).

$$\mathbf{P}_i = \begin{bmatrix} \mathbf{R}_i & \mathbf{0}_3 & \mathbf{0}_3 & \mathbf{0}_3 \\ \mathbf{0}_3 & \mathbf{R}_i & \mathbf{0}_3 & \mathbf{0}_3 \\ \mathbf{0}_3 & \mathbf{0}_3 & \mathbf{R}_i & \mathbf{0}_3 \\ \mathbf{0}_3 & \mathbf{0}_3 & \mathbf{0}_3 & \mathbf{R}_i \end{bmatrix} \tag{3.8}$$

The matrices $\boldsymbol{R}_i$ inside the stiffness permutation matrix $\boldsymbol{P}_i$ are the rotation matrices reported in Equation (3.9).
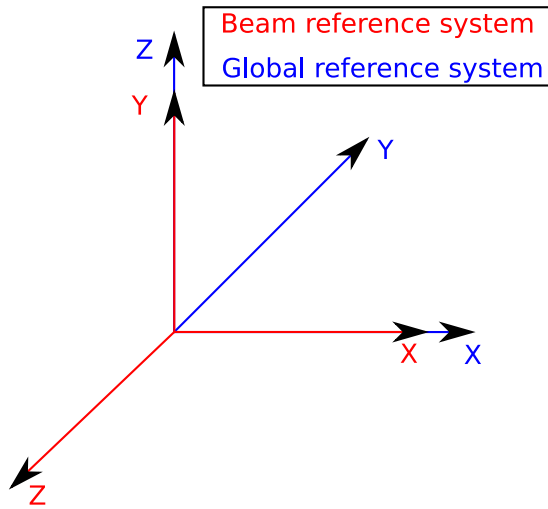
Figure 3.4: Beam and global reference systems

$$\mathbf{R}_i = \begin{bmatrix} \cos(\alpha) & -\sin(\alpha) & 0 \\ 0 & 0 & -1 \\ \sin(\alpha) & \cos(\alpha) & 0 \end{bmatrix} \tag{3.9}$$

The reference system transformation of the stiffness matrix is made through the relation:

$$^{R_g}\mathbf{K} = \mathbf{P}_i^{-1} \, {}^{R_i}\mathbf{K}^i \, \mathbf{P}_i \tag{3.10}$$

where $\mathbf{R}_i$ and $\mathbf{R}_g$ represent the beam reference system and the global reference system. After all these passages the stiffness matrix of the beam i, in the global coordinate system, can be expressed as:

$$^{R_g}\mathbf{K}^i = \begin{bmatrix} {}^{R_g}\mathbf{K}^i_{u,u} & {}^{R_g}\mathbf{K}^i_{u,v} \\ {}^{R_g}\mathbf{K}^i_{v,u} & {}^{R_g}\mathbf{K}^i_{v,v} \end{bmatrix} \tag{3.11}$$

3.4.1 Stiffness matrix assembly

Once the stiffness matrix of each beam element is expressed in the global reference system it is possible to assembly the overall stiffness matrix of the structure. The

assembly process needs an incidence matrix, this matrix contains in the first row the first node of the beam and in the second row the second node. The incidence matrix for the considered structure is :

$$\mathbf{Inc} = \begin{bmatrix} 1 & 2 & 5 & 6 & 8 & 7 & 11 & 12 & 14 & 13 & 17 & 18 \\ 3 & 4 & 7 & 8 & 9 & 10 & 13 & 14 & 15 & 16 & 19 & 20 \end{bmatrix} \tag{3.12}$$

The index ^{R_g} is suppressed in the following passages in order to simply the notation.

The assembly process of the stiffness matrix needs the knowledge of the DoF of each node in order to insert the single elements of the beam stiffness matrix in the right position of the overall stiffness matrix. The DoF, reported in Equation (3.13), are calculated from the incidence matrix and from the knowledge of the DoF of each node.

$$\mathrm{Beams}_{DoF} = \begin{bmatrix} 1 & 2 & 3 & 4 & 5 & 6 & 13 & 14 & 15 & 16 & 17 & 18 \\ 7 & 8 & 9 & 10 & 11 & 12 & 19 & 20 & 21 & 22 & 23 & 24 \\ 25 & 26 & 27 & 28 & 29 & 30 & 37 & 38 & 39 & 40 & 41 & 42 \\ 31 & 32 & 33 & 34 & 35 & 36 & 43 & 44 & 45 & 46 & 47 & 48 \\ 43 & 44 & 45 & 46 & 47 & 48 & 49 & 50 & 51 & 52 & 53 & 54 \\ 37 & 38 & 39 & 40 & 41 & 42 & 55 & 56 & 57 & 58 & 59 & 60 \\ 61 & 62 & 63 & 64 & 65 & 66 & 73 & 74 & 75 & 76 & 77 & 78 \\ 67 & 68 & 69 & 70 & 71 & 72 & 79 & 80 & 81 & 82 & 83 & 84 \\ 79 & 80 & 81 & 82 & 83 & 84 & 85 & 86 & 87 & 88 & 89 & 90 \\ 73 & 74 & 75 & 76 & 77 & 78 & 91 & 92 & 93 & 94 & 95 & 96 \\ 97 & 98 & 99 & 100 & 101 & 102 & 109 & 110 & 111 & 112 & 113 & 114 \\ 103 & 104 & 105 & 106 & 107 & 108 & 115 & 116 & 117 & 118 & 119 & 120 \end{bmatrix} \tag{3.13}$$

In Equation (3.13) the rows represent the beam elements (twelve) while the columns represent the degrees of freedom of the beams (twelve). The first six elements of the rows are the DoF of the first nodes of the beams, the other six elements are the DoF of the second ones. The overall stiffness matrix assembled results to be

$$^{R_g}K_T = \begin{bmatrix} K_{1,1} & 0 & K_{1,3} & 0 & 0 & 0 & 0 & 0 & 0 & 0 & 0 & 0 & 0 & 0 & 0 & 0 & 0 & 0 & 0 & 0 \\ 0 & K_{2,2} & 0 & K_{2,4} & 0 & 0 & 0 & 0 & 0 & 0 & 0 & 0 & 0 & 0 & 0 & 0 & 0 & 0 & 0 & 0 \\ K_{3,1} & 0 & K_{3,3} & 0 & 0 & 0 & 0 & 0 & 0 & 0 & 0 & 0 & 0 & 0 & 0 & 0 & 0 & 0 & 0 & 0 \\ 0 & K_{4,2} & 0 & K_{4,4} & 0 & 0 & 0 & 0 & 0 & 0 & 0 & 0 & 0 & 0 & 0 & 0 & 0 & 0 & 0 & 0 \\ 0 & 0 & 0 & 0 & K_{5,5} & 0 & K_{5,7} & 0 & 0 & 0 & 0 & 0 & 0 & 0 & 0 & 0 & 0 & 0 & 0 & 0 \\ 0 & 0 & 0 & 0 & 0 & K_{6,6} & 0 & K_{6,8} & 0 & 0 & 0 & 0 & 0 & 0 & 0 & 0 & 0 & 0 & 0 & 0 \\ 0 & 0 & 0 & 0 & K_{7,5} & 0 & 2\,K_{7,7} & 0 & 0 & K_{7,10} & 0 & 0 & 0 & 0 & 0 & 0 & 0 & 0 & 0 & 0 \\ 0 & 0 & 0 & 0 & 0 & K_{8,6} & 0 & 2\,K_{8,8} & K_{8,9} & 0 & 0 & 0 & 0 & 0 & 0 & 0 & 0 & 0 & 0 & 0 \\ 0 & 0 & 0 & 0 & 0 & 0 & 0 & K_{9,8} & K_{9,9} & 0 & 0 & 0 & 0 & 0 & 0 & 0 & 0 & 0 & 0 & 0 \\ 0 & 0 & 0 & 0 & 0 & 0 & K_{10,7} & 0 & 0 & K_{10,10} & 0 & 0 & 0 & 0 & 0 & 0 & 0 & 0 & 0 & 0 \\ 0 & 0 & 0 & 0 & 0 & 0 & 0 & 0 & 0 & 0 & K_{11,11} & 0 & K_{11,13} & 0 & 0 & 0 & 0 & 0 & 0 & 0 \\ 0 & 0 & 0 & 0 & 0 & 0 & 0 & 0 & 0 & 0 & 0 & K_{12,12} & 0 & K_{12,14} & 0 & 0 & 0 & 0 & 0 & 0 \\ 0 & 0 & 0 & 0 & 0 & 0 & 0 & 0 & 0 & 0 & K_{13,11} & 0 & 2\,K_{13,13} & 0 & 0 & K_{13,16} & 0 & 0 & 0 & 0 \\ 0 & 0 & 0 & 0 & 0 & 0 & 0 & 0 & 0 & 0 & 0 & K_{14,12} & 0 & 2\,K_{14,14} & K_{14,15} & 0 & 0 & 0 & 0 & 0 \\ 0 & 0 & 0 & 0 & 0 & 0 & 0 & 0 & 0 & 0 & 0 & 0 & 0 & K_{15,14} & K_{15,15} & 0 & 0 & 0 & 0 & 0 \\ 0 & 0 & 0 & 0 & 0 & 0 & 0 & 0 & 0 & 0 & 0 & 0 & K_{16,13} & 0 & 0 & K_{16,16} & 0 & 0 & 0 & 0 \\ 0 & 0 & 0 & 0 & 0 & 0 & 0 & 0 & 0 & 0 & 0 & 0 & 0 & 0 & 0 & 0 & K_{17,17} & 0 & K_{17,19} & 0 \\ 0 & 0 & 0 & 0 & 0 & 0 & 0 & 0 & 0 & 0 & 0 & 0 & 0 & 0 & 0 & 0 & 0 & K_{18,18} & 0 & K_{18,20} \\ 0 & 0 & 0 & 0 & 0 & 0 & 0 & 0 & 0 & 0 & 0 & 0 & 0 & 0 & 0 & 0 & K_{19,17} & 0 & K_{19,19} & 0 \\ 0 & 0 & 0 & 0 & 0 & 0 & 0 & 0 & 0 & 0 & 0 & 0 & 0 & 0 & 0 & 0 & 0 & K_{20,18} & 0 & K_{20,20} \end{bmatrix} \tag{3.14}$$

The assembly process, used for the stiffness matrix, was performed also for the force and displacement vectors shown below:

$$\mathbf{F}_T = \begin{bmatrix} \mathbf{F}_1^T & \mathbf{F}_2^T & \dots & \mathbf{F}_{19}^T & \mathbf{F}_{20}^T \end{bmatrix}^T \tag{3.15}$$

$$\mathbf{\Delta X}_T = \begin{bmatrix} \mathbf{\Delta X}_1^T & \mathbf{\Delta X}_2^T & \dots & \mathbf{\Delta X}_{19}^T & \mathbf{\Delta X}_{20}^T \end{bmatrix}^T \tag{3.16}$$

3.5 Revolute joints

The joints of the structure are considered with two different nodes for each joint because it is necessary to allow the rotation around the axis $\vec{y}$. Without considering a relation between the nodes which compose a joint, the stiffness matrix results to be defined null. There are two different ways in which the joints can be modellized. The first one considers the kinematic relations that govern the joints, whereas the second one the joints with their own stiffness. The second method is closer to the real problem but the stiffness of the joints need to be identified.

3.5.1 Kinematic relation between the nodal displacements

The kinematic relations are the bonds between the rotations and translations of the two nodes that make a joint. They are imposed considering equal the translation along the axis x, y, z and the rotation around the axis x and z of the two nodes which compose a joint. The rotation around the axis y is allowed because is the rotation that lets the structure to move. The following equations express the kinematics relations for a joint:

$$\begin{cases} u_1 - u_2 = 0 \\ v_1 - v_2 = 0 \\ w_1 - w_2 = 0 \\ \theta_{x_1} - \theta_{x_2} = 0 \\ \theta_{z_1} - \theta_{z_2} = 0 \end{cases} \tag{3.17}$$

Writing Equation (3.17) in matrix form we obtain:

$$\begin{bmatrix} \boldsymbol{A}_{u,v} & -\boldsymbol{A}_{u,v} \end{bmatrix} \begin{bmatrix} \boldsymbol{P}_u \\ \boldsymbol{\delta}_u \\ \boldsymbol{P}_v \\ \boldsymbol{\delta}_v \end{bmatrix} = \begin{bmatrix} \boldsymbol{0}_{3,1} \\ \boldsymbol{0}_{2,1} \end{bmatrix} \tag{3.18}$$

Where

$$\boldsymbol{A}_{u,v} = \begin{bmatrix} 1 & 0 & 0 & 0 & 0 & 0 \\ 0 & 1 & 0 & 0 & 0 & 0 \\ 0 & 0 & 1 & 0 & 0 & 0 \\ 0 & 0 & 0 & 1 & 0 & 0 \\ 0 & 0 & 0 & 0 & 0 & 1 \end{bmatrix} \tag{3.19}$$

$$\boldsymbol{P} = \begin{bmatrix} u \\ v \\ w \end{bmatrix} \tag{3.20}$$

$$\boldsymbol{\delta} = \begin{bmatrix} \theta_x \\ \theta_y \\ \theta_z \end{bmatrix} \tag{3.21}$$

Since the pantograph is made by ten revolute joints, a 50×120 matrix is created for gathering all the kinematics relations of the nodes. For the assembly of the

overall kinematic relations a matrix containing the nodes couples, which compose a joint, is needed:

$$\boldsymbol{Lj} = \begin{bmatrix} 1 & 3 & 4 & 7 & 9 & 10 & 13 & 15 & 16 & 19 \\ 2 & 5 & 6 & 8 & 11 & 12 & 14 & 17 & 18 & 20 \end{bmatrix} \tag{3.22}$$

The assembled matrix results to be:

$$\boldsymbol{A}_T = \begin{bmatrix} \boldsymbol{A}_{lp_1} & \boldsymbol{0}_{20,36} & \boldsymbol{0}_{20,36} \\ \boldsymbol{0}_{15,48} & \boldsymbol{A}_{lp_2} & \boldsymbol{0}_{15,36} \\ \boldsymbol{0}_{15,48} & \boldsymbol{0}_{15,36} & \boldsymbol{A}_{lp_3} \end{bmatrix} \tag{3.23}$$

Where

$$\boldsymbol{A}_{lp_1} = \begin{bmatrix} \boldsymbol{A}_{1,2} & -\boldsymbol{A}_{1,2} & \boldsymbol{0}_{5,6} & \boldsymbol{0}_{5,6} & \boldsymbol{0}_{5,6} & \boldsymbol{0}_{5,6} & \boldsymbol{0}_{5,6} & \boldsymbol{0}_{5,6} \\ \boldsymbol{0}_{5,6} & \boldsymbol{0}_{5,6} & \boldsymbol{A}_{3,5} & \boldsymbol{0}_{5,6} & -\boldsymbol{A}_{3,5} & \boldsymbol{0}_{5,6} & \boldsymbol{0}_{5,6} & \boldsymbol{0}_{5,6} \\ \boldsymbol{0}_{5,6} & \boldsymbol{0}_{5,6} & \boldsymbol{0}_{5,6} & \boldsymbol{A}_{4,6} & \boldsymbol{0}_{5,6} & -\boldsymbol{A}_{4,6} & \boldsymbol{0}_{5,6} & \boldsymbol{0}_{5,6} \\ \boldsymbol{0}_{5,6} & \boldsymbol{0}_{5,6} & \boldsymbol{0}_{5,6} & \boldsymbol{0}_{5,6} & \boldsymbol{0}_{5,6} & \boldsymbol{0}_{5,6} & \boldsymbol{A}_{7,8} & -\boldsymbol{A}_{7,8} \end{bmatrix}$$

$$\boldsymbol{A}_{lp_2} = \begin{bmatrix} \boldsymbol{A}_{9,11} & \boldsymbol{0}_{5,6} & -\boldsymbol{A}_{9,11} & \boldsymbol{0}_{5,6} & \boldsymbol{0}_{5,6} & \boldsymbol{0}_{5,6} \\ \boldsymbol{0}_{5,6} & \boldsymbol{A}_{10,12} & \boldsymbol{0}_{5,6} & -\boldsymbol{A}_{10,12} & \boldsymbol{0}_{5,6} & \boldsymbol{0}_{5,6} \\ \boldsymbol{0}_{5,6} & \boldsymbol{0}_{5,6} & \boldsymbol{0}_{5,6} & \boldsymbol{0}_{5,6} & \boldsymbol{A}_{13,14} & -\boldsymbol{A}_{13,14} \end{bmatrix} \tag{3.24}$$

$$\boldsymbol{A}_{lp3} = \begin{bmatrix} \boldsymbol{A}_{15,17} & \boldsymbol{0}_{5,6} & -\boldsymbol{A}_{15,17} & \boldsymbol{0}_{5,6} & \boldsymbol{0}_{5,6} & \boldsymbol{0}_{5,6} \\ \boldsymbol{0}_{5,6} & \boldsymbol{A}_{16,18} & \boldsymbol{0}_{5,6} & -\boldsymbol{A}_{16,18} & \boldsymbol{0}_{5,6} & \boldsymbol{0}_{5,6} \\ \boldsymbol{0}_{5,6} & \boldsymbol{0}_{5,6} & \boldsymbol{0}_{5,6} & \boldsymbol{0}_{5,6} & \boldsymbol{A}_{19,20} & -\boldsymbol{A}_{19,20} \end{bmatrix}$$

The final expression of the kinematic relations is:

$$\boldsymbol{A}_T \, \boldsymbol{\Delta X}_T = \boldsymbol{0}_{50,1} \tag{3.25}$$

3.5.2 Stiffness of the joints

The passive revolute joints can be modelled as a beam element with length equal to zero. The only characteristics of the joint stiffness matrix that are not null are the ones on the diagonal.

$$K_j = \begin{bmatrix} K_n & -K_n \\ -K_n & K_n \end{bmatrix} \tag{3.26}$$

where

$$K_n = \begin{bmatrix} 10^{13} & & & & & \\ & 10^{13} & & & \boldsymbol{0} & \\ & & 10^{13} & & & \\ & & & 10^{13} & & \\ & \boldsymbol{0} & & & 10^{13} & \\ & & & & & 10^{-1} \end{bmatrix} \tag{3.27}$$

The matrix K_n contains the axial stiffness, in the first three positions, and the rotational stiffness, in the other three. The revolute joints have one rotation allowed whereas the movements in the other directions are blocked. To achieve this, one of the stiffnesses has to be very low and the other ones have to be very high. In the case under investigation the movement allowed is the rotation around the axis $\vec{z}$ (in the beam reference system). The real stiffness of the joints is one of the parameter to identify, therefore, as first attempt, it was considered as $10^{13}\,\mathrm{N\,m^{-1}}$ for the linear stiffness, $10^{13}\,\mathrm{N\,m^{-1}\,rad}$ and $10^{-1}\,\mathrm{N\,m^{-1}\,rad}$ for the

rotational, where the last one is the rotational stiffness around $\vec{z}$.

As for the stiffness matrix of the structure, the stiffness matrix of the joint has to be placed in the global reference system, therefore a rotation matrix is used. The rotation matrix is the same as the one described before, see Equation (3.8), where the angle α was considered equal to zero because the two nodes, which make a joint, end in the same position and they do not have a relative orientation. The joint stiffness matrix was calculated through Equation (3.28) and it can be assembled inside the overall stiffness matrix with the same procedure described before, but considering the Equation (3.22) instead of Equation (3.12).

$$^{R_g}\boldsymbol{K} = \boldsymbol{P}_i^{-1} \,^{R_i}\boldsymbol{K}_j \, \boldsymbol{P}_i \tag{3.28}$$

3.6 Boundary conditions

The overall stiffness matrix is still defined null because the structure is not bounded, therefore it is necessary to insert the boundary conditions.

The points B_0 has the translation along the axis $\vec{z}$ blocked and along $\vec{x}$ the coordinate q_1 impose the position. On the other hand the point B_1 has the translation along $\vec{x}$ blocked and along $\vec{z}$ imposed by the coordinate q_2. Furthermore the rotation around $\vec{x}$ and $\vec{z}$ are not allowed because they would bring the pantograph out of his plane. Considering these premises, it is necessary to block the three translations and two of the three rotations of the points B_0 and B_1. With this purpose the following conditions have to be imposed:

$$\begin{cases} d\boldsymbol{P}_1 = d\boldsymbol{P}_2 = 0 \\ \boldsymbol{\theta}_{x_1} = \boldsymbol{\theta}_{z_1} = \boldsymbol{\theta}_{x_2} = \boldsymbol{\theta}_{z_2} = 0 \end{cases} \tag{3.29}$$

$$\begin{cases} d\boldsymbol{P}_7 = d\boldsymbol{P}_8 = 0 \\ \boldsymbol{\theta}_{x_7} = \boldsymbol{\theta}_{z_7} = \boldsymbol{\theta}_{x_8} = \boldsymbol{\theta}_{z_8} = 0 \end{cases} \tag{3.30}$$

The application of the boundary conditions entails a modification in the stiffness matrix and in the force and displacement vectors. A suppression of the rows and the columns which correspond to the fixed degrees of freedom make the stiffness matrix not defined null. The stiffness matrix with the boundary conditions applied is called $^{R_g}\boldsymbol{K}$. The same procedure has to be applied to the rows of the vector $\boldsymbol{\Delta X}_T$ and $\boldsymbol{F}_T$ that become $\boldsymbol{\Delta X}$ and $\boldsymbol{F}$. For the matrix $\boldsymbol{A}_T$ the columns linked to the fixed degrees of freedom and the rows made by only zero have to be deleted. In the case of using the method of kinematic relations, the stiffness matrix is semi-defined positive, therefore it couldn't be invertible. Whereas if the stiffness of the joints method is considered, the stiffness matrix is defined positive therefore it is invertible.

3.7 Energetic studies

The aim of the elastic model is to characterize the relation Equation (3.31) which describes the bound between force and displacement.

$$^{R_g}\boldsymbol{F} = {}^{R_g}\boldsymbol{K} \ {}^{R_g}\boldsymbol{\Delta X} \tag{3.31}$$

Considering the previous dissertation, a distinction between the model which considers the kinematic relations and the one which considers the stiffness of the joints needs to be made.

3.7.1 Kinematic relation

The matrix $\boldsymbol{K}$ is not defined positive because the links are not bounded to each other.

The insertion of the kinematic relations can be reduced to the identification of the minimum of the potential energy V (Equation (3.32)) with the surrounding conditions expressed by the Equations (3.29) and (3.30).

$$V = \frac{1}{2} \, \boldsymbol{\Delta X}^T \, \boldsymbol{K} \, \boldsymbol{\Delta X} - \boldsymbol{\Delta X}^T \, \boldsymbol{F} \tag{3.32}$$

The research of the minimum is made by the Lagrange multiplicator vectors whose correspond to the fifty surrounding conditions

$$V^* = V + [\boldsymbol{A} \, \boldsymbol{\Delta X}]^T \, \boldsymbol{\lambda}_m \tag{3.33}$$

The minimum can be achieved imposing the derivative equal to zero

$$\begin{cases} \frac{\partial V^*}{\partial \boldsymbol{\Delta X}} = 0 \\[2mm] \frac{\partial V^*}{\partial \boldsymbol{\lambda}} = 0 \end{cases} \tag{3.34}$$

therefore one can obtain the following equation:

$$\begin{bmatrix} \boldsymbol{K} & \boldsymbol{A}^T \\ \boldsymbol{A} & \boldsymbol{0}_{40} \end{bmatrix} \begin{bmatrix} \boldsymbol{\Delta X} \\ \boldsymbol{\lambda} \end{bmatrix} = \begin{bmatrix} \boldsymbol{F} \\ \boldsymbol{0}_{40,1} \end{bmatrix} \tag{3.35}$$

The Equation (3.35) can be simplified as

$$\boldsymbol{K}_G \, \boldsymbol{\Delta X}_G \ = \ \boldsymbol{F}_G \tag{3.36}$$

Where

$$\boldsymbol{K}_G = \begin{bmatrix} \boldsymbol{K} & \boldsymbol{A}^T \\ \boldsymbol{A} & \boldsymbol{0}_{40} \end{bmatrix}$$

$$\boldsymbol{\Delta X}_G = \begin{bmatrix} \boldsymbol{\Delta X} \\ \boldsymbol{\lambda} \end{bmatrix} \tag{3.37}$$

$$\boldsymbol{F}_G = \begin{bmatrix} \boldsymbol{F} \\ \boldsymbol{0}_{40,1} \end{bmatrix}$$

With the boundary and the surrounding conditions, the stiffness matrix $\boldsymbol{K}_G$ is symmetric and positive defined, therefore it is invertible and the displacements are calculated inverting the Equation (3.36) as follow:

$$\boldsymbol{\Delta X}_G \; = \; \boldsymbol{K}_G^{-1} \; \boldsymbol{F}_G \tag{3.38}$$

3.7.2 Joint stiffness

Differently from Section 3.7.1 the stiffness matrix is invertible, therefore the search of the minimum of a function is not needed. It is sufficient to verify that $\boldsymbol{\Delta X}$ respects the relation (3.36)

$$\boldsymbol{K}_G \, \boldsymbol{\Delta X}_G \; = \; \boldsymbol{F}_G$$

3.7.3 Differences between the two methods

The two methods provide similar results but, considering the stiffness of the joints, the elastic model results more accurate and closer to the reality. This because there is a small deflection in the joints that is not taken into account by the kinematic relations method. With the stiffness of the joints method the revolute joints are considered as beam elements with a length equal to zero and with their own stiffness.

3.8 Verification with Catia® model

The first verification of the elastic Model was performed comparing the results obtained with a finite element model developed on Catia® during previous studies [13]. Different positions and loads configuration were tested in order to prove the coherence of the two models. In Table 3.1 are reported the tested configurations and results.

Table 3.1: Results of the comparison between the Matlab® and Catia® elastic model

q1 [m]	q2 [m]	Load [N]	End-effector displacement in [mm]			
			$\vec{x}$		$\vec{z}$	
			Matlab® model	Catia® model	Matlab® model	Catia® model
0.15	-0.075	-100+WF	-1.903	-1.915	-2.236	-2.251
0.1	-0.125	-50	-1.109	-1.119	-1.920	-1.937
-0.05	-0.175	-150+WF	-1.651	-1.663	-7.979	-8.036
0.01	-0.225	-75	-0.081	-0.082	-3.405	-3.434

WF means 'Weight Force'

There is a small gap between the displacement obtained with the Matlab$^{\circledR}$ model and with the Catia$^{\circledR}$ one. This is probably due to the definition of the mesh size and to the numerical approximation made by Catia$^{\circledR}$.

3.9 Experimental validation

Once the geometrical and elastic models were developed, an experimental validation was done in order to evaluate the goodness of the two models.
The experiments consider two different configurations with two different applied loads, both reported in Table 3.2. The goal of this experimental validation was to

Table 3.2: First real model test parameters

Measure	Load [kg]	q_1 [m]	q_2 [m]
1.1	4.196	0.1243	-0.26904
1.2	9.154	0.1243	-0.26908
2.1	4.196	0.1243	-0.15695
2.2	9.196	0.1243	-0.15695

understand if both the geometrical and elastic model were correct. For this scope the same configuration of the pantograph was tested with two different loads, in order to obtain a relative displacement and to analyse separately the geometrical and elastic perspective.
The elastic model was used to calculate the displacement between the first and the second load and the results were compared with the measured end-effector displacement between the two loads. The results are summarized in Table 3.3.

Table 3.3: Results of the comparison between the Matlab model and the measurements on the real mock-up

(a) Position of the end-effector with the first and with the second load

Measure	X position [m]		Z position [m]	
	Calculated	Measured	Calculated	Measured
1.1	-0.3055	-0.3013	-0.9442	-0,9435
1.2	-0.3061	-0.3019	-0.9458	-0.9453
2.1	-0.3077	-0.3035	-0.5520	-0,5516
2.2	-0.3082	-0.3039	-0.5540	-0.5538

(b) End-effector displacement between the first and second load

Measure	X displacement [mm]		Z displacement [mm]	
	Calculated	Measured	Calculated	Measured
1.1	-	-	-	-
1.2	0.68899	0.6222	1.6287	1.7613
2.1	-	-	-	-
2.2	0.4783	0.4176	2.0241	2.1957

The Matlab® model does not consider neither the elastic nor the geometrical calibration. The absence of the calibration is the cause of the differences between the Matlab® model and the real values of the end-effector positions and displacements. We note that, despite from the calibration, the values are quite similar therefore the model can be considered correct. One can also observe that the $\vec{z}$ end-effector displacements, obtained from the real model, are bigger than the one calculated through Matlab®. This is due to the fact that the joints were considered more stiff (about $1 \times 10^{13}\,\mathrm{N\,m^{-1}}$) than in the reality, therefore the smaller deformations were expected. With the displacements in the $\vec{x}$ direction the evaluation of the correctness of the Matlab® model is more difficult.

CHAPTER 4

Elasto-geometrical calibration

The analytical models, as described in Chapters 2 and 3, have some parameters which are unknown, therefore they need to be estimated through an identification procedure. The parameters that we are going to identify are the stiffness of the joints and the geometrical errors of the structure. The end-effector position is influenced by different parameters such as:

- Geometrical errors

    - Manufacturing errors.

    - Assembly errors.

- Measuring errors

    - Intrinsic error of Nikon K610 optical CMM.

    - Errors due to the inaccuracy of the SpaceProbe[1].

    - Errors due to difficulties in the measures, such as hard access to the point to measure and measure of the centre of a joint starting from the measure of the centre of a circle.

    - Propagation of the errors in case of indirect measures.

    - Errors on the measures of the mass applied on the structure.

- Errors due to temperature

- Errors caused by the deformation of the external frame due to the weight of the pantograph

The performances of the geometrical identification could be strongly influenced by the errors described above. Whereas the identification of the joints stiffness is not influenced by these errors because, as described in Section 4.1, it is made considering the difference between the deformation with one load and with a higher load in the same position. Therefore all the errors linked to the position, such as the geometrical errors and the measuring errors, are neglected (this was

---

[1]The SpaceProbe is a touch trigger probe which measures discrete points in the space. It was used for measure the centre of the joints and all the points on the mock-up

taken as an hypothesis). The other errors were not considered because the only ones which remain are linked to intrinsic error of the measuring system that cannot be deleted.

4.1 Identification of the stiffness of the joints

The first step in the calibration is the identification of the stiffness of the joints. It comes before the geometrical errors identification because it is made from a comparison between the end-effector position with two different loads. With the scope of identifying the joints stiffness in case of different loads and to increase the number of equations, three loads were used. The first load is approximately 7 kg and it is the reference one, the other two are approximately 11.8 kg and 16.6 kg and they represent the second load that is compared with the reference one in order to obtain the displacement. This, as described above, means that the geometrical errors are neglected and moreover, for this step, the geometrical identification is not needed.
The identification goes through the calculation of two displacements for each pantograph configuration. The first one is the difference between the end-effector position with the first load and with the lighter of the other loads, the second displacement comes from the difference between the first load and the heavier of the other loads. The two displacements become four equations considering the two directions $\vec{x}$ and $\vec{z}$. These displacements are measured on the real mock-up and calculated with the Matlab® model. Therefore one obtains the errors between the real and the calculated displacements. There are two[2] ways to manage these errors. The first one is sum the errors and minimize it, whereas the second way is to put together the $\vec{x}$ and $\vec{z}$ errors (with the vector addition) and minimize the sum of the errors.   The minimization of the errors, which considers the vector addition, could give better results because the scope of the calibration is to minimize the errors along both $\vec{x}$ and $\vec{z}$ direction. Nevertheless it can also cause some problems because it does not consider the sign of the errors (the vector addition goes through the square root and the squared of the values). On the other hand the minimization of the sum of the errors finds the best compromise between all the errors without focusing the attention on the global end-effector errors (the one coming from the vector addition). A comparison of the two methods is reported in Section 5.4.1.

---

[2]Actually there is a third option that is to write an analytical model, function of the coordinates q_1, q_2 and the joints stiffness. This was performed using the Matlab® symbolic toolbox and, therefore, convert it with the function 'MatlabFunction' into a anonymous function. The function obtained is the inverted stiffness matrix of the overall system and it has the scope of writing the problem in this form:

$$inv(\boldsymbol{K})\boldsymbol{F} - \boldsymbol{\Delta X} = \boldsymbol{0} \tag{4.1}$$

Because a function is impossible to invert in Matlab®, the inversion of the stiffness matrix was performed with the symbolic toolbox but, after the check of the matrix invertibility, it was impossible to perform because of the high complexity of the calculus.

A bisection method was used for the identification. Starting from a range of the stiffness of the joints which was plausible, we decreased the interval until the minimum of the errors was reached.

4.2   Identification of the geometrical errors

Once the elastic deflection, due to the load applied, is known, we can make a comparison between the end-effector positions and angles measured and calculated through the Matlab® model. The displacements, due to the wrench, are calculated analytically and then we obtain the end-effector positions, in absence of any load, subtracting the displacement from the end-effector position measured. Therefore, from the comparison between the end-effector positions without any wrench measured and calculated we perform the identification of the geometrical errors due to manufacturing and assembling inaccuracies. The errors can be calculated through the Jacobian matrix as explained in Section 2.3. Equation (2.10) is reported in order to simplify the reading.

$$\boldsymbol{\delta P} = \boldsymbol{J} \ \boldsymbol{\delta K} \tag{4.2}$$

In the calibration equations there are 14 parameters to identify, but they are not all identifiable, therefore, before solving the Equation (4.2), it is essential to define the identifiable parameters. Starting from Equation (4.2) we consider that $\boldsymbol{J}$ has dimension $n \cdot m$, where n represents the number of parameters to identify and m the number of equations used for the identification. Taking into account that r is the rank of the Jacobian matrix, the system can be written as

$$\boldsymbol{\delta P} = \begin{bmatrix} \boldsymbol{J_1} & \boldsymbol{J_2} \end{bmatrix} \begin{bmatrix} \boldsymbol{\delta K}_1 \\ \boldsymbol{\delta K}_2 \end{bmatrix} \tag{4.3}$$

where $\boldsymbol{J}_1$ contains the r linear independent columns of $\boldsymbol{J}$, while $\boldsymbol{J}_2$ contains the linear dependent ones. It is possible to define the matrix $\boldsymbol{\beta}$ of the constant coefficients such that

$$\boldsymbol{J}_2 = \boldsymbol{J}_1 \boldsymbol{\beta} \tag{4.4}$$

Combining Equations (4.3) and (4.4) we obtain:

$$\boldsymbol{\delta P} = \boldsymbol{J}_1 \ \boldsymbol{\delta K}_r \tag{4.5}$$

where

$$\boldsymbol{\delta K}_r = \boldsymbol{\delta K}_1 + \boldsymbol{\beta} \ \boldsymbol{\delta K}_2 \tag{4.6}$$

To calculate the matrices $\boldsymbol{J}_1$ and $\boldsymbol{J}_2$ the QR decomposition of the Jacobian matrix is used, as explained in [1] and [12]. For the details of the calculation see Appendix B.

Once the matrix $\boldsymbol{\beta}$ is known, we can calculate the geometrical errors inverting Equation (4.5). Theoretically the non identifiable parameters are the ones whose

correspond a zero[3] element on the diagonal of the matrix $\boldsymbol{\beta}$. The expression of the identifiable parameters, as linear combination of the non identifiable parameters, is given by Equation (4.6).

To verify the accuracy of the method, the condition number of the Jacobian matrix is used. The condition number of a matrix, considering the system $Ax = b$, is an index on how much the solution x is accurate considering the approximations on A. Therefore the condition number reveals if the matrix is well-approximated or not. A value close to one means that the matrix is well-conditioned, therefore the inverse can be calculated with a good accuracy, whereas the further it is from one, the biggest are the numerical errors in the inversion.

4.2.1   Monte Carlo methods

The Monte Carlo methods are used to solve a problem through the generation of random intercorrelated values of a parameter in order to obtain the numerical solutions of a function. They are used when an analytic study is difficult or impossible. They are also employed to simulate systems with a big number of DoF and to evaluate problems with uncertainty in the inputs. The last one is the case that we evaluate because it translates uncertainties in the input to uncertainties in the output. The application of the Monte Carlo methods needs the knowledge of the statistic distribution of the input variables. In the case of an unknown distribution one can use the Markov Chain Monte Carlo (MCMC) sampler.

4.2.1.1   Chosen of the random number generator and distribution

The chosen of the random number generator is the heart of the Monte Carlo method. The random numbers need to be independent and to have a certain distribution, which is the same of the variables they represent. According to [8], a good random number generator needs to have the following properties:

- The generator should pass a battery of simple statistical tests designed to detect deviations from uniformity and independence.

- It should be based on sound mathematical principles.

- The stream of random numbers is reproducible for store the complete stream in memory.

- It should produce random number in a fast and efficient way.

- The period should be large (in the order of 10^{50}) in order to avoid problems with duplication and dependence.

In order to avoid a tedious dissertation on the different classes of random number generators, only two different generators are presented. They are normally used in the main programming languages and have overall good performances.

---

[3]With zero we mean the numerical zero for double precision according to IEEE 754

- *Combined multiple recursive generators*: they have excellent statical properties, are simple, have large period and are moderately fast.

- *Twisted general feedback shift register generators*: they have good equidistributional properties, are among the fastest generators and have long periods. they are the default Matlab® generators.

The Matlab® default generator is good enough for the purpose of this work, therefore it was the used one.

The distribution of the uncertainty on the parameters was considered as Gaussian with a null mean value and a variance depending on the parameter type.

4.2.1.2   Implementation

In Table 4.1 one can find the different possible causes of an end-effector position error and their variance. The identification of the sources of error was linked to

Table 4.1: Imposed errors and their variance

Parameter	Variance of the error
Horizontal coordinate q_1	$0.1\,\mathrm{mm}$
Vertical coordinate q_2	$0.1\,\mathrm{mm}$
Length of links	$1\,\mathrm{mm}$
Joints stiffness	$0.02 \times 10^6\,\mathrm{N\,m^{-1}}$
Joints centre	$1.5\,\mathrm{mm}$
Joints position	$0.1\,\mathrm{mm}$
Mass applied as a load	$0.005\,\mathrm{kg}$

the measure procedure itself, for the detailed procedure see Section 5.3. One can find below the error sources considered in the Monte Carlo Method.

- *Coordinates q_1 and q_2*: the errors come from the inaccuracy on the position of the led.

- *Length of the links*: this errors come from the manufacturing and assembly errors.

- *Joints stiffness*: errors due to the stiffness identification and to the nonlinearity of the structure.

- *Joints centre*: these errors come from the procedure used for the measurement of the centre of a joint. The position of the centre of a joint is obtained from the measure of the centre of a circle. The circle is measured from the external ring of the bearing or from the head of the screw that hold together the links. Both the external ring and the crew are not perfectly centred, therefore we have to consider the procedure as a source of errors. Additional sources of error are the propagation of the errors due to an indirect measure and the errors in the measurement of the circle.

- *Joints position*: the position of the joint was calculated through a dynamic reference systems, as offset from a led, or derived from the position of more than one led. Therefore there are errors due to indirect measures.

- *Mass applied as a load*: there is an error in the measurement of the mass due to the intrinsic error of the balance.

This errors were added to their nominal value and then the end-effector position was calculated, therefore it was compared with the one calculated without the errors. This procedure was repeated for one hundred times for each one of the different identification procedures (which consider different measures for the identification) listed in Section 4.2.2. The results are available in Table 4.2.

Table 4.2: Results of the Monte Carlo analysis: end-effector position errors after the identification of the geometrical errors

Identification type	Error along $\vec{x}$ [mm]			Error along $\vec{z}$ [mm]		
	Mean	Max	Variance	Mean	Max	Variance
End-effector	0.8104	2.4351	0.2443	0.6873	2.0174	0.1546
End-effector + nodes A11,A12	0.9088	2.4610	0.2799	0.7100	1.9225	0.1468
Angles $\theta_A,\theta_{A32},\theta_{A3}$	2.4141	6.2315	1.9022	1.5675	4.0168	0.5921
End-effector + Angles $\theta_A,\theta_{A32},\theta_{A3}$	0.8661	2.3434	0.2405	0.7196	1.9320	0.1309
End-effector + Angles $\theta_A,\theta_{A21},\theta_{A2}$	0.8605	2.2631	0.2436	0.7076	1.8018	0.1205
Without identification	2.7875	6.8799		2.0583	5.2271	

4.2.1.3 Conclusions

The Monte Carlo study demonstrates that the identification procedure produces an increment in the accuracy of the geometrical model. A focus on the different parameters to measure for the identification is presented in the chapter below. Nevertheless the smallest error is obtained from the identification through the measures on the end-effector position, even if the identification through the other measures, with the exception of the measures on the angles $\theta_A,\theta_{A32},\theta_{A3}$, has similar results.
From the Monte Carlo method we can observe the performance of the identification procedure. The maximum end-effector position accuracy achievable is approximately ± 2.5 mm.

4.2.2 Simulations

The identification of the geometrical errors is strongly influenced by the parameters used to evaluate Equation (4.2). In Section 4.2.1 we observe the behaviour of the identification procedure from a rigorous point of view. This section has the scope of focussing the attention on the different choices for the parameters to measure for the identification. Therefore, different simulations were performed in order to choose which are the best parameters to measure, as a means to identify the geometrical errors. Different pantograph configurations were tested in order to verify the accuracy in the entirely working area. The noise was not taken into account, whereas random geometrical errors, uniformly distributed, were considered. The imposed errors have a maximum value equal to $\pm 1 \, \text{mm}$, this choice comes from the reflection that we want to understand the performances of the calibration method in the worst condition possible. The procedure used consists in the definition of the two driven coordinates q_1 and q_2 in such a way that the entire work area is reached. The end-effector positions were calculated through the geometrical model with the addition of the geometrical errors. The end-effector positions obtained above were compared with the end-effector positions obtained without considering the geometrical errors. Once the $\boldsymbol{\delta P}$ was obtained, the identification was performed, as described in the beginning of the chapter. There are three key indexes in the geometrical error identification. The first one is the number of the identifiable parameters, the second one is the accuracy on the geometrical errors estimation and the last one is the end-effector position accuracy. Below there is a comparison between the identification with the measures on different parameters.

4.2.2.1 End-effector positions

The end-effector position accuracy is the goal of the calibration, therefore the measures on the end-effector are a good starting point to perform the identification of the geometrical errors. In case of measures on the end-effector, Equation (4.2) becomes:

$$
\begin{bmatrix} \boldsymbol{\delta P}_1 \\ \boldsymbol{\delta P}_2 \\ \vdots \\ \boldsymbol{\delta P}_{n-1} \\ \boldsymbol{\delta P}_n \end{bmatrix} = \begin{bmatrix} \boldsymbol{J_1} \\ \boldsymbol{J_2} \\ \vdots \\ \boldsymbol{J_{n-1}} \\ \boldsymbol{J_n} \end{bmatrix} \begin{bmatrix} \boldsymbol{\delta K} \end{bmatrix} \tag{4.7}
$$

where n is the number of measures taken. The number of measures have to be bigger than the number of parameters to identify in order to obtain an overdetermined system.

Simulations results   The geometrical errors added were chosen randomly therefore, to make a sensitivity analysis, the calibration was repeated three times in order to measure the robustness of the calibration procedure. The comparison between the imposed and the estimated geometrical errors is reported in Table 4.3,

whereas the end-effector position errors are reported in Table 4.4 and Figs. 4.1 and 4.2.

Table 4.3: Mean and Maximum errors on the end-effector position considering the geometrical errors identified through the end-effector position

| | | Simulation | | | | | |
| | | First | | Second | | Third | |
		Wo.I.	W.I.	Wo.I.	W.I.	Wo.I.	W.I.
$\vec{x}$ Error [mm]	Max	17.8974	7.8229	10.1081	0.7288	12.6308	0.3382
	Mean	2.3993	0.3125	1.5143	0.0762	14.3134	0.0967
$\vec{z}$ Error [mm]	Max	18.1491	4.8364	8.7915	0.3941	2.8064	0.3573
	Mean	4.6268	0.1727	1.7886	0.0388	6.0514	0.0779

Wo.I. means 'Without identification'
W.I. means 'With identification'

Table 4.4: Geometrical errors identification through the end-effector position

Parameter	Simulation									Combination of other parameters
	First			Second			Third			
	I.E.	E.E	Δ.E.	I.E.	E.E	Δ.E.	I.E.	E.E	Δ.E.	
q_1	-0.1	-0.1338	0.0337	0.4	0.3900	0.0100	-0.5	-0.4920	0.0080	Independent value
q_2	-0.9	-0.9584	0.0584	-0.1	-0.1280	0.0280	-0.7	-0.7309	0.0309	Independent value
$L_{1,1}^u$	-0.4	-1.2058	0.8058	-0.7	-0.5272	0.1728	-0.8	-1.7546	0.9546	$L_{1,1}^u + \frac{4L_{22}^l}{15} - \frac{2L_{31}^u}{5} - \frac{2L_{21}^u}{3}$
$L_{1,2}^u$	-0.3	0.1992	0.4992	-0.9	-0.3951	0.5049	0.3	0.0991	0.2009	$L_{1,2}^u + \frac{4L_{21}^u}{15} - \frac{2L_{31}^l}{5} - \frac{2L_{21}^l}{3}$
$L_{1,1}^l$	-0.9	-1.703	0.8030	-1	-1.2717	0.2717	0.6	1.0874	0.4875	$L_{1,1}^l + \frac{4L_{21}^u}{15} - \frac{2L_{22}^l}{3} - \frac{2L_{32}^l}{5}$
$L_{1,2}^l$	-0.4	-0.5291	0.1291	0.1	0.0082	0.0918	0.4	1.1636	0.7636	$L_{1,2}^l + \frac{4L_{21}^l}{15} - \frac{2L_{22}^u}{3} - \frac{2L_{32}^u}{5}$
$L_{2,1}^u$	0.2	n.i.	/	-0.5	n.i.	/	-0.8	n.i.	/	
$L_{2,2}^u$	0.1	n.i.	/	0.6	n.i.	/	0.1	n.i.	/	
$L_{2,1}^l$	-1	n.i.	/	-0.7	n.i.	/	1	n.i.	/	
$L_{2,2}^l$	0.7	n.i.	/	-0.8	n.i.	/	0.8	n.i.	/	
$L_{3,1}^u$	0.9	n.i.	/	0.7	n.i.	/	-0.1	n.i.	/	
$L_{3,2}^u$	1	n.i.	/	-0.8	n.i.	/	-0.9	n.i.	/	
$L_{3,1}^l$	0.7	n.i.	/	0.4	n.i.	/	-0.9	n.i.	/	
$L_{3,2}^l$	1	n.i.	/	0.6	n.i.	/	0.7	n.i.	/	

I.E. means 'Imposed errors [mm]'

E.E. means 'Estimated errors [mm]'

Δ.E. means 'Difference between the imposed and estimated errors [mm]'

n.i. means 'Non identifiable parameter'

Conclusions The results show that there are only six out of fourteen errors identifiable. Furthermore considering a maximum error equal to ± 1 mm the errors on the end-effector position change a lot depending on the geometrical errors configuration. In Figures 4.1a and 4.1b we observe that there are a big oscillations on the errors between the real position (the one that considers the geometrical errors) and the one without the geometrical errors. Moreover the errors increase increasing the number of the measures. The measures were taken on a grid defined by ten different positions of q_1 and ten of q_2, therefore the measures from one to ten have different q_1 but the same q_2, similarly for the measures from eleven to twenty and the following ones. Hence, the errors increase going from the top to the bottom of the grid and have an oscillation going from the left to the right part of the working area. Whereas in Figure 4.1c there still is the oscillation of the error going from left to right but there is not an identifiable behaviour of the error going from the top to the bottom of the grid. The 3D behaviour of the error in the first simulation is reported in Figure 4.2. We also observe that the accuracy on the end-effector positions changes a lot with different configurations of the errors, as reported in Table 4.3. The decrement of the oscillations amplitude, with a period of ten measures, was analysed and it depends from the values of the errors. If positive errors are predominant, there is a decrement of the errors from the left to the right of the measure grid, but, if there are a preponderance of negative errors, the errors should increase going from the left to the right of the grid.

The identification procedure reduces a lot the errors on the end-effector position, as one can see in Figure 4.1 the blue line is close to zero (except for one configuration). Therefore the geometrical errors identification achieve an improvement of the model performances. Unfortunately there still is a small oscillation of the error in phase with the errors in absence of the geometrical errors identification.
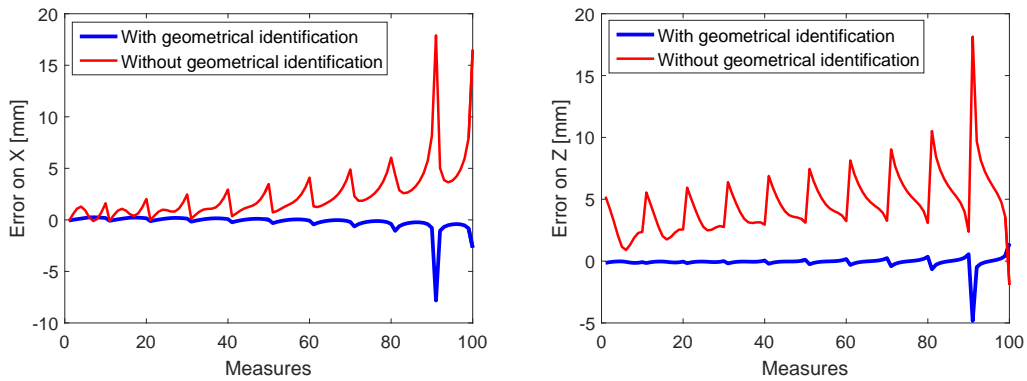
(a.1) Comparison along $\vec{x}$ direction
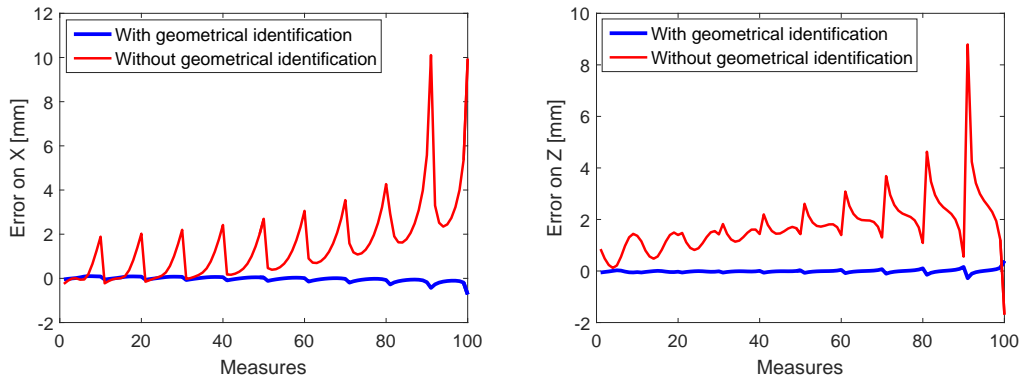
(a.2) Comparison along $\vec{z}$ direction

(a) First simulation

(b.1) Comparison along $\vec{x}$ direction

(b.2) Comparison along $\vec{z}$ direction

(b) Second simulation
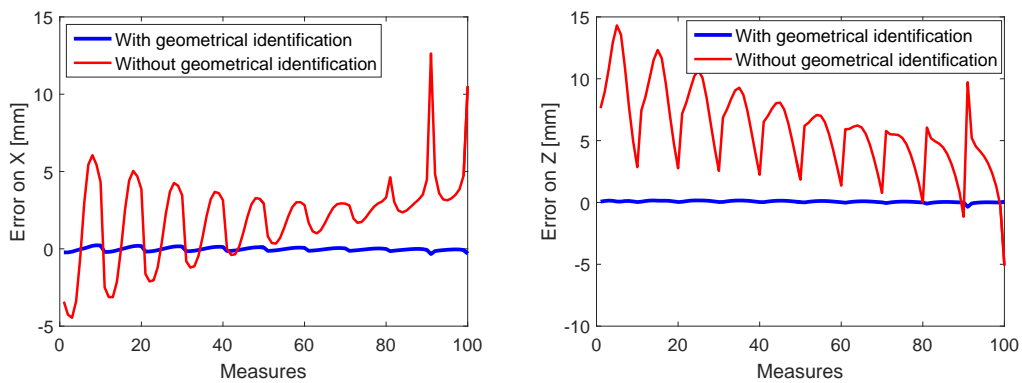
(c.1) Comparison along $\vec{x}$ direction

(c.2) Comparison along $\vec{z}$ direction

(c) Third simulation

Figure 4.1: Comparison between the end-effector position with and without the geometrical errors identified through the end-effector position

(a) First simulation

(b) Second simulation

(c) Third simulation
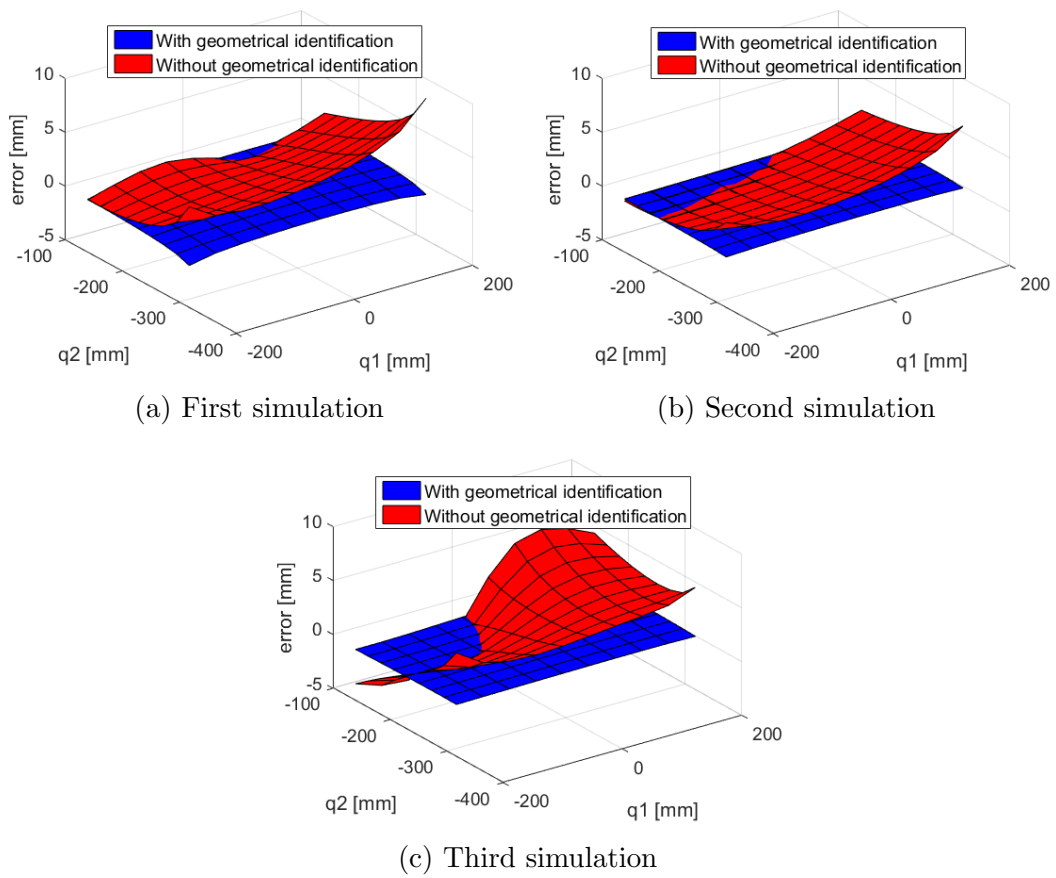
Figure 4.2: Comparison between the end-effector errors with and without the geometrical errors identified through the end-effector position

4.2.2.2 End-effector position and angles θ_A, $\theta_{A_{21}}$, θ_{A_2}

In order to increase the number of the identifiable parameters, the identification through the end-effector position plus the angles θ_{A_2}, $\theta_{A_{21}}$ and $\theta_{A_{22}}$ was considered. The chosen angles should give the information to identify the errors on the second loop of the pantograph. The knowledge of these errors should increase the accuracy on the end-effector position due to the amplification factor (explained in Section 2.2.1). In this case Equation (4.2) becomes

$$
\begin{bmatrix} \boldsymbol{\delta P} \\ \boldsymbol{\delta\theta}_{A2} \\ \boldsymbol{\delta\theta}_{A21} \\ \boldsymbol{\delta\theta}_{A22} \end{bmatrix} = \begin{bmatrix} \boldsymbol{J_P} \\ \boldsymbol{J_{\theta A2}} \\ \boldsymbol{J_{\theta A21}} \\ \boldsymbol{J_{\theta A22}} \end{bmatrix} \begin{bmatrix} \boldsymbol{\delta K} \end{bmatrix}^{\mathrm{d}} \tag{4.8}
$$

where

$$
\begin{aligned}
\boldsymbol{\delta P} &= \begin{bmatrix} \boldsymbol{\delta P}_1 & \boldsymbol{\delta P}_2 & \cdots & \boldsymbol{\delta P}_{n-1} & \boldsymbol{\delta P}_n \end{bmatrix}^T \\
\boldsymbol{\delta\theta}_{A2} &= \begin{bmatrix} \boldsymbol{\delta\theta}_{A_1} & \boldsymbol{\delta\theta}_{A_2} & \cdots & \boldsymbol{\delta\theta}_{A_{n-1}} & \boldsymbol{\delta\theta}_{A_n} \end{bmatrix}^T \\
\boldsymbol{\delta\theta}_{A21} &= \begin{bmatrix} \boldsymbol{\delta\theta}_{A21_1} & \boldsymbol{\delta\theta}_{A21_2} & \cdots & \boldsymbol{\delta\theta}_{A21_{n-1}} & \boldsymbol{\delta\theta}_{A21_n} \end{bmatrix}^T \\
\boldsymbol{\delta\theta}_{A22} &= \begin{bmatrix} \boldsymbol{\delta\theta}_{A2_1} & \boldsymbol{\delta\theta}_{A2_2} & \cdots & \boldsymbol{\delta\theta}_{A2_{n-1}} & \boldsymbol{\delta\theta}_{A2_n} \end{bmatrix}^T
\end{aligned} \tag{4.9}
$$

To avoid errors due to the different measure units of the end-effector position and the angles, the Jacobian matrix and the vector, which contains the positions and angles errors, were normalized, therefore Equation (4.8) becomes:

$$
\begin{bmatrix} \frac{\boldsymbol{\delta P}}{\|\boldsymbol{\delta P}\|} \\ \frac{\boldsymbol{\delta\theta}_A}{\|\boldsymbol{\delta\theta}_A\|} \\ \frac{\boldsymbol{\delta\theta}_{A21}}{\|\boldsymbol{\delta\theta}_{A21}\|} \\ \frac{\boldsymbol{\delta\theta}_{A2}}{\|\boldsymbol{\delta\theta}_{A2}\|} \end{bmatrix} = \begin{bmatrix} \frac{\boldsymbol{J_P}}{\|\boldsymbol{\delta P}\|} \\ \frac{\boldsymbol{J_{\theta A}}}{\|\boldsymbol{\delta\theta}_A\|} \\ \frac{\boldsymbol{J_{\theta A21}}}{\|\boldsymbol{\delta\theta}_{A21}\|} \\ \frac{\boldsymbol{J_{\theta A2}}}{\|\boldsymbol{\delta\theta}_{A2}\|} \end{bmatrix} \begin{bmatrix} \boldsymbol{\delta K} \end{bmatrix} \tag{4.10}
$$

An additional advantage to use a grater number of parameters in the identification is the increase of the number of the equations available.

Simulations results   A comparison between the imposed and the estimated errors is reported in Table 4.5, whereas Table 4.6 explains if the parameters are estimated independently, through a linear combination of the not-identifiable parameters, furthermore in Table 4.7 there are the errors on the end-effector position considering the identified parameters.

ᵈ The disposition of the terms were chosen in order to simplify the assembly in the Matlab®

Table 4.5: Geometrical errors identification through the end-effector position and the angles θ_A, $\theta_{A_{21}}$, θ_{A_2}

Parameter	Simulation								
	First			Second			Third		
	I.E.	E.E	Δ.E.	I.E.	E.E	Δ.E.	I.E.	E.E	Δ.E.
q_1	-0.1	-0.1645	0.6447	0.4	0.3913	0.0087	-0.5	-0.5266	0.0266
q_2	-0.9	-0.8952	0.0048	-0.1	-0.1143	0.0143	-0.7	-0.6937	0.0063
$L_{1,1}^u$	-0.4	-0.4777	0.0777	-0.7	-0.7218	0.2175	-0.8	-0.8196	0.0196
$L_{1,2}^u$	-0.3	0.22034	0.0797	-0.9	-0.8707	0.0293	0.3	0.3297	0.0297
$L_{1,1}^l$	-0.9	-0.9814	0.0814	-1	-1.066	0.0660	0.6	0.5861	0.0139
$L_{1,2}^l$	-0.4	-0.5250	0.1250	0.1	0.0738	0.0262	0.4	0.3521	0.0479
$L_{2,1}^u$	0.2	n.i.	/	-0.5	0.0205	0.5205	-0.8	-0.9080	0.1080
$L_{2,2}^u$	0.1	1.1403	1.0403	0.6	-0.3400	0.9400	0.1	-0.8485	0.9485
$L_{2,1}^l$	-1	n.i.	/	-0.7	-1.6482	0.9483	1	n.i.	/
$L_{2,2}^l$	0.7	0.6440	0.0560	-0.8	-0.2174	0.5826	0.8	0.6514	0.1486
$L_{3,1}^u$	0.9	0.5482	0.3518	0.7	n.i.	/	-0.1	n.i.	/
$L_{3,2}^u$	1	-0.0525	1.0525	-0.8	n.i.	/	-0.9	0.1691	1.0691
$L_{3,1}^l$	0.7	-0.2002	0.9002	0.4	1.3627	0.9627	-0.9	0.0378	0.9378
$L_{3,2}^l$	1	0.9278	0.0722	0.6	-0.0831	0.6831	0.7	0.7780	0.0779

I.E. means 'Imposed errors [mm]'

E.E. means 'Estimated errors [mm]'

Δ.E. means 'Difference between the imposed and estimated errors [mm]'

n.i. means 'Non identifiable parameter'

Table 4.6: Combination of the other parameters with the identification through the end-effector position and the angles θ_A, $\theta_{A_{21}}$, θ_{A_2}

Parameter	Combination of other parameters		
	First simulation	Second simulation	Third simulation
q_1	Independent value	Independent value	Independent value
q_2	Independent value	Independent value	Independent value
$L^u_{1,1}$	Independent value	Independent value	Independent value
$L^u_{1,2}$	Independent value	Independent value	Independent value
$L^l_{1,1}$	Independent value	Independent value	Independent value
$L^l_{1,2}$	Independent value	Independent value	Independent value
$L^u_{2,1}$	/	$L^u_{21} + L^u_{31}$	$L^u_{21} + L^u_{31}$
$L^u_{2,2}$	$L^u_{2,2} - L^l_{21}$	$L^u_{22} + L^u_{32}$	$L^u_{22} - L^l_{21}$
$L^l_{2,1}$	/	$L^l_{21} + L^u_{32}$	/
$L^l_{2,2}$	$L^l_{2,2} - L^u_{21}$	$L^l_{22} + L^u_{31}$	$L^l_{22} + L^u_{31}$
$L^u_{3,1}$	$L^u_{3,1} + L^u_{21}$	/	/
$L^u_{3,2}$	$L^u_{3,2} + L^l_{21}$	/	$L^l_{21} + L^u_{32}$
$L^l_{3,1}$	$L^l_{3,1} + L^l_{21}$	$L^l_{31} - L^u_{32}$	$L^l_{21} + L^l_{31}$
$L^l_{3,2}$	$L^l_{3,2} + L^u_{21}$	$L^l_{32} - L^u_{31}$	$L^l_{32} - L^u_{31}$

Conclusions   Considering the end-effector position and the angles θ_A, $\theta_{A_{21}}$, θ_{A_2} in the identification procedure, the number of the identifiable parameters increases, going from six to twelve, in comparison with the identification based on the end-effector position only. There still are oscillations in the end-effector position errors but the increment in the model accuracy is outstanding, as reported in Table 4.7.
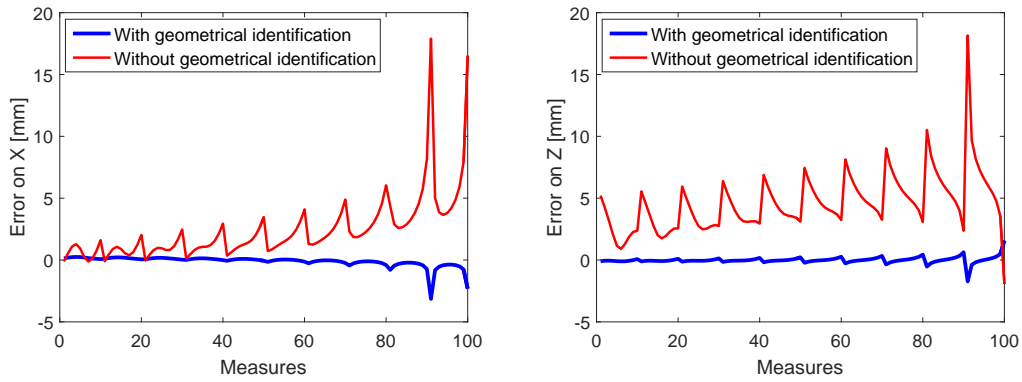
(a.1) Comparison along $\vec{x}$ direction
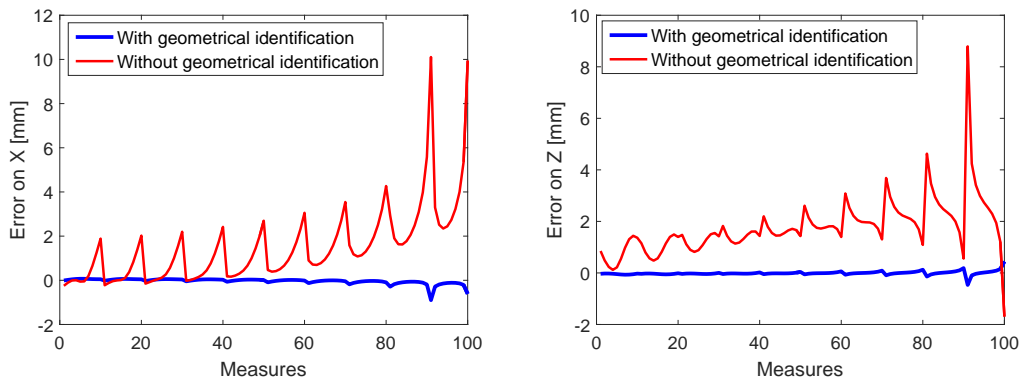
(a.2) Comparison along $\vec{z}$ direction

(a) First simulation

(b.1) Comparison along $\vec{x}$ direction

(b.2) Comparison along $\vec{z}$ direction

(b) Second simulation
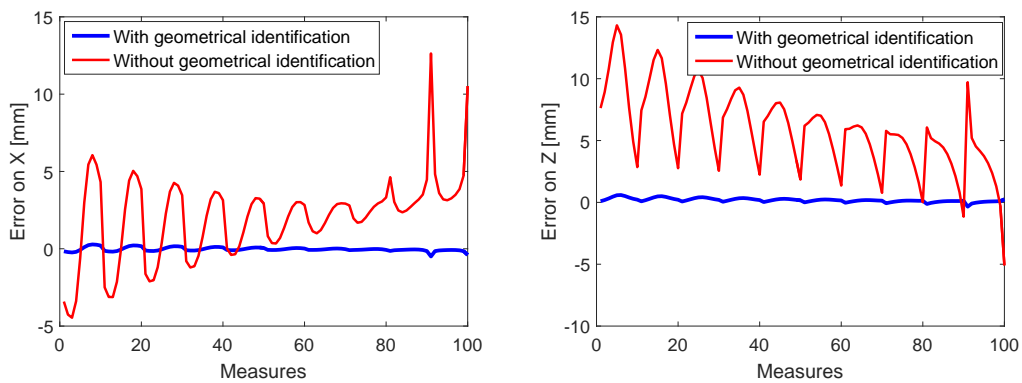
(c.1) Comparison along $\vec{x}$ direction

(c.2) Comparison along $\vec{z}$ direction

(c) Third simulation

Figure 4.3: Comparison between the end-effector position with and without the geometrical errors identified through the end-effector position and the angles θ_A, $\theta_{A_{21}}$, θ_{A_2}

Table 4.7: Mean and Maximum errors on the end-effector position considering the geometrical errors identified through the end-effector position and the angles θ_A, $\theta_{A_{21}}$, θ_{A_2}

		Simulation					
		First		Second		Third	
		Wo.I.	W.I.	Wo.I.	W.I.	Wo.I.	W.I.
$\vec{x}$ Error [mm]	Max	17.8974	3.1454	10.1081	0.8996	12.6308	0.4983
	Mean	2.3993	0.2314	1.5143	0.0733	2.8064	0.1017
$\vec{z}$ Error [mm]	Max	18.1491	1.7308	8.7915	0.4665	14.3134	0.5950
	Mean	4.6268	0.1488	1.7886	0.0452	6.0514	0.1992

Wo.I. means 'Without identification'
W.I. means 'With identification'

(a) First simulation

(b) Second simulation

(c) Third simulation
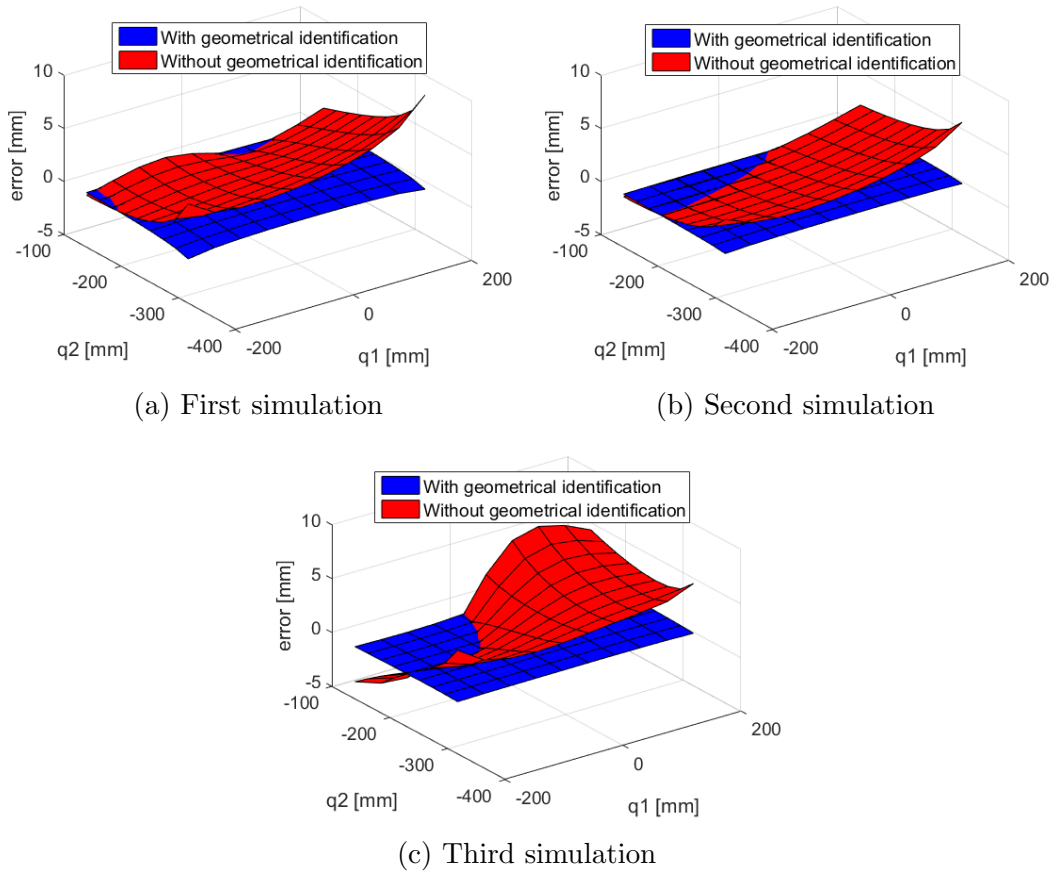
Figure 4.4: Comparison between the end-effector errors with and without the geometrical errors identified through the end-effector position and the angles θ_A, $\theta_{A_{21}}$, θ_{A_2}

4.2.2.3 Position of the end-effector and the points A_{11} and A_{12}

The procedure is the same as the one reported in Section 4.2.2.2 but, in order to avoid measure units problems and the propagation of the errors[5], we consider the position of the joints instead of the angles. Equation (4.2) becomes:

$$
\begin{bmatrix} \boldsymbol{\delta P} \\ \boldsymbol{\delta P}_{A11} \\ \boldsymbol{\delta P}_{A12} \end{bmatrix} = \begin{bmatrix} \boldsymbol{J_P} \\ \boldsymbol{J_{P A11}} \\ \boldsymbol{J_{P A12}} \end{bmatrix} \begin{bmatrix} \boldsymbol{\delta K} \end{bmatrix} \tag{4.11}
$$

Simulations results In Table 4.8 one finds the results of the identification. Moreover in Table 4.9 and Fig. 4.5 one finds the end-effector position errors comparison for the three simulations.

---

[5] The calculation of the angles came from the knowledge of the position of the joints, therefore instead of one error on the measure , that one has for the position of a joint, there are more errors that affect the measure of an angle

Table 4.8: Geometrical errors identification through the end-effector position and the points A_{11} and A_{12}

Parameter	Simulation									Combination of other parameters
	First			Second			Third			
	I.E.	E.E	Δ.E.	I.E.	E.E	Δ.E.	I.E.	E.E	Δ.E.	
q_1	-0.1	-0.2613	0.1613	0.4	0.3634	0.0366	-0.5	-0.4876	0.0124	Independent value
q_2	-0.9	-0.5903	0.3097	-0.1	0.06455	0.1646	-0.7	-0.3955	0.3045	Independent value
$L_{1,1}^u$	-0.4	-0.5577	0.1577	-0.7	-0.7594	0.0594	-0.8	-0.8247	0.0247	Independent value
$L_{1,2}^u$	-0.3	1.6556	1.9556	-0.9	-0.5546	0.3454	0.3	1.2506	0.9507	Independent value
$L_{1,1}^l$	-0.9	-1.1067	0.2056	-1	-1.1219	0.1220	0.6	0.4009	0.1991	Independent value
$L_{1,2}^l$	-0.4	0.0325	0.4325	0.1	-0.0348	0.1348	0.4	-0.0206	0.4207	Independent value
$L_{2,1}^u$	0.2	2.1575	1.9575	-0.5	0.0718	0.5718	-0.8	-0.9629	0.1629	$\frac{2L_{32}^l}{7} + L_{21}^u + \frac{5L_{31}^u}{7}$
$L_{2,2}^u$	0.1	2.4956	2.3956	0.6	0.4051	0.1950	0.1	0.0946	0.0054	$\frac{2L_{31}^l}{7} + L_{22}^u + \frac{5L_{32}^u}{7}$
$L_{2,1}^l$	-1	3.5383	4.5383	-0.7	0.1449	0.8449	1	2.1978	1.1978	$L_{22}^l + \frac{5L_{32}^l}{7} + \frac{2L_{31}^u}{7}$
$L_{2,2}^l$	0.7	2.4209	1.7209	-0.8	-0.0493	0.7507	0.8	1.4345	0.6345	$L_{22}^l + \frac{5L_{32}^l}{7} + \frac{2L_{31}^u}{7}$
$L_{3,1}^u$	0.9	n.i.	/	0.7	n.i.	/	-0.1	n.i.	/	/
$L_{3,2}^u$	1	n.i.	/	-0.8	n.i.	/	-0.9	n.i.	/	/
$L_{3,1}^l$	0.7	n.i.	/	0.4	n.i.	/	-0.9	n.i.	/	/
$L_{3,2}^l$	1	n.i.	/	0.6	n.i.	/	0.7	n.i.	/	/

I.E. means 'Imposed errors [mm]'

E.E. means 'Estimated errors [mm]'

Δ.E. means 'Difference between the imposed and estimated errors [mm]'

n.i. means 'Non identifiable parameter'

Table 4.9: Mean and Maximum errors on the end-effector position considering the geometrical errors identified through the end-effector position and the points A_{11} and A_{12}

| | | Simulation | | | | | |
| | | First | | Second | | Third | |
		Wo.I.	W.I.	Wo.I.	W.I.	Wo.I.	W.I.
$\vec{x}$ Error [mm]	Max	17.8974	2.4836	10.1081	1.0690	12.6308	1.0926
	Mean	2.3993	0.4430	1.5143	0.2150	14.3134	0.3006
$\vec{z}$ Error [mm]	Max	18.1491	1.2758	8.7915	0.5787	2.8064	0.8893
	Mean	4.6268	0.2653	1.7886	0.1343	6.0514	0.4489

Wo.I. means 'Without identification'
W.I. means 'With identification'

Conclusions The results of the simulations are similar to the ones in Sections 4.2.2.1 and 4.2.2.2, with the exception of the number of the identified parameters which is ten. This entails a bigger oscillation in the end-effector errors although there still remains a significant improvement in the model performances, as one sees in Figure 4.5.
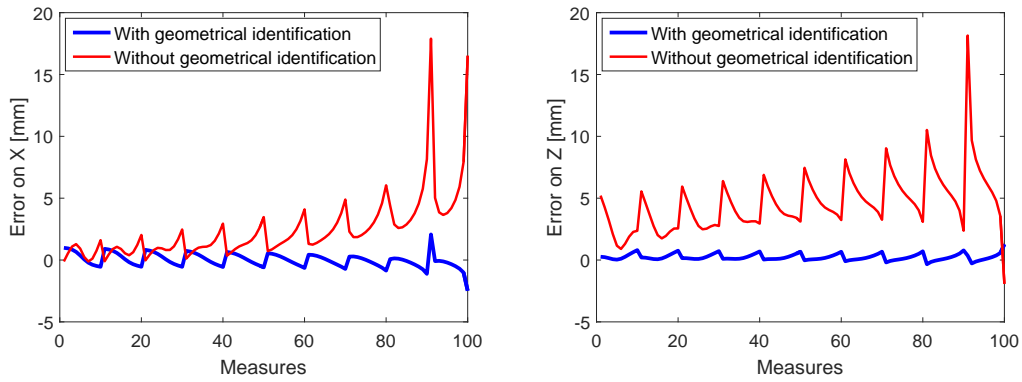
(a.1) Comparison along $\vec{x}$ direction
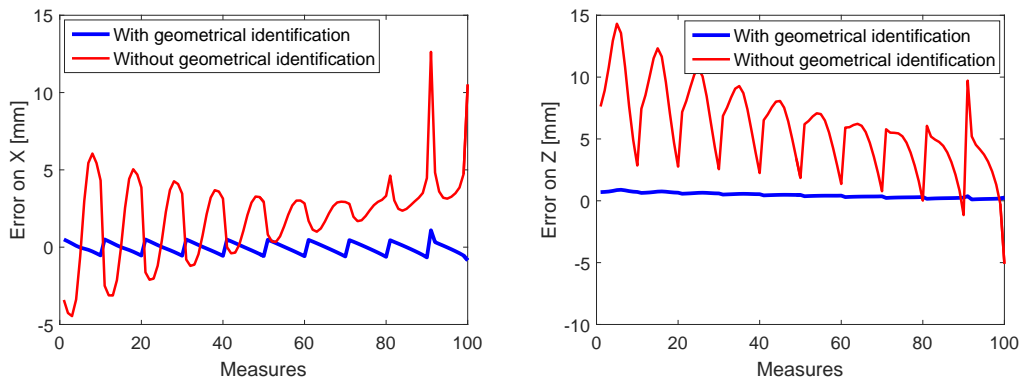
(a.2) Comparison along $\vec{z}$ direction

(a) First simulation

(b.1) Comparison along $\vec{x}$ direction

(b.2) Comparison along $\vec{z}$ direction

(b) Second simulation
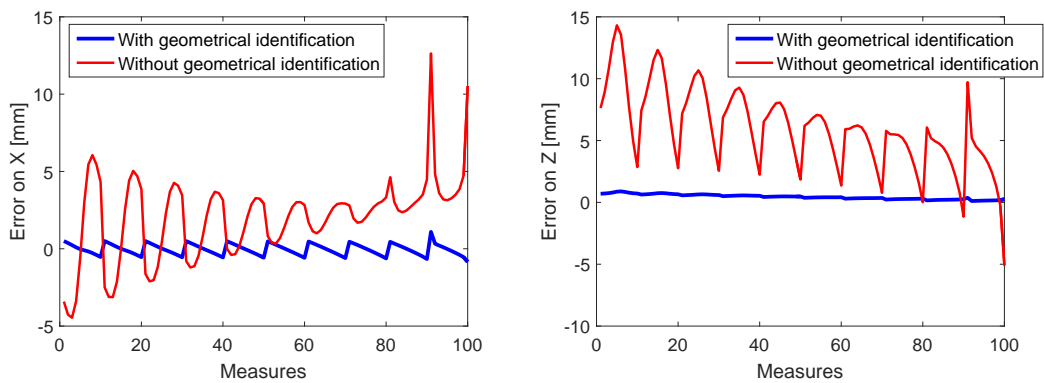
(c.1) Comparison along $\vec{x}$ direction

(c.2) Comparison along $\vec{z}$ direction

(c) Third simulation

Figure 4.5: Comparison between the end-effector position with and without the geometrical errors identified through the end-effector position and the points A_{11} and A_{12}

(a) First simulation

(b) Second simulation

(c) Third simulation
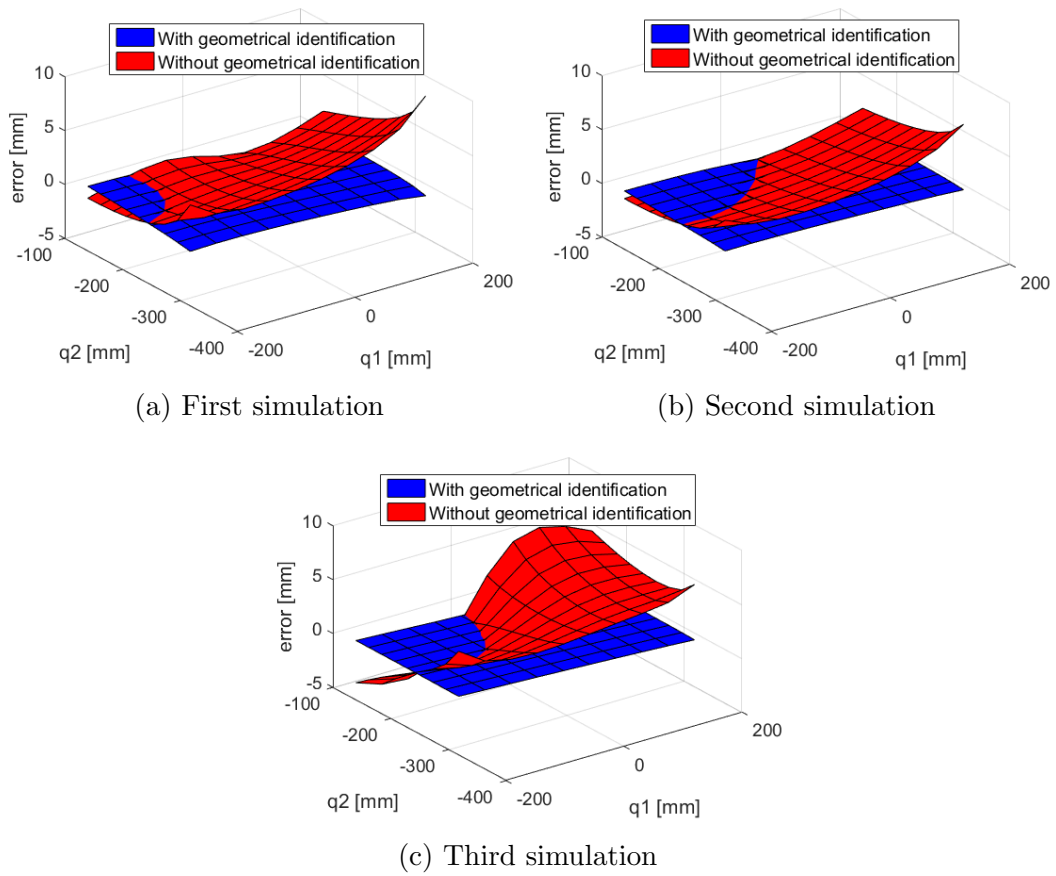
Figure 4.6: Comparison between the end-effector errors with and without the geometrical errors identified through the end-effector position and the points A_{11} and A_{12}

4.2.2.4   End-effector position and angles θ_A, $\theta_{A_{32}}$, θ_{A_3}

Another possibility is to consider the end-effector position and the third-loop angles, therefore, following the procedure explained in Section 4.2, Equation (4.2) becomes

$$
\begin{bmatrix} \dfrac{\delta P}{\|\delta P\|} \\[2mm] \dfrac{\delta\theta_A}{\|\delta\theta_A\|} \\[2mm] \dfrac{\delta\theta_{A32}}{\|\delta\theta_{A32}\|} \\[2mm] \dfrac{\delta\theta_{A3}}{\|\delta\theta_{A3}\|} \end{bmatrix} = \begin{bmatrix} \dfrac{J_P}{\|\delta P\|} \\[2mm] \dfrac{J_{\theta A}}{\|\delta\theta_A\|} \\[2mm] \dfrac{J_{\theta A32}}{\|\delta\theta_{A32}\|} \\[2mm] \dfrac{J_{\theta A3}}{\|\delta\theta_{A3}\|} \end{bmatrix} \begin{bmatrix} \delta K \end{bmatrix} \tag{4.12}
$$

Simulations results   Table 4.10 shows the results of the simulation whereas Table 4.11 reports the linear dependence of the identified parameters from the non-identifiable ones. In Figure 4.7 and Table 4.12 is reported the comparison between the Matlab® model, with the parameter identification through the measures on the end-effector position plus the third loop angles, and the Matlab® model without the identification. Furthermore Table 4.12 shows also the performances achieved through the identification.

Table 4.10: Geometrical errors identification through the end-effector position and the angles θ_A, $\theta_{A_{32}}$, θ_{A_3}

Parameter	Simulation								
	First			Second			Third		
	I.E.	E.E	Δ.E.	I.E.	E.E	Δ.E.	I.E.	E.E	Δ.E.
q_1	-0.1	-0.1379	0.0379	0.4	0.4029	0.0029	-0.5	-0.5189	0.0189
q_2	-0.9	-0.9023	0.0023	-0.1	-0.1175	0.0175	-0.7	-0.6989	0.0011
$L_{1,1}^u$	-0.4	-0.4577	0.0576	-0.7	-0.7130	0.0130	-0.8	-0.8119	0.0119
$L_{1,2}^u$	-0.3	-0.4674	0.1674	-0.9	-1.117	0.2170	0.3	0.3708	0.0707
$L_{1,1}^l$	-0.9	-0.9897	0.0897	-1	-1.0696	0.0696	0.6	0.5847	0.0153
$L_{1,2}^l$	-0.4	-0.2692	0.1308	0.1	0.3332	0.2331	0.4	0.2920	0.1080
$L_{2,1}^u$	0.2	1.0536	0.8536	-0.5	0.4903	0.9903	-0.8	-1.032	0.2320
$L_{2,2}^u$	0.1	0.9687	0.8687	0.6	1.5339	0.9339	0.1	-0.8581	0.9581
$L_{2,1}^l$	-1	-0.3483	0.6517	-0.7	n.i.	/	1	n.i.	/
$L_{2,2}^l$	0.7	1.5515	0.8515	-0.8	0.0084	0.8084	0.8	0.5884	0.2116
$L_{3,1}^u$	0.9	n.i.	/	0.7	n.i.	/	-0.1	n.i.	/
$L_{3,2}^u$	1	n.i.	/	-0.8	-2.0249	1.2249	-0.9	0.1834	1.0834
$L_{3,1}^l$	0.7	-0.3270	1.027	0.4	-0.7402	1.1402	-0.9	0.1346	1.0346
$L_{3,2}^l$	1	0.1126	0.8874	0.6	-0.1485	0.7485	0.7	0.7968	0.0968

I.E. means 'Imposed errors [mm]'

E.E. means 'Estimated errors [mm]'

Δ.E. means 'Difference between the imposed and estimated errors [mm]'

n.i. means 'Non identifiable parameter'

Table 4.11: Combination of the other parameters with the identification through the end-effector position and the angles θ_A, $\theta_{A_{32}}$, θ_{A_3}

Parameter	Combination of other parameters		
	First simulation	Second simulation	Third simulation
q_1	Independent value	Independent value	Independent value
q_2	Independent value	Independent value	Independent value
$L_{1,1}^u$	Independent value	Independent value	Independent value
$L_{1,2}^u$	Independent value	Independent value	Independent value
$L_{1,1}^l$	Independent value	Independent value	Independent value
$L_{1,2}^l$	Independent value	Independent value	Independent value
$L_{2,1}^u$	$L_{21}^u + L_{31}^u$	$L_{21}^u + L_{31}^u$	$L_{21}^u + L_{31}^u$
$L_{2,2}^u$	$L_{22}^u + L_{32}^u$	$L_{22}^u - L_{21}^l$	$L_{22}^u - L_{21}^l$
$L_{2,1}^l$	$L_{21}^l + L_{32}^u$	/	/
$L_{2,2}^l$	$L_{22}^l + L_{31}^u$	$L_{22}^l + L_{31}^u$	$L_{22}^l + L_{31}^u$
$L_{3,1}^u$	/	/	/
$L_{3,2}^u$	/	$L_{21}^l + L_{32}^u$	$L_{21}^l + L_{32}^u$
$L_{3,1}^l$	$L_{31}^l - L_{32}^u$	$L_{21}^l + L_{31}^l$	$L_{21}^l + L_{31}^l$
$L_{3,2}^l$	$L_{32}^l - L_{31}^u$	$L_{32}^l - L_{31}^u$	$L_{32}^l - L_{31}^u$

Conclusions The identifiable geometrical errors are twelve and the model with the identified parameters has approximately the same performances as with the identification through the measures on the end-effector position plus the first loop angles.
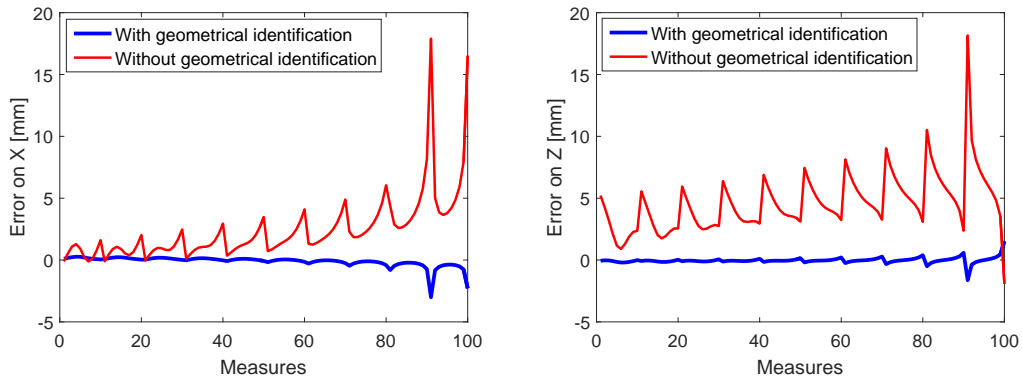
(a.1) Comparison along $\vec{x}$ direction
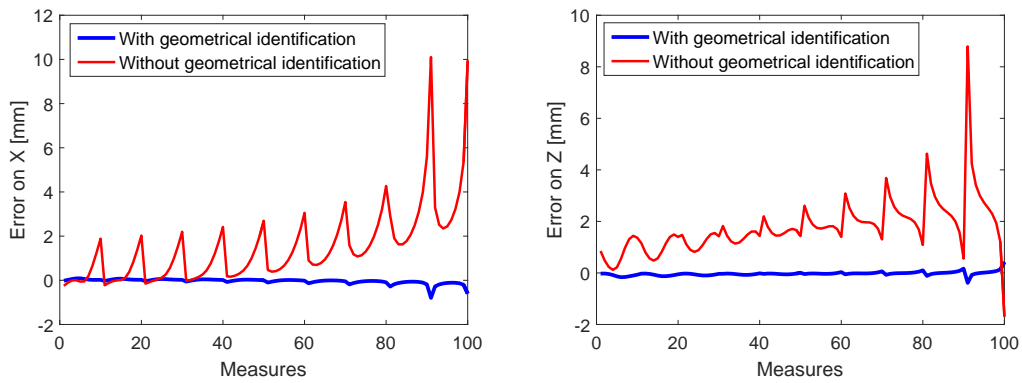
(a.2) Comparison along $\vec{z}$ direction

(a) First simulation

(b.1) Comparison along $\vec{x}$ direction

(b.2) Comparison along $\vec{z}$ direction

(b) Second simulation
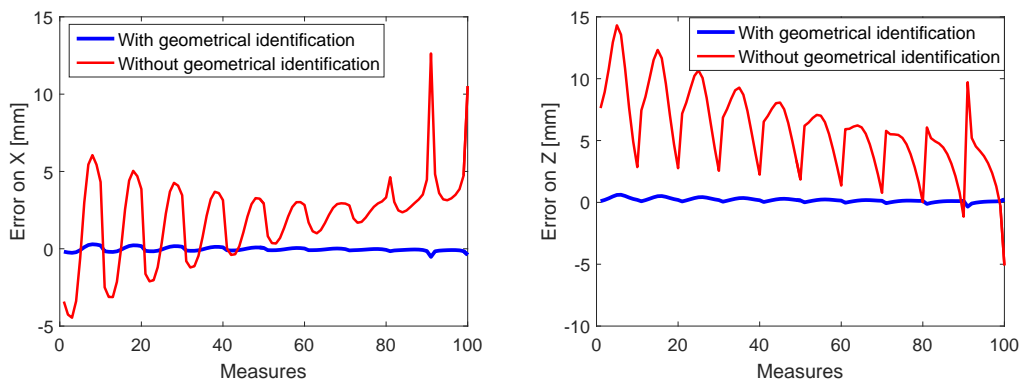
(c.1) Comparison along $\vec{x}$ direction

(c.2) Comparison along $\vec{z}$ direction

(c) Third simulation

Figure 4.7: Comparison between the end-effector position with and without the geometrical errors identified through the end-effector position and the angles θ_A, $\theta_{A_{32}}$, θ_{A_3}

Table 4.12: Mean and Maximum errors error on the end-effector position considering the geometrical errors identified through the end-effector position and the angles θ_A, $\theta_{A_{32}}$, θ_{A_3}

		Simulation					
		First		Second		Third	
		Wo.I.	W.I.	Wo.I.	W.I.	Wo.I.	W.I.
$\vec{x}$ Error [mm]	Max	17.8974	3.0090.	10.1081	0.7979	12.6308	0.5255
	Mean	2.3993	0.2301	1.5143	0.0705	14.3134	0.1105
$\vec{z}$ Error [mm]	Max	18.1491	1.6289	8.7915	0.4245	2.8064	0.6166
	Mean	4.6268	0.1411	1.7886	0.0566	6.0514	0.1993

Wo.I. means 'Without identification'
W.I. means 'With identification'

(a) First simulation

(b) Second simulation

(c) Third simulation

Figure 4.8: Comparison between the end-effector errors with and without the geometrical errors identified through the end-effector position and the angles θ_A, $\theta_{A_{32}}$, θ_{A_3}

4.2.2.5 Results of the simulations

The results of the simulations are summarized in the following tables and figures. In all the three simulations there is an increment in the performances of the model.
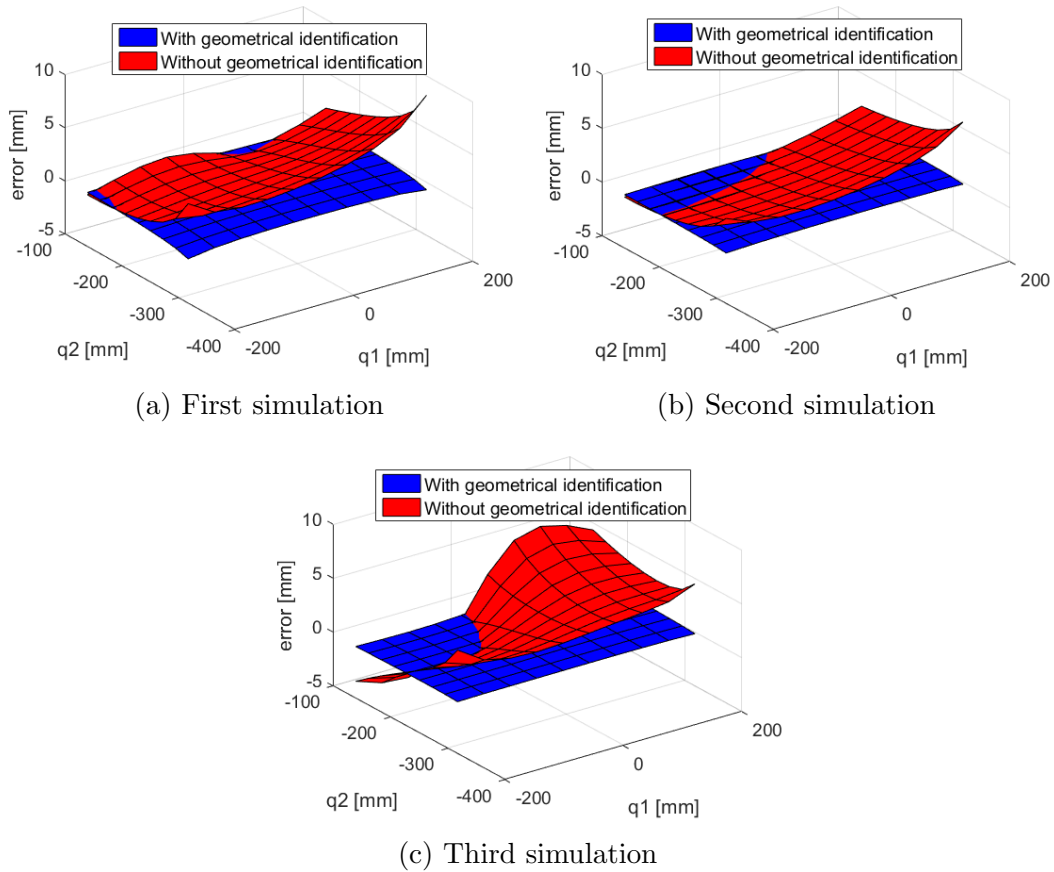
There are three main things to consider in order to take the best choice of the parameters to measure for the identification:

1. The increment in the accuracy of the model.

2. The number of the geometrical errors identifiable

3. The accuracy in the identification procedure

In Table 4.13 is reported the number of the identifiable parameters and the accuracy of the model with the identified geometrical errors. The results are largely influenced by the values of the geometrical errors.

Scope of this paragraph is to evaluate which are the best points to measure. The maximum value of the end-effector position errors was considered as the most important value to minimize, therefore it is reported in Table 4.13. The main reason is that the maximum error on the end-effector positions represents the upper limit of the precision of the pantograph. From the results reported in Table 4.13 is not possible to identify the best measure points, therefore, to analyse the increment in the accuracy on the end-effector position, we consider Table 4.14. In the last row of Table 4.14 one sees that the identification through the measures on the end-effector plus the angles θ_A, $\theta_{A_{32}}$, θ_{A_3} entails the best increment in the accuracy. With the scope of choosing the best points to measure further consideration were made. The Monte Carlo method, described in Section 4.2.1, does not supply the best points to measure but the measures on the end-effector position plus the angles provide the best results in terms of accuracy. Moreover the best measure points found by the Monte Carlo method provide the biggest number of identifiable parameters. A further aspect to evaluate is the accuracy on the identified parameters, reported in Figure 4.9. The identification with the measures on the end-effector plus the angles entails a smaller error, with the exclusion of Figure 4.9b where the best measure configuration is not easily distinguishable.

In conclusion, the identification through the measures on the end-effector position and angles is the best choice. The choice of the angles θ_A, $\theta_{A_{32}}$, θ_{A_3} entail slightly better performances than with the angles θ_A, $\theta_{A_{21}}$, θ_{A_2}, therefore the end-effector plus the third loop angles are the best points to measure for the geometrical calibration.

Table 4.13: Number of the identifiable parameters and the maximum errors on the end-effector position with a comparison between the different parameters measured for the identification of the geometrical errors

		E.F.	E.F. θ_A $\theta_{A_{21}}$ θ_{A_2}	E.F. A_{11} A_{12}	E.F. θ_A $\theta_{A_{32}}$ θ_{A_3}
Identifiable parameters		6	12	10	12
1st simulation	$\vec{x}$ error [mm]	7.8229	3.1454	2.4836	3.0090
	$\vec{z}$ error [mm]	4.8364	1.7308	1.2758	1.6289
2nd simulation	$\vec{x}$ error [mm]	0.7288	0.8996	1.0690	0.7979
	$\vec{z}$ error [mm]	0.3941	0.4665	0.5787	0.4245
3rd simulation	$\vec{x}$ error [mm]	0.3382	0.4983	1.0926	0.5255
	$\vec{z}$ error [mm]	0.3573	0.5950	0.8893	0.6166

Table 4.14: Comparison between the identification through the different parameters measured in terms of accuracy percentage increment in the end-effector position

		E.F.	E.F. θ_A $\theta_{A_{21}}$ θ_{A_2}	E.F. A_{11} A_{12}	E.F. θ_A $\theta_{A_{32}}$ θ_{A_3}
1st simulation	$\vec{x}$ error	56.29%	82.43%	86.12%	83.19%
	$\vec{z}$ error	73.35%	90.46%	92.97%	91.02%
2nd simulation	$\vec{x}$ error	92.79%	91.10%	89.42%	92.10%
	$\vec{z}$ error	95.52%	94.69%	93.42%	95.17%
3rd simulation	$\vec{x}$ error	97.32%	96.05%	91.35%	95.84%
	$\vec{z}$ error	87.27%	78.80%	68.31%	78.03%
Mean value		**83.76%**	**88.92%**	**86.93%**	**89.23%**
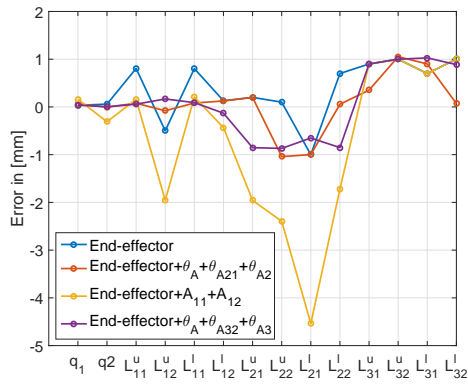
(a) First simulation
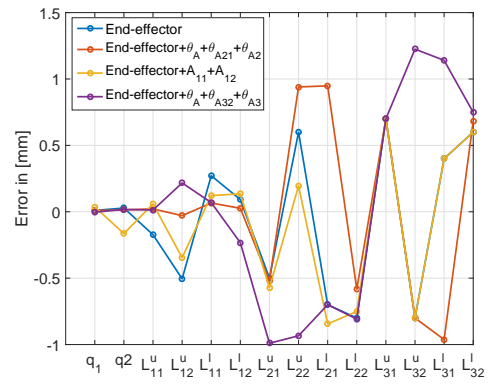
(b) Second simulation
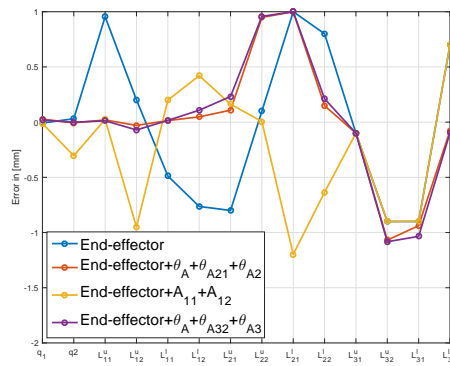
(c) Third simulation

Figure 4.9: Error in the identification of the geometrical errors

CHAPTER 5

System mock-up, measure procedure and results

The calibration of the analytical model was performed through experiments, therefore it is necessary to chose the correct experimental set-up and the parameters to identify in order to make the identification the most accurate possible.

5.1 Experimental set-up
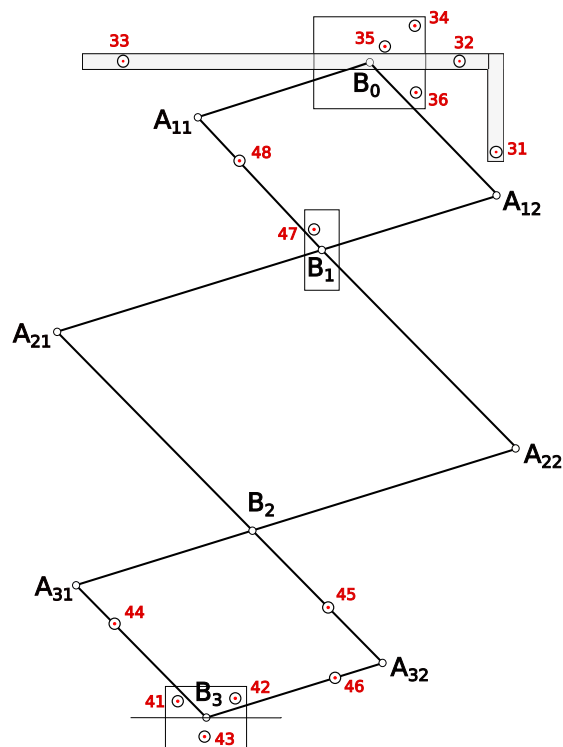
Figure 5.1: Led set-up

The parameters to identify are the two driven coordinates q_1 and q_2, the end-effector position and the angles necessary to characterize the structure. To provide the information needed, the *Nikon K610* measuring system was used. This led configuration gives let us to follow the points which we want to measure. As

displayed in Figure 5.1 fourteen is the minimum number of led required in order to obtain the parameters needed. The first digit of the name of the led represents the port of the measuring system controller in which the led is set, whereas the second digit represent the number of the led connected to the considered port and goes from one to six for the port three and from one to eight for port four. In Table 5.1 the purpose of each led is described. Through the camera is possible to

Table 5.1: Led number and their purpose

Led name	What it represents
31 32 33	Define the dynamic frame attached to the main reference system
34 35 36	Define the dynamic frame connected to the point B_0, which is the horizontal driven coordinate
41 42 43	Define the dynamic frame connected to the end-effector
44	Defines the point A_{31}
45 46	Define the points A_{32} and B_2
47	Defines the point B_1, which represents the vertical driven coordinate
48	Defines the point A_{11}

follow the led in the workspace whereas with a dynamic reference system is possible to know the position of the origin of this reference system, which represents a point to measure A dynamic frame is defined by a centre, which is the point to measure, and by three led. Considering, for example, the point B_0, as reported in Figure 5.1, it was taken as the centre of a circle using the Spaceprobe. To increase the precision and avoid measure errors, three circles were taken. Three circle centres were interpolated to obtain the most accurate centre of the bearing that makes the point B_0. The dynamic frame, made by the led 34, 35 and 36, is attached to the point B_0. Measuring the position of the three led we obtain a vector made by six elements, the first three represent the position of B_0, and other three represent the orientation of the dynamic frame. There are two other possibilities to obtain the position of a point. The first one can be used only if the led and the point don't change their distance and orientation in the space. For example the point B_1. In this case the offset between the led 47 and the point B_1 was calculated as the difference between the position of the led 47 and the position of the point B_1 (using the Spaceprobe and interpolating three centre

of circles as described for B_0). Therefore between the led and the point B_1 was considered fixed during all the measurements. The second possibility, known the position of one led, is to take the offset between the led and the point. The knowledge of the offset is not enough for calculate the position of a point because the orientation between the led and the point changes, therefore more informations are needed. Assuming to know the position of the led and the point P_1, as reported in Figure 5.2, we can use the *Cosines law*, reported in Equation (5.1), to calculate the necessaries angles. Once the angle α is calculated, through the angles γ and θ we can obtain the Equation (5.4) which gives the position of the point P_2.

$$\alpha = \arccos \left(\frac{\overline{P_2 P_1}^2 + \overline{Led\ P_1}^2 - \overline{P_2\ Led}^2}{2\ \overline{P_2 P_1}\ \overline{Led\ P_1}} \right) \tag{5.1}$$

$$\gamma = ata2\left((Z_{Led} - Z_{P_1}), (X_{Led} - X_{P_1})\right) \tag{5.2}$$

$$\theta = \gamma + \alpha \tag{5.3}$$

Therefore one obtains

$$P_2 = \begin{bmatrix} X_{P_1} + \overline{P_2 P_1}\ \cos(\theta) \\ 0 \\ Y_{P_1} + \overline{P_2 P_1}\ \sin(\theta) \end{bmatrix} \tag{5.4}$$

The described processes are used to calculate the position of the points of the structure needed for the identification of the elastic and geometrical parameters.
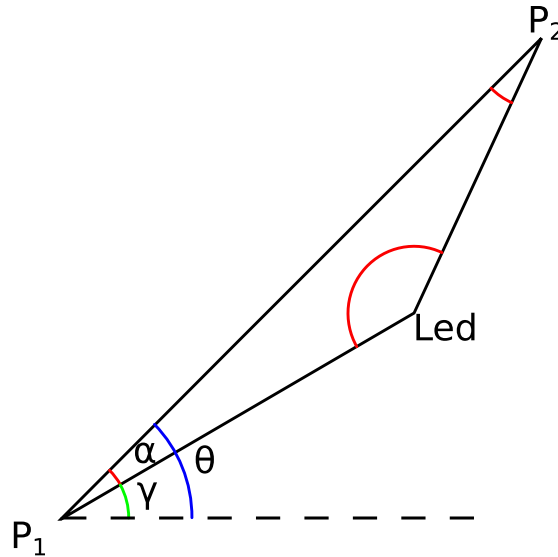
Figure 5.2: Explanation of the *Cosines law*

5.2 Description of the model

The studied structure is shown in Figure 5.3. It was made with eight[1] aluminium links connected with bearings. The properties of the material used are reported in Table 5.2 and the geometrical properties in Tables 5.3 and 5.4.
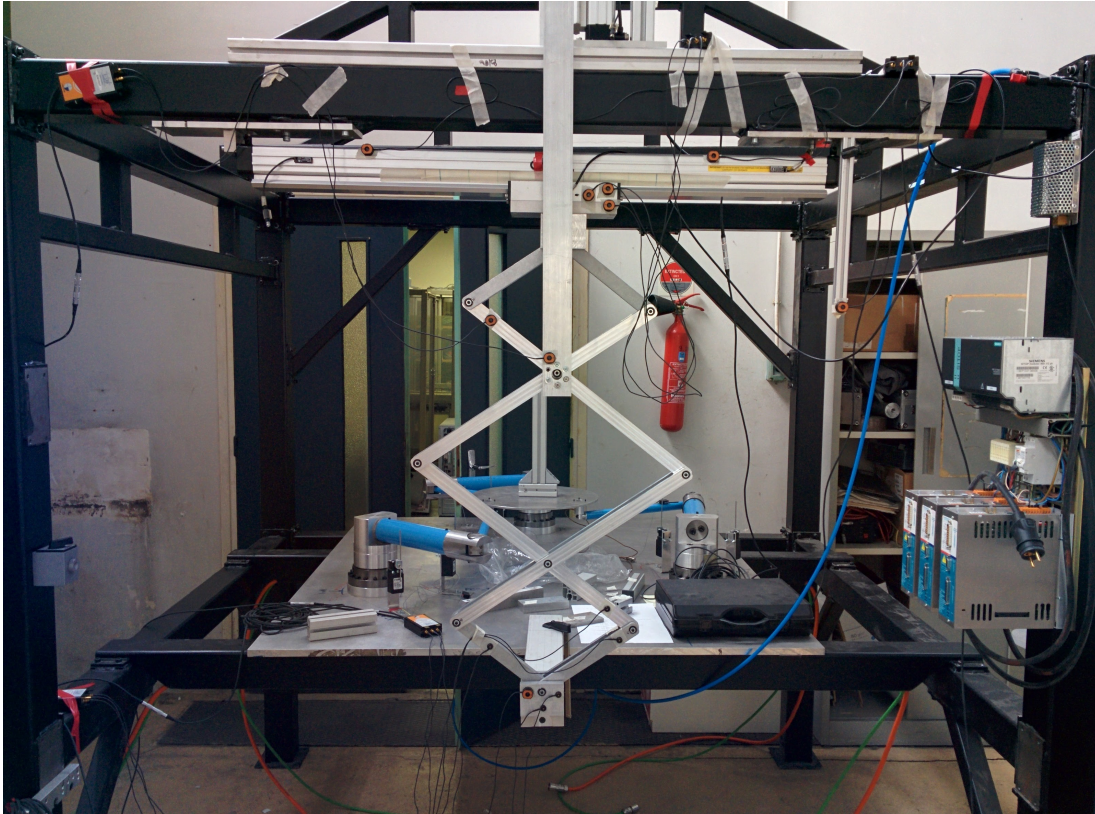
Figure 5.3: Pantograph real mock-up

Table 5.2: Material properties of the structure

Material	Young's modulus	Coulomb's modulus	Poisson modulus	Density
Aluminium	70 GPa	2.6 GPa	0.346	2710 kg m^{-3}

---

[1]In the dissertation was considered twelve links instead of eight because they actually represent the finite elements due to the assumption introduced by the *Finite element method*.

Table 5.3: Area properties of the links

Cross sectional area	I_y	I_z	J
4×10^{-4} m	8.533×10^{-9} m	10^{-8} m	10^{-8} m

Table 5.4: Length of the links

$L_{1,1}^u$ [m]	$L_{1,2}^u$ [m]	$L_{1,1}^l$ [m]	$L_{1,2}^l$ [m]	$L_{2,1}^u$ [m]	$L_{2,2}^u$ [m]	$L_{2,1}^l$ [m]	$L_{2,2}^l$ [m]	$L_{3,1}^u$ [m]	$L_{3,2}^u$ [m]	$L_{3,1}^l$ [m]	$L_{3,2}^l$ [m]
0.2	0.2	0.2	0.2	0.3	0.3	0.3	0.3	0.2	0.2	0.2	0.2

5.3 Measurement steps

Once the led are placed, as describe before, it is necessary to pursue the following steps in order to define all the parameters needed for the identification of the elastic and geometrical characteristics of the structure.

- Definition of the frames

  1 Define the plane in which project all the points. The plane which contains B_0 is the plane taken as reference plane.

  2 Define the $\vec{x}$ and $\vec{z}$ axis using two point for each direction (for each point create a cloud of points and interpolate them in order to increase the accuracy).

  3 The main static frame is defined through the definition of the axis and the origin (intersection of the axis).

  4 Attached to the static frame a dynamic frame is created using the led 31, 32 and 33.

  5 Taking with the SpaceProbe the point B_0 and create a dynamic frame attached to this point with the led 34, 35 and 36.

  6 Repeat the previous step with the point B_3 and the led 41, 42 and 43.

- Definition of the joint of the structure

  1 Measure with the SpaceProbe the point B_1 and calculate the offset from the led 47. The offset is the same for all the configurations.

  2 Take with the SpaceProbe the point $A_{1,1}$ and calculate the offset from the led 48.

  3 Repeat the previous step consider the points B_2, $A_{3,1}$ and $A_{3,2}$ with the led 45, 44 and 46.

- Measurements

1 Define the number of measures needed and create a grid in the workspace.

2 For each couple of coordinates q_1 and q_2,which define the grid, measure the position of the led.

3 Repeat the measure with three different loads in order to have the measures to perform the calibration of the joint stiffness.

Knowing the position of the led mentioned before, the angles necessary to identify the geometrical parameters can be calculated using the *Law of cosines.*

5.3.1 Measures

A real-time analysis of the results was performed during the measurements. The measures, in terms of end-effector position and angles, were compared with the ones obtained through the analytical model. The measured coordinates q_1 and q_2 were used as input for the analytical model in order to obtain a correct comparison. Table 5.5 shows an example of the comparison between the measures and the analytical model. From Table 5.5b, we note that the calculated and measured position are different, this is due to the absence of the calibration, moreover we could see that the z coordinate increase increasing the load and that the delta position between different loads, reported in Table 5.5c, also increase increasing the load. Therefore we could conclude that the measures and the model are coherent. The coherence is also shown in Figure 5.4 where we could observe the differences between the measure and the non-calibrated model. Moreover, from Table 5.5a, we note that the coordinate q_2 is influenced by the applied load, this is due to the elastic deformation of the structure that lead this coordinate.

Table 5.5: Example of comparison between the measures and the analytical model

(a) Load and driven coordinates

Measure number	Load [kg]	$q_1[\mathrm{m}]$	$q_2[\mathrm{m}]$
10	7,1030	0,0713	-0,1915
	11,8690	0,0713	-0,1915
	16,6360	0,0713	-0,1915
22	7,1030	0.0716	-0.2704
	11,8690	0.0716	-0.2705
	16,6360	0.0716	-0.2705

(b) End-effector position with the three different loads

Measure number	Load	x coordinate		z coordinate	
		Calculated	Measured	Calculated	Measured
10	1st	-0.1785	-0.1735	-0.6742	-0.6753
	2nd	-0.1787	-0.1737	-0.6765	-0.6779
	3rd	-0.1788	-0.1738	-0.6788	-0.6805
22	1st	-0.1780	-0.1720	-0.9496	-0.9507
	2nd	-0.1777	-0.1718	-0.9514	-0.9533
	3rd	-0.1774	-0.1714	-0.9532	-0.9548

(c) End-effector displacement between the first and the second load and between the first and the third load

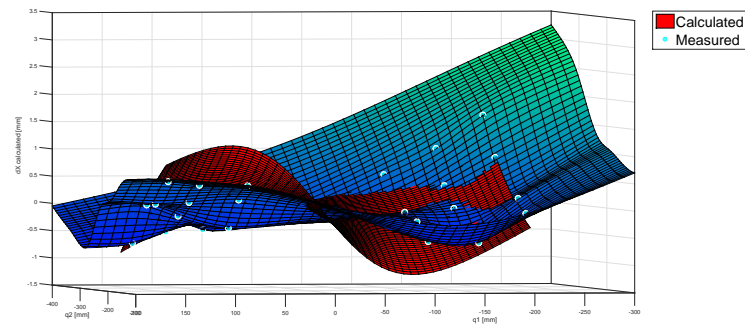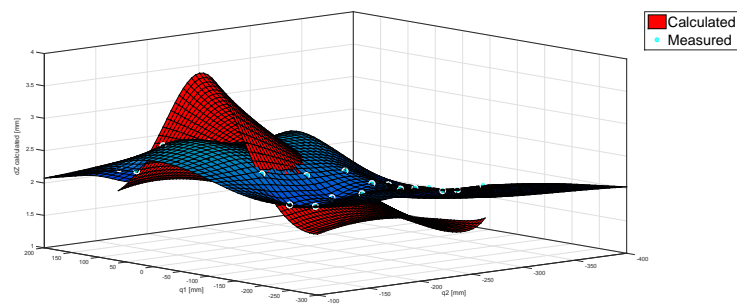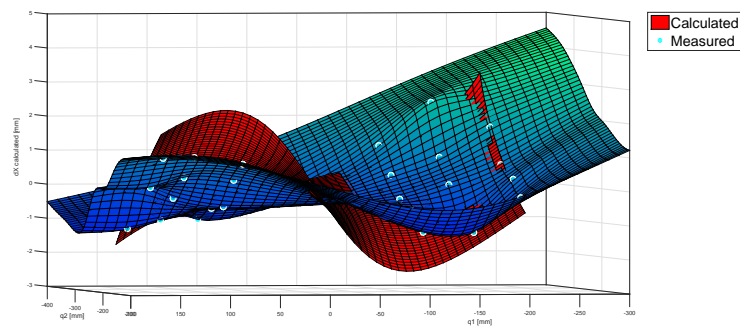| Measure number	Displacement	$\vec{x}$ displacement		$\vec{z}$ displacement	
		Calculated	Measured	Calculated	Measured
10	1st-2nd	0.2286	0.1742	2.2788	2.6094
	1st-3rd	0.3675	0.2916	4.5828	5.2604
22	1st-2nd	-0.3470	-0.2035	1.7745	2.5706
	1st-3rd	-0.6362	-0.6048	3.5611	4.1106

(a) $\vec{x}$ displacement between the first and second load

(b) $\vec{z}$ displacement between the first and second load

(c) $\vec{x}$ displacement between the first and third load
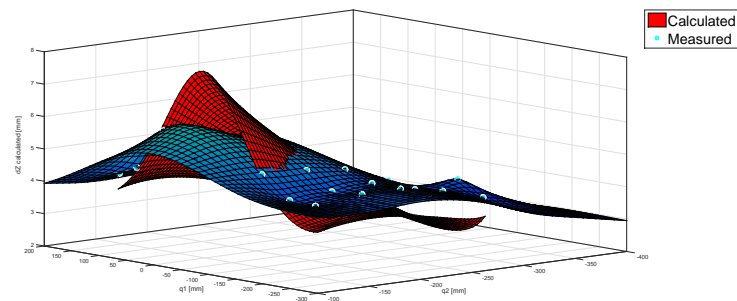
(d) $\vec{z}$ displacement between the first and third load

Figure 5.4: Comparison between the displacement obtained from the measure and from the analytical model

5.4 Results

The scope of the measures is to make the identification of both the joints stiffness and the geometrical errors. The identification steps are described in Chapter 4.

5.4.1 Stiffness of the joints

Two different methods were used in order to identify the stiffness of the joints. The first method considers the vector addition of the $\vec{x}$ and $\vec{z}$ errors, where the errors are calculated subtracting the measured displacement from the one calculated by the Matlab® model. The second method consists in minimizing the sum of the errors. A comparison was made in order to point out the best method.

The two methods generate similar results, as shown in Table 5.6 and Fig. 5.5. Using the sum of the errors, we obtain bigger errors along $\vec{z}$ but smaller along $\vec{x}$, whereas the vector addition (which uses the Pitagora's theorem) of the errors entails smaller position errors. The choice of the method, as described in Section 4.1, depends on the purpose of the work. The minimization of the errors along $\vec{x}$ and $\vec{z}$ is the scope of the calibration, therefore the method that gives the best results is the sum of the errors. The stiffness of the joints is therefore considered as $3.3152 \times 10^6 \, \text{N} \, \text{m}^{-1}$. However the accuracy on the end-effector displacement is quite big, considering that the pantograph is used as a coordinate measuring arm.

Table 5.6: Comparison between the vector addition of the errors and the sum of the errors methods

(a) Comparison of the two methods with the errors on the end-effector displacement from the first to the second load

Method used	Mean end-effector error [mm]			Max absolute end-effector error [mm]		
	Error along $\vec{x}$	Error along $\vec{z}$	Position error	Error along $\vec{x}$	Error along $\vec{z}$	Position error
Vector addition of the errors	-0.0301	0.0936	0.2034	0.2209	0.5835	0.6020
Sum of the errors	-0.0289	0.1039	0.2042	0.2114	0.5922	0.6104

(b) Comparison of the two methods with the errors on the end-effector displacement from the first to the third load

Method used	Mean end-effector error [mm]			Max absolute end-effector error [mm]		
	Error along $\vec{x}$	Error along $\vec{z}$	Position error	Error along $\vec{x}$	Error along $\vec{z}$	Position error
Vector addition of the errors	-0.1035	0.1859	0.3487	0.4174	0.4916	0.6727
Sum of the errors	-0.1012	0.2065	0.3525	0.3984	0.5161	0.6451
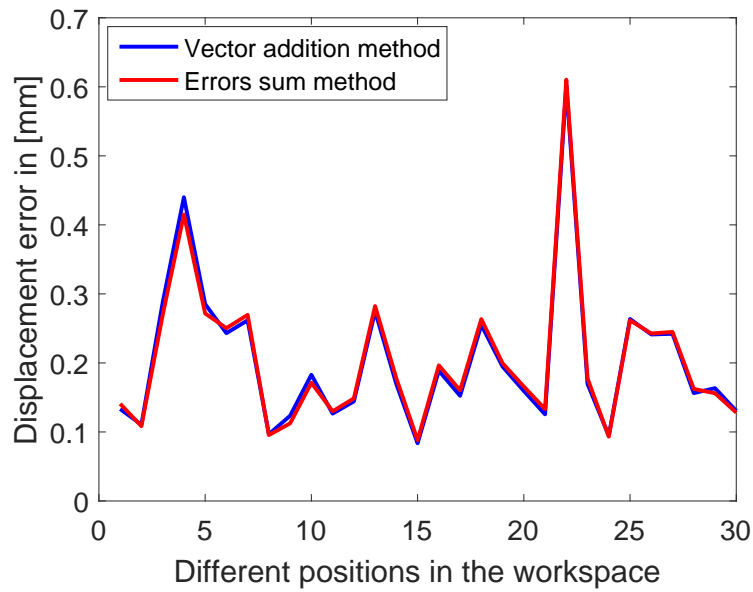
(a) Comparison of the two methods with the errors on the end-effector displacement from the first to the second load

(b) Comparison of the two methods with the errors on the end-effector displacement from the first to the third load
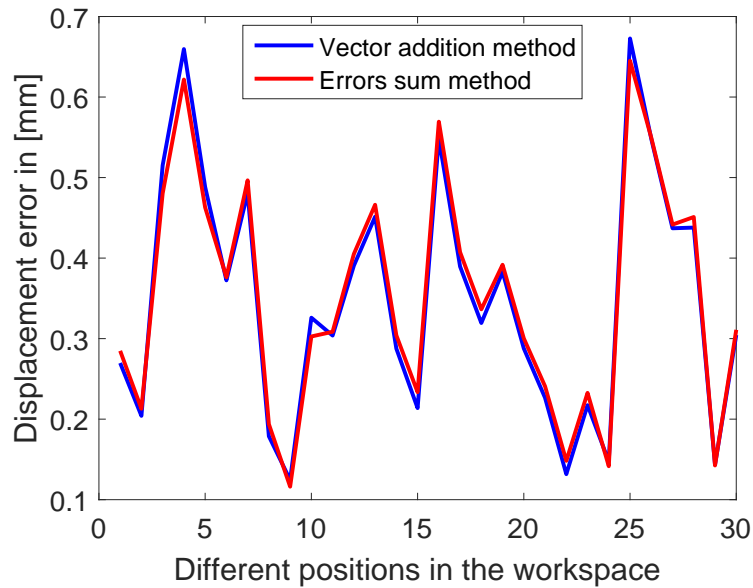
Figure 5.5: Comparison of the displacement error between the vector addition of the errors and the sum of the errors methods

5.4.2 Identification of the geometrical errors

The simulations reported in Section 4.2.2 demonstrate that the identification through the measures on the end-effector and the angles θ_A, $\theta_{A_{32}}$, θ_{A_3} is the best compromise for the geometrical errors identification. Despite this, the identification though the measures on the end-effector position was considered as a means of comparison for its good performances in terms of accuracy on the end-effector position.

Once the stiffness of the joints was obtained, the measures can be used for the geometrical errors identification, as described in Section 4.2. The identification uses the measures with the lightest load for the identification and the measures with the other loads to verify the results.

The identification through the measures on the end-effector and the angles θ_A, $\theta_{A_{32}}$, θ_{A_3} entails the results reported in Table 5.7a and Fig. 5.6a. There is a big increment in the accuracy of the Matlab$^{\circledR}$ model along the $\vec{x}$ direction, whereas along $\vec{z}$ the errors identification slightly increases the accuracy of the model. This is due to the fact that the errors along $\vec{x}$ are twice as much the errors along $\vec{z}$, therefore the identification procedure tends to find the geometrical errors in order to achieve the best compromise between the reduction of both errors. If an error is bigger, it tends to minimize it, instead of minimize the other one. This behaviour is clearly visible in Figure 5.6a. The mean and maximum values of the errors, reported in Table 5.7a, explain that the errors are generally quite small but there is a quite big one. The errors along $\vec{x}$ have some big and some very small values, the same for the errors along $\vec{z}$ but with a decreasing trend. The cyclic behaviour of the errors means that they depend on the configuration of the pantograph. Therefore there is not a constant trend through the different configurations.

In Table 5.7 and Fig. 5.6 there is a comparison between the errors on the end-effector positions with the identification through the measures on the end-effector and on the end-effector plus the last loop angles. The identification through the measures on the end-effector only achieve better results in terms of mean value, whereas for the errors along $\vec{z}$ there is a configuration with a big error. The cyclic behaviour reported in Figure 5.6a is not shown in Figure 5.6b where there is not a specific walk. As reported in Section 4.2.2.5, the identification through the measures on the end-effector plus the third loops angles has a big number of the identifiable geometrical errors.

In order to obtain the smallest maximum value of the errors, the identification through the end-effector and the angles θ_A, $\theta_{A_{32}}$, θ_{A_3} is the best choice. The identified parameters from the method chosen are reported in Table 5.8.

Table 5.7: Comparison, through the mean and the maximum value, of the end-effector position errors with and without the geometrical identification

(a) Identification with the measures on the end-effector position and the angles θ_A, $\theta_{A_{32}}$, θ_{A_3}

	Mean error in [mm]			Maximum error in [mm]		
	$\vec{x}$	$\vec{z}$	v.a.	$\vec{x}$	$\vec{z}$	v.a.
with calibration	-0.2793	0.4187	0.9646	1.4089	1.1777	1.6760
without calibration	-5.3407	1.1288	5.5515	6.9714	3.3882	7.5537

v.a. means vector addition

(b) Identification with the measures on the end-effector position

	Mean error in [mm]			Maximum error in [mm]		
	$\vec{x}$	$\vec{z}$	v.a.	$\vec{x}$	$\vec{z}$	v.a.
with calibration	-0.1000	0.1496	0.6519	1.3395	2.4872	2.6013
without calibration	-5.3407	1.1288	5.5515	6.9714	3.3882	7.5537

v.a. means vector addition

Table 5.8: Geometrical errors identified from the measure with the identification through the measures on the end-effector plus the angles θ_A, $\theta_{A_{32}}$, θ_{A_3}

Parameter	value [mm]
q_1	-0.9386
q_2	1.2029
$L_{1,1}^u$	-1.2209
$L_{1,2}^u$	1.3316
$L_{1,1}^l$	-1.2530
$L_{1,2}^l$	-0.3716
$L_{2,1}^u$	1.9141
$L_{2,2}^u$	3.1189
$L_{2,1}^l$	7.2667
$L_{2,2}^l$	not identified
$L_{3,1}^u$	-2.3152
$L_{3,2}^u$	not identified
$L_{3,1}^l$	-2.3114
$L_{3,2}^l$	-0.5704

(a.1) $\vec{x}$ errors

(a.2) $\vec{z}$ errors
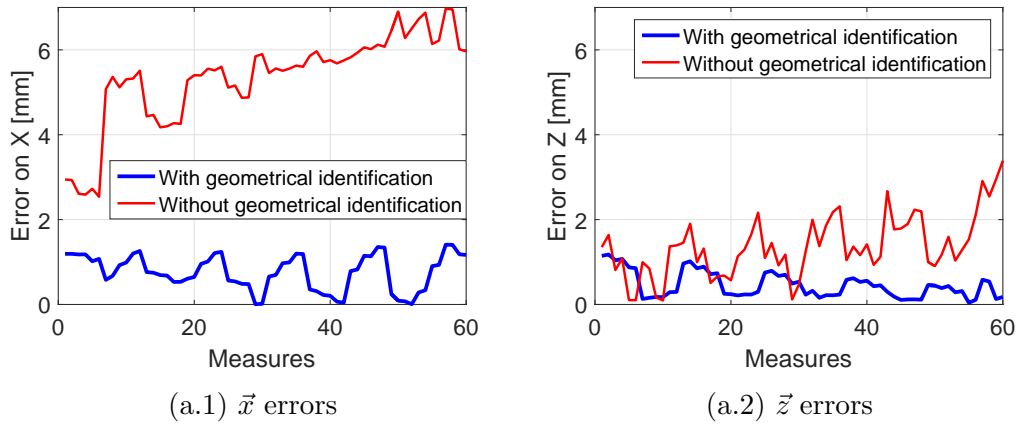
(a) Identification through the measures on the end-effector position and the angles θ_A, $\theta_{A_{32}}$, θ_{A_3}

(b.1) $\vec{x}$ errors

(b.2) $\vec{z}$ errors
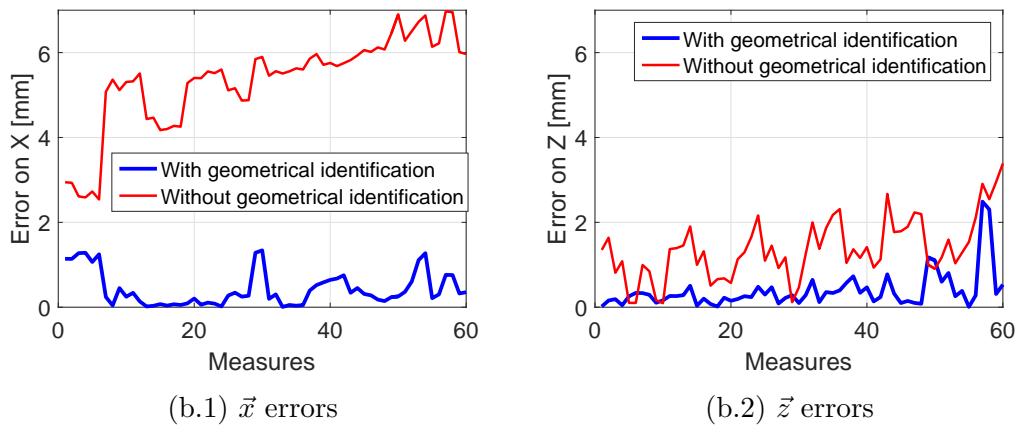
(b) Identification through the measures on the end-effector position

Figure 5.6: Comparison of the end-effector position errors with and without the geometrical calibration

CHAPTER 6

Conclusions and future perspectives

The calibration of the pantograph is the main purpose of this work; therefore a Matlab® model was developed in order to predict the end-effector position. The model presents some unknown parameters and some uncertainties:

- Stiffness of the joints

- Geometrical errors

- Temperature deformation of the structure

- Measuring system errors

- Oscillations of the model during the measure

- Deformation of the frame in which the pantograph is mounted

- Errors in the measure of the centre of the joints

A calibration procedure was developed in order to identify the joints stiffness and the geometrical parameters errors. The effect of the temperature was not taken into account. The measuring system errors and the errors due to the measure of the centre of the joints can not be avoided, while the effect of the oscillation of the structure was reduced applying a load on the end-effector. The deformation of the frame was considered negligible.

The calibration and the analysis of these uncertainties have the purpose of increment the performances of the model.

The results, reported in Table 6.1, show that the end-effector position error has a quite small mean value, whereas the maximum errors is bigger than $1.5\,mm$. Since the PKM accuracy is $\pm 0.25\,mm$, the maximum error obtained is far too big.

Table 6.1: Errors on the end-effector position after the elastic and geometrical calibration

Error direction	Mean error in [mm]	Maximum error in [mm]
$\vec{x}$	-0.2793	1.4089
$\vec{z}$	0.4187	1.1777
vector addition	0.9646	1.6760

The loss in the CMA accuracy is the consequence of the approximations made during the modelling. Some critic considerations were made in order to understand the cause of the low accuracy:

- There is a non-linear behaviour in the identification of the stiffness of the joints. As showed in Figure 5.5 the displacement errors change a lot going from a point of the workspace to another one. Therefore, the hypothesis of considering the stiffness of the joints equal for each joint should be reviewed.

- The use in Section 4.2 of the Jacobian matrix entails a linear approximation of the behaviour of the geometrical errors. The results of both the simulations, reported in Section 4.2, and the results of the comparison with the measures, showed in Figure 5.6, demonstrate that there is a correlation of the errors with the position in the workspace. The linear approximation needs therefore to be reviewed.

- The pantograph is not suitable to take the measures in an easy and accurate way, therefore the measures of the position of the joints are not accurate.

The hypotheses made during the modelling are correct, nevertheless the simplifications introduced can cause small errors and the sum of these errors can compromise the accuracy of the model. Despite this, the benefit of the method presented is clearly visible from the comparison proposed in Table 5.7. Future works can therefore increase the accuracy of the hypotheses here made. For example, the hypothesis about the equality of the stiffness of the joints could be investigated with an accurate measure of the stiffness of each joint. Moreover the identification through a non-linear technique can improve the accuracy, especially in the geometrical errors identification. A self-calibration approach, through the use of encoders on the passive joints, could be performed simultaneously with the external calibration. Moving toward the increment of the accuracy, it is possible to perform the elastic and geometrical identifications together. This can avoid errors due to the simplifications introduced by considering the two models as independent.

Bibliography

[1] Sébastien Besnard and Wisama Khalil. Identifiable parameters for parallel robots kinematic calibration. In *Proceedings 2001 ICRA. IEEE International Conference on Robotics and Automation*, volume 3, pages 2859–2866. IEEE, 2001.

[2] Claudio R Boër, Lorenzo Molinari-Tosatti, and K Scott Smith. *Parallel kinematic machines: theoretical aspects and industrial requirements*. Springer Science & Business Media, 2012.

[3] Yu-Jen Chiu and Ming-Hwei Perng. Self-calibration of a general hexapod manipulator with enhanced precision in 5-dof motions. *Mechanism and Machine Theory*, 39(1):1–23, 2004.

[4] Dominique Deblaise, Xavier Hernot, and Patrick Maurine. A systematic analytical method for pkm stiffness matrix calculation. In *Proceedings 2006 IEEE International Conference on Robotics and Automation*, pages 4213–4219. IEEE, 2006.

[5] Giorgio Diana and Federico Cheli. *Dinamica dei sistemi meccanici*. Polipress, 2010.

[6] EE Hernández Martínez, CS López-Cajún, JC Jáuregui Correa, et al. Calibration of parallel manipulators and their application to machine tools. a state of the art survey.

[7] Alexandr Klimchik, Anatol Pashkevich, Damien Chablat, and Geir Hovland. Compliance error compensation technique for parallel robots composed of non-perfect serial chains. *Robotics and Computer-Integrated Manufacturing*, 29(2):385–393, 2013.

[8] Dirk P Kroese, Thomas Taimre, and Zdravko I Botev. *Handbook of Monte Carlo Methods*, volume 706. John Wiley & Sons, 2013.

[9] Ana C Majarena, Jorge Santolaria, David Samper, and Juan J Aguilar. An overview of kinematic and calibration models using internal/external sensors or constraints to improve the behavior of spatial parallel mechanisms. *Sensors*, 10(11):10256–10297, 2010.

[10] Amit J Patel and Kornel F Ehmann. Calibration of a hexapod machine tool using a redundant leg. *International Journal of Machine Tools and Manufacture*, 40(4):489–512, 2000.

[11] YD Patel and PM George. Parallel manipulators applications, a survey. *Modern Mechanical Engineering*, 2012.

[12] Maurine Patrick and Quinet Jean-François. *L'étalonnage des robots manipulateurs industriels*. Lavoisier, 2013.

[13] Mathieu Rognant and Patrick Maurine. Elasto-geometrical modelling of a pantographic linkage used as coordinate measuring arm for pkm applications. In *Proceedings of the IFToMM 2007 World Congress*, 2007.

[14] Daniel Schütz and Friedrich M Wahl. *Robotic Systems for Handling and Assembly*, volume 67. Springer, 2010.

[15] Hanqi Zhuang. Self-calibration of parallel mechanisms with a case study on stewart platforms. *IEEE Transactions on Robotics and Automation*, 13(3): 387–397, 1997.

Appendix A

Jacobian matrices

Section 2.3 describes how to calculate the Jacobian matrices, in this appendix the details of the calculus are being explained.

The Jacobian matrix is defined as the matrix which contains the partial derivatives of the considered function. In this case it describes the dependence of the position errors from the geometrical parameters errors. Considering the generic point P, the correlation between the position errors and the geometrical errors is defined as follow

$$\boldsymbol{\delta P} = \boldsymbol{J}\,\boldsymbol{\delta K} \tag{A.1}$$

The pantograph is dived in three different loop, each loop is described with four points, therefore there will be four Jacobian matrices for each loop.

A.0.3   First loop

The first loop is described with the points A_{11}, A_{12}, B_0 and B_1. Equation (A.2) describes the geometrical parameter from which the points depend.

$$\begin{cases} \boldsymbol{\delta A}_{1,j} = \boldsymbol{J}_{A_{1,j}} \begin{bmatrix} \delta q_1 & \delta q_1 & \delta L_{1,j}^T \end{bmatrix}^T \\[2mm] \boldsymbol{\delta B}_i = \boldsymbol{J}_{B_i} \begin{bmatrix} \delta q_1 & \delta q_1 & \delta L_{1,j}^T \end{bmatrix}^T \end{cases} \tag{A.2}$$

where

$$\delta L_{1,j} = \begin{bmatrix} \delta L_{1,1}^u & \delta L_{1,2}^u & \delta L_{1,1}^l & \delta L_{1,2}^l \end{bmatrix}^T \tag{A.3}$$

For obtaining the Jacobian matrix it is necessary to use the following equation

$$\begin{bmatrix} \frac{\partial A_1}{\partial x_1} & \frac{\partial A_1}{\partial x_2} \\[2mm] \frac{\partial A_2}{\partial x_1} & \frac{\partial A_2}{\partial x_2} \end{bmatrix} \begin{bmatrix} \delta x_1 \\[2mm] \delta x_2 \end{bmatrix} + \begin{bmatrix} \frac{\partial A_1}{\partial q_1} & \frac{\partial A_1}{\partial q_2} & \frac{\partial A_1}{\partial l_1} & \frac{\partial A_1}{\partial l_2} & \frac{\partial A_{11}}{\partial l_3} & \frac{\partial A_{11}}{\partial l_4} \\[2mm] \frac{\partial A_2}{\partial q_1} & \frac{\partial A_2}{\partial q_2} & \frac{\partial A_2}{\partial l_1} & \frac{\partial A_2}{\partial l_2} & \frac{\partial A_2}{\partial l_3} & \frac{\partial A_2}{\partial l_4} \end{bmatrix} \begin{bmatrix} \delta q_1 \\[2mm] \delta q_2 \\[2mm] \delta l_1 \\[2mm] \delta l_2 \\[2mm] \delta l_3 \\[2mm] \delta l_4 \end{bmatrix} = \begin{bmatrix} 0 \\[2mm] 0 \end{bmatrix} \tag{A.4}$$

that becomes

$$
\begin{bmatrix} \delta x_1 \\ \delta x_2 \end{bmatrix} = - \underbrace{\begin{bmatrix} \frac{\partial A_1}{\partial x_1} & \frac{\partial A_1}{\partial x_2} \\ \frac{\partial A_2}{\partial x_1} & \frac{\partial A_2}{\partial x_2} \end{bmatrix}^{-1} \begin{bmatrix} \frac{\partial A_1}{\partial q_1} & \frac{\partial A_1}{\partial q_2} & \frac{\partial A_1}{\partial l_1} & \frac{\partial A_1}{\partial l_2} & \frac{\partial A_{11}}{\partial l_3} & \frac{\partial A_{11}}{\partial l_4} \\ \frac{\partial A_2}{\partial q_1} & \frac{\partial A_2}{\partial q_2} & \frac{\partial A_2}{\partial l_1} & \frac{\partial A_2}{\partial l_2} & \frac{\partial A_2}{\partial l_3} & \frac{\partial A_2}{\partial l_4} \end{bmatrix}}_{J} \begin{bmatrix} \delta q_1 \\ \delta q_2 \\ \delta l_1 \\ \delta l_2 \\ \delta l_3 \\ \delta l_4 \end{bmatrix}
$$

(A.5)

The point B_0 is described with the following formula

$$
\begin{cases} X_{B_0} = q_1 \\ Z_{B_0} = 0 \end{cases}
$$

(A.6)

Deriving the Equation (A.6) by the parameters described before, one obtains

$$
J_{B_0} = - \begin{bmatrix} 1 & 0 \\ 0 & 1 \end{bmatrix}^{-1} \begin{bmatrix} -1 & 0 & 0 & 0 & 0 & 0 \\ 0 & 0 & 0 & 0 & 0 & 0 \end{bmatrix}
$$

(A.7)

As for the point B_0, the point B_1 is described by

$$
\begin{cases} X_{B_1} = 0 \\ Z_{B_1} = q_2 \end{cases}
$$

(A.8)

therefore the Jacobian becomes

$$
J_{B_0} = - \begin{bmatrix} 1 & 0 \\ 0 & 1 \end{bmatrix}^{-1} \begin{bmatrix} 0 & 0 & 0 & 0 & 0 & 0 \\ 0 & -1 & 0 & 0 & 0 & 0 \end{bmatrix}
$$

(A.9)

The point A_{11} and A_{12} are characterize by the following formulas

$$
\begin{cases} (X_{A_{1,1}} - X_{B_0})^2 + (Z_{A_{1,1}} - Z_{B_0})^2 = {L_{1,1}^u}^2 \\ (X_{A_{1,1}} - X_{B_1})^2 + (Z_{A_{1,1}} - Z_{B_1})^2 = {L_{1,1}^l}^2 \end{cases}
$$

$$
\begin{cases} (X_{A_{1,2}} - X_{B_0})^2 + (Z_{A_{1,2}} - Z_{B_0})^2 = {L_{1,2}^u}^2 \\ (X_{A_{1,2}} - X_{B_1})^2 + (Z_{A_{1,2}} - Z_{B_1})^2 = {L_{1,2}^l}^2 \end{cases}
$$

(A.10)

hence the Jacobian matrices $J_{A_{11}}$ and $J_{A_{12}}$, according with Equation 2.14, are

$$
J^i_{A_{11}} = \begin{bmatrix} 2X_{A_{11}} - 2X_{B_0} & 2Z_{A_{11}} - 2Z_{B_0} \\ 2X_{A_{11}} - 2X_{B_1} & 2Z_{A_{11}} - 2Z_{B_1} \end{bmatrix}^{-1}
$$
$$
\begin{bmatrix} -2X_{A_{11}} + 2X_{B_0} & -2Z_{A_{11}} + 2Z_{B_0} & 0 & 0 & -2L_{11}^u & 0 & 0 & 0 \\ 0 & 0 & -2X_{A_{11}} + 2X_{B_1} & -2Z_{A_{11}} + 2Z_{B_1} & 0 & 0 & -2L_{11}^l & 0 \end{bmatrix}
$$

(A.11)

$$
J^i_{A_{12}} = \begin{bmatrix} 2X_{A_{12}} - 2X_{B_0} & 2Z_{A_{12}} - 2Z_{B_0} \\ 2X_{A_{12}} - 2X_{B_1} & 2Z_{A_{12}} - 2Z_{B_1} \end{bmatrix}^{-1}
$$
$$
\begin{bmatrix} -2X_{A_{12}} + 2X_{B_0} & -2Z_{A_{12}} + 2Z_{B_0} & 0 & 0 & -2L_{12}^u & 0 & 0 & 0 \\ 0 & 0 & -2X_{A_{12}} + 2X_{B_1} & -2Z_{A_{12}} + 2Z_{B_1} & 0 & 0 & -2L_{12}^l & 0 \end{bmatrix}
$$

(A.12)

Therefore using the permutation matrix, as explained in Section 2.3, one obtains the Jacobian matrices $\boldsymbol{J}_{A_{11}}$ and $\boldsymbol{J}_{A_{12}}$ in the form expressed in Equation (A.5).

A.0.4 Second and third loop

The procedure described for the first loop was applied also for the second and the third loops.

The points A_{21} and A_{22} are calculated as follow

$$A_{2,1} = A_{1,2} + \frac{L_{1,2}^l + L_{2,1}^u}{L_{1,2}^l}(B_1 - A_{1,2})$$
$$A_{2,2} = A_{1,1} + \frac{L_{1,1}^l + L_{2,2}^u}{L_{1,1}^l}(B_1 - A_{1,1})$$

(A.13)

therefore the Jacobian matrices are

$$J_{A_{21}}^i = \begin{bmatrix} 1 & 0 \\ 0 & 1 \end{bmatrix}^{-1}$$
$$\begin{bmatrix} -1+\frac{L_{12}^l+L_{21}^u}{L_{12}^l} & 0 & -\frac{L_{12}^l+L_{21}^u}{L_{12}^l} & 0 & 0 & 0 & 0 & -\frac{X_{B_1}-X_{A_{12}}}{L_{12}^l}+\frac{(L_{12}^l+L_{21}^u)(X_{B_1}-X_{A_{12}})}{(L_{12}^l)^2} & -\frac{X_{B_1}-X_{A_{12}}}{L_{12}^l} & 0 & 0 & 0 \\ 0 & -1+\frac{L_{12}^l+L_{21}^u}{L_{12}^l} & 0 & -\frac{L_{12}^l+L_{21}^u}{L_{12}^l} & 0 & 0 & 0 & -\frac{Z_{B_1}-Z_{A_{12}}}{L_{12}^l}+\frac{(L_{12}^l+L_{21}^u)(Z_{B_1}-Z_{A_{12}})}{(L_{12}^l)^2} & -\frac{Z_{B_1}-Z_{A_{12}}}{L_{12}^l} & 0 & 0 & 0 \end{bmatrix}$$

(A.14)

$$J_{A_{22}}^i = \begin{bmatrix} 1 & 0 \\ 0 & 1 \end{bmatrix}^{-1}$$
$$\begin{bmatrix} -1+\frac{L_{11}^l+L_{22}^u}{L_{11}^l} & 0 & -\frac{L_{11}^l+L_{22}^u}{L_{11}^l} & 0 & 0 & 0 & -\frac{X_{B_1}-X_{A_{11}}}{L_{11}^l}+\frac{(L_{11}^l+L_{22}^u)(X_{B_1}-X_{A_{11}})}{(L_{11}^l)^2} & 0 & 0 & -\frac{X_{B_1}-X_{A_{11}}}{L_{11}^l} & 0 & 0 \\ 0 & -1+\frac{L_{11}^l+L_{22}^u}{L_{11}^l} & 0 & -\frac{L_{11}^l+L_{22}^u}{L_{11}^l} & 0 & 0 & -\frac{Z_{B_1}-Z_{A_{11}}}{L_{11}^l}+\frac{(L_{11}^l+L_{22}^u)(Z_{B_1}-Z_{A_{11}})}{(L_{11}^l)^2} & 0 & 0 & -\frac{Z_{B_1}-Z_{A_{11}}}{L_{11}^l} & 0 & 0 \end{bmatrix}$$

(A.15)

The point B_2 is defined as

$$\begin{cases} (X_{B_2} - X_{A_{2,1}})^2 + (Z_{B_2} - Z_{A_{2,1}})^2 = L_{2,1}^l{}^2 \\ (X_{B_2} - X_{A_{2,2}})^2 + (Z_{B_2} - Z_{A_{2,2}})^2 = L_{2,2}^l{}^2 \end{cases}$$

(A.16)

hence the matrix $J_{B_2}^i$ becomes

$$J_{B_2}^i = \begin{bmatrix} 2X_{B_2}-2X_{A_{21}} & 2Z_{B_2}-2Z_{A_{21}} \\ 2X_{B_2}-2X_{A_{22}} & 2Z_{B_2}-2Z_{A_{22}} \end{bmatrix}^{-1}$$
$$\begin{bmatrix} 2X_{A_{21}}-2X_{B_2} & 2Z_{A_{21}}-2Z_{B_2} & 0 & 0 & 0 & 0 & -2L_{21}^l & 0 \\ 0 & 0 & 2X_{A_{22}}-2X_{B_2} & 2Z_{A_{22}}-2Z_{B_2} & 0 & 0 & 0 & -2L_{22}^l \end{bmatrix}$$

(A.17)

As explained in Section 2.3, it is necessary to refer the Jacobian matrices to all the previously loops parameters, therefore the Jacobian matrices calculated have to be multiplied by the permutation matrices reported in Equation (2.20). Afterwards one can obtain the Jacobian matrices $J_{A_{21}}$, $J_{A_{22}}$ and J_{B_2}.

The calculation of $J_{A_{31}}$, $J_{A_{32}}$ and J_{B_3} has to be done exactly in the same way as for the second loop.

Appendix B

QR decomposition

The calculus of the matrix $\boldsymbol{\beta}$ is made by the following steps

1. Calculation of the permutation matrix P such that

$$\boldsymbol{J}\, P = [\boldsymbol{J}_1 \quad \boldsymbol{J}_2] \tag{B.1}$$

2. Through the QR decomposition one obtains

$$[\boldsymbol{J}_1 \quad \boldsymbol{J}_2] = [\boldsymbol{Q}_1 \quad \boldsymbol{Q}_2] \begin{bmatrix} \boldsymbol{R}_1 & \boldsymbol{R}_2 \\ 0 & 0 \end{bmatrix} \tag{B.2}$$

3. Knowing the matricex $\boldsymbol{R}_1$ and $\boldsymbol{R}_2$ one can calculate the matrix $\boldsymbol{\beta}$ as

$$\boldsymbol{\beta} = \boldsymbol{R}_1^{-1}\, \boldsymbol{R}_2 \tag{B.3}$$

The matrices $\boldsymbol{Q}$, $\boldsymbol{R}$ and $\boldsymbol{\beta}$ are calculated through the Matlab$^{\circledR}$ function qr.